NASA Contractor Report 198390

Materials Compatibility With Uranium Fluorides at High Temperatures

S. Anghaie, R.J. Hanrahan, Jr., and Z.E. Erkmen
University of Florida
Gainesville, Florida

April 1996

Prepared for
Lewis Research Center
Under Contract NAS3–26314

National Aeronautics and
Space Administration

PART I

Interaction of Uranium Tetrafluoride in the Liquid and Vapor Phase With Urania and Thoria

ABSTRACT

The objective of an ongoing study being conducted by the Innovative Nuclear Space Power and Propulsion Institute (INSPI) at the University of Florida, is to find suitable materials for use in contact with uranium tetrafluoride from approximately 1200 to 3000 C. This temperature range encompasses both the liquid and gas phase of UF_4. In this project ceramic materials were investigated which have been used in the fuel of nuclear reactors. These materials, if compatible with UF_4, would be extremely valuable due to their very high melting temperatures, familiar chemistry, and well characterized nuclear properties. Experiments were conducted on thorium dioxide (ThO_2) and uranium dioxide (UO_2). Samples were exposed to liquid UF_4 at 1100 C and to UF_4 vaporized at above 1450 C. Exposures took place in a graphite crucible inside an evacuated quartz tube. An inductive heating system was used to heat the crucible and thereby the UF_4. Use of the quartz tube allowed direct observation of the ongoing reactions.

At the conclusion of each exposure samples of residual gases diluted with nitrogen were run through a gas chromatograph (GC) to determine which gases were released as corrosion products. Subsequent to each experiment remaining samples were weighed then photographed at 2.5x magnification. Power samples of the surface scales and the bulk samples were then prepared for x-ray diffraction analysis (XRD) to determine composition. Data from the GC and XRD were then correlated with equilibrium reaction product data obtained from F*A*C*T to determine the reactions present. Surface analysis of the samples was conducted using Scanning Electron Microscopy (SEM) to examine the scales formed at high magnification, and Energy Dispersive X-Ray Spectroscopy (EDS), to qualitatively determine the elements present

in various parts of the scales.

Experiments with uranium dioxide showed that although UO_2 does not react significantly with UF_4, it does dissolve in liquid UF_4 and apparently suffers from ablation when exposed to UF_4 vapor. Thoria did react with UF_4 in both the liquid and gas phase exposures, forming a mixture of uranium dioxide and uranium-thorium oxyfluorides.

TABLE OF CONTENTS

LIST OF FIGURES
(Figures Located at the end of Part I)

INTRODUCTION

There has been considerable interest, particularly in the field of space power, in gas core nuclear reactors since the mid 1950s.[1] Gas core reactors should possess high efficiency and compact operation due to the extremely high fuel and working fluid temperatures which could be achieved with suitable materials. Unfortunately there is only a very small selection of volatile compounds of uranium which may be used as the fuel in a gas core reactor. Most designs up until recently employed UF_6 as the probable working fluid. UF_6 vaporizes at 56.2 C at 1 atmosphere.[2] Research on UF_6 at elevated temperatures over the past 10 years has shown that in the presence of other materials UF_6 rapidly dissociates at temperatures above roughly 700 C.[3,4,12]. Most gas core reactor designs require peak fuel temperatures well in excess of 700 C[2]. Therefore current work has shifted to using UF_4 as the fuel. The present design being investigated at the Innovative Nuclear Space Power Institute (INSPI) at the University of Florida is referred to as the UltraHigh Temperature Vapor Core Reactor (UTVR). The UTVR utilizes a mixture of UF_4 fuel and a metal fluoride working fluid with MHD power conversion. The UTVR has the following approximate cycle temperatures as the stated goal:[6] (K is used instead of C as this reflects the original source)

Reactor Fluids Temperature: 4000 - 5000 K

Component Temperature Range: 1200 - 2500 K

Energy Conversion Temperature Range: 2100 - 2500 K

Radiator Temperature Range: 1600 - 2100 K

Of particular importance here is the component temperature range listed above. Over this range UF_4 goes from a saturated liquid to full vaporization. Components therefore must be either constructed or coated with material which is stable with respect to this temperature

range, chemical reaction with UF_4 in both liquid and vapor, possible high temperature gas ablation, and very intense radiation fields (neutron, gamma, charged particle, and fission fragment).

Several of the ceramic materials used as fuel in nuclear reactors are already known to possess at least two of the above properties: high temperature stability and resistance to intense radiation fields. Additionally, these materials could potentially take the form of a solid fissile material of a chosen enrichment. This could then act as a "driver fuel" for the reactor, maintaining at all times a fixed base quantity of fuel in chosen areas of the reactor.

For this investigation two materials were chosen, uranium dioxide ($U0_2$) and thorium dioxide ($Th0_2$). These materials were studied separately in the experiments conducted, however both previous literature[20] and our experimental results show that they may be treated as components of a single UO_2-THO_2-UF_4 ternary system.

The fuel mixture in the UTVR is expected to be roughly 95% KF and 5% UF_4.[5] As a first approximation, UF_4 is expected to be the most corrosive element of the fuel therefore all initial experiments involve exposure of samples to pure UF_4. This assumption implies that any material stable in UF_4 should perform exceptionally well in the actual system. The conservatism of this assumption is important when considering that in service, the fuel mixture would also contain thermal and radiolytic decomposition products which would in all likelihood greatly increase the complexity and rate of the overall corrosion process.

In studying a metal exposed to a corrosive environment, focus is usually upon the formation of a solid inert reaction product scale which prevents further reaction of the metal. A classic example of this is aluminum, which is thermodynamically unstable in air, but forms a scale of Al_2O_3 on the surface which prevents further oxidation. In contrast, ceramic materials

are generally chosen for application in corrosive environments in which they have been shown to be inherently chemically inert or at least react very slowly. Formation of a scale on the surface of the ceramic then could be taken to indicate that one should rather use a different ceramic material with the same composition as the scale. This fact changes the interpretation of familiar methods used for determining material compatibility in corrosive environments. In use of the gravimetric method for example when applied to ceramics, an increase in weight does not necessarily imply compatibility, since formation of a surface scale may not be desired. Loss of weight however may still be used to determine reaction rate constants, assuming the weight loss is consistent, reproducible and preferably not accompanied by scale formation. In any case, the most probable reaction product scales to be formed on thoria or urania in reaction with fluorine are thorium oxyfluorides, all possess melting temperatures far below the operating temperatures of the proposed UTVR. Therefore formation of a fluoride on materials studied in this investigation is not desirable.

Since this study is interested in reactions between potential materials and UF_4 and not in reaction rates as such, no attempt was made to obtain maximum density samples or to exercise any other control over sample microstructure. If the samples showed any significant resistance to attack by UF_4, manufacture of materials with the optimum microstructure is the logical next step. Every effort was made however to obtain samples with high chemical purity, in order to minimize the possibility of impurity complexed reactions.

Literature Survey

A literature survey was conducted to gather data from previous investigations of systems involving either ThO_2 or UO_2 and UF_4 at high temperatures. Due to the importance of these two ceramics to the nuclear industry, and the use of fluoride compounds as intermediates in

the production and enrichment of the metals extensive work has been done on fluorination reactions of the oxides with either HF or free fluorine.[7,8] Uranium tetrafluoride is drastically more stable than HF, and no hydrogen should be present in the exposure system therefore papers dealing with fluorination in HF were not reviewed. The dehydration of all elements of the experimental apparatus and reagents is obviously of great importance however. The general Chemistry of UO_2, ThO_2, and UF_4 were summarized in three supplemental volumes of the Gmelin handbook of inorganic chemistry published between 1978 and 1982.[9,10,11] This recent compilation, combined with the classic work by Seaborg and Katz[8] rendered papers published on the general chemistry of these compounds largely redundant to this survey. Methods used to study corrosion of oxide ceramics in a uranium fluoride atmosphere, with specific emphasis on methods available to our lab, was covered thoroughly by Collins.[12] Therefore this literature survey concentrates primarily on previous work involving uranium or thorium dioxide reacted with uranium tetrafluoride, in order to predict any corrosive reactions above 1000 C, with additional emphasis on works involving application to gas or liquid core reactors, or related systems.

Due to its position as the highest melting point oxide ceramic, thoria has been tested extensively for use in high temperature systems. Of particular interest to the UTVR design are two papers published analyzing ThO_2 for application to magneto hydro dynamic (MHD) systems. Arthur and Hepworth tested a number of metals and oxides in an oxidizing atmosphere at 2200 C and determined that thoria could be used as an insulator for an MHD duct.[13] Nagahiro et. al. conducted tests of ThO_2, ZrO_2, and MgO for the same applications, however the ThO_2 was tested at 2400 C. In this case they once again determined that thoria was a "promising" material for MHD systems.[14]

Thoria has also been extensively used for its chemical stability. Of particular interest in this field is the use of thoria as a lining for crucibles used in fluoride systems. In 1952 O'Driscoll and Tee analyzed the free energies for reaction between UF_4 and $Th0_2$, BeO, CaO, $Zr0_2$, $A1_20_3$, and MgO to determine which material would be best used as a liner for the magnesium reduction of UF_4 to U metal and concluded that ThO_2 was the best candidate.[15] Wathen in 1958 received a British patent for the use of ThO_2 as a crucible for the thermorefining of U metal at 1700 C.[16]

Extensive work was done through the early 1970s on the chemistry of solid solutions of ThO_2 and $U0_2$, due to their application as an integral fuel and breeding material for nuclear reactors. Most of these works dealt with the systems at relatively low temperatures in inert atmospheres. The solidus and liquidus temperatures in the UO_2-ThO_2 system were determined in 1970.[17] Tagawa, in 1975 published a study of the reaction between uranium tetrafluoride and uranium mononitride at temperatures up to 950 C.[25] This study is of interest here not because of its direct relation to the present work but because of the experimental apparatus used. The UN-UF_4 mixture was placed in an open nickel crucible which was housed in a quartz vacuum chamber, much like the one used in the present experiment. UF_4 expelled from the nickel crucible was observed to condense on the quartz and react to form UO_2 and SiF_4. This phenomenon was independently verified in the present work using a combination of gas chromatography and qualitative x-ray diffraction analysis.

The definitive work to date on the UO_2 - ThO_2 - UF_4 system was performed by Fonteneau and Lucas in 1969.[18,19] They studied this system at 1100 C by preparing uranium as a uranate and thorium as a hydroxide, the mixture of which was dried and held at 1100 C in a hydrogen filled nickel tube for 48 hours. The resulting U-Th-O structure was then

combined with UF_4, sealed in nickel, heated to 1100 C, and then quenched. The phases present in the final product were then determined using x-ray diffraction. This procedure was repeated at numerous Th/U/F ratios in order to produce the phase diagram at 1100 C, which is reproduced in Figure 1. No follow up investigations of this system, or any experiments involving gas phase UF_4 exposures of oxide ceramics have been published.

The literature survey reveals that although considerable work has been done on the fluorination of thorium dioxide and uranium dioxide, very little work has been done on the reaction of these oxides with UF_4 particularly where UF_4 is a vapor. If UF_4 were to dissociate extensively at high temperatures, corrosion of the oxides will undoubtedly result. There is however, no conclusive evidence of extensive fluorination reactions between UF_4 and either UO_2 or ThO_2. The work by Fontenau and Lucas on the liquid phase reaction products does reveal that UO_2 should dissolve in molten UF_4, the kinetics of which may be assumed to be fairly rapid based on the work of Greenfield and Hyde, who studied the solubility of UO_2 in a mixed UF_4 metal fluoride melt at 1250 C.[20] This investigation therefore proceeded in order to determine the gas phase compatibilities, as well as to estimate the rate of dissolution of UO_2 in UF_4 and determine the compatibility of ThO_2 with UF_4 at 1100 C.

Theoretical Methods

The first step in determining whether a given ceramic material will perform well in a corrosive environment is to examine the thermodynamics of any probable reactions. By determining the equilibrium reaction products, materials which should be inert in the corrosive medium may be identified. Although this method does not provide any information on reaction kinetics, at the temperatures of interest in this study reactions may approach equilibrium so rapidly that measurement of reaction rates is unimportant. Accordingly all of the systems

examined in this study were analyzed for equilibrium products using the EQUILIB module of the F*A*C*T codes (see Appendix B). This provided predictions of the corrosion products produced by the reactions, however since much of the data was based on extrapolation from significantly lower temperatures, in all cases experiments were carried out even if the code predicted that the materials were incompatible with UF_4.

Accompanying the thermodynamic analysis of the samples, analysis of phase diagrams for the reacting systems of interest is required. Conveniently a phase diagram for this system was produced based on the work of Fontenau and Lucas. This diagram is reproduced in Figure 1. Examining this diagram reveals that although the F*A*C*T analysis indicates that UO_2 is stable in UF_4, (see appendix B) UO_2 may not be considered compatible in the liquid range of UF_4 since these two species exhibit infinite miscibility. Since the rate of dissolution of UO_2 solid in UF_4 liquid is unknown, an experiment to observe this reaction was carried out. Multiple experiments with UF_4 vaporized at approximately 1450 C were also conducted as the reactions in the gas phase were expected to be qualitatively and quantitatively .different from those in the liquid phase.

Experimental Methods

In a preliminary study such as this, where the primary emphasis is on identifying potential engineering materials rather than determining reaction kinetics or thermodynamic quantities, there are a limited number of practical techniques to study the reacting system. Primary among these are direct observation of the reaction, measurement of weight change (discontinuous gravimetric method), and determination of solid reaction products using X-ray diffraction and gaseous products using gas chromatography. Surface analysis may be carried

out using optical microscopy, scanning electron microscopy (SEM), and energy dispersive x-ray spectroscopy (EDS). Each of these methods is discussed individually below.

Using a quartz tube as the vacuum chamber surrounding the graphite reaction vessel allowed the liquid phase reactions to be directly observed in progress. A schematic of the reaction system and photographs of the actual system are provided in Figures 2, 3, and 4. Therefore it was straightforward to determine when a reaction was occurring which resulted in damage to the sample and to judge the appropriate duration for a given exposure. The same system was used for vapor phase exposures. However in this case direct observation was rendered difficult by the rapid fogging of the quartz tube by deposition of UF_4 and assorted reaction by-products. The duration of gas phase exposures was limited by the volume of UF_4 which the reaction vessel could hold. Continuous exposures in excess of roughly 10 minutes were impractical. This duration was ample for identifying the gas phase reactions however.

A common quantitative method for determining reaction rates of a solid with a liquid or gas is monitoring the weight change over time (gravimetric method).[12] This technique may be employed either continuously or discontinuously. The continuous method typically consists of suspending the sample from a wire attached to a microbalance and recording the weight change with time of the reaction. Due to problems with corrosion of the suspending wire and condensation of UF_4 on the cool components of the microbalance the continuous gravimetric method was deemed inappropriate to this study. The discontinuous method involves exposing samples at the same temperature/pressure etc. for varying lengths of time. This data may be employed to produce a weight change versus time plot. As discussed earlier, interpretation of this data when applied to ceramic corrosion is potentially misleading. In general steady increase or decrease in weight with time both may indicate incompatibility. Although an

increase in weight may indicate growth of a stable scale on the surface of the sample, this is undesirable since the objective of using a ceramic is to have a materials which is inert. Ideally the positive or negative weight change should rapidly approach a maximum or minimum value which does not change significantly with further exposure.

The chemical composition of solid reaction products may be determined using X-Ray Diffraction (XRD). This method is based on the fact that a given compound will produce a characteristic pattern of diffracted X-ray$_s$ whether the compound is pure or part of a mixture in solid or powder form. The chemical is identified by matching its pattern with a known pattern recorded by the Joint Committee on Powder Diffraction Standards (JCPDS).[21] Powder samples were prepared and mounted in our lab. The samples were analyzed by the Major Analytic Instrumentation Center (MAIC) at the University of Florida. Results provided by the MAIC were then checked manually in order to verify the identification of the compounds detected.

Early in this project it was realized that a significant fraction of the corrosion products were stable gases. Since determining which gases were being produced by the reactions could help to guide us to the predominant corrosion path, a thermal conductivity gas chromatograph (F&M model 810) was obtained and overhauled for use as a by-product gas analyzer (Figure 5). The key to G.C. is separation of a small sample of mixed gases (diluted in an inert carrier gas) into its constituents. The sample separates as it passes through the chromatographic column due to the varying affinity of the constituent gases for the packing of the column. Column packings must therefore be chosen which are effective in separating the unknown gas sample.

As the gases leave the column they pass through a detector which produces a small positive voltage to be read on a chart recorder. Gases are therefore identified by the characteristic time it takes for them to pass through the column. Quantitative information may be obtained from the height of the voltage peak, proportional to the volume of sample gas passing through the detector. For this system a thermal conductivity detector was used. The chromatographic column consisted of a seven foot length of 0.14 inch i.d. 304 stainless steel packed with washed molecular sieve 13x. The use of molecular sieve allows separation of all fixed gases (except nitrogen from argon and CO_2 which is permanently adsorbed on the column).[21,22]

Scanning electron microscopy (SEM) is a useful technique for studying extremely fine details of the topography and microstructure of a surface scale. In the SEM a beam of electrons strikes the sample in a rastered pattern. Secondary electrons emitted from the surface of the sample are collected into a photomultiplier, the output of which is sent to a CRT producing an image of the surface. High contrast is possible due to the sensitive dependence of secondary electron yield on the topography of the sample. SEM may be used with any solid material, although insulators generally must be coated with a conductive film to improve resolution. Under good conditions, details on the order of 1E-8 M may be resolved.[23]

In conjunction with the SEM, Energy Dispersive X-ray Spectroscopy (EDS) may be used to determine the elements present at the surface of a sample. The electrons striking the surface of the sample in the SEM leave some of the atoms in an excited state. These atoms may then decay to their ground state by emission of characteristic x-rays. By measuring the energy of the x-rays using a lithium drifted silicon (SiLi) or planar high purity germanium (HPGE) spectrometer the elements present may be determined qualitatively. By collecting

x-ray counts versus energy on a multi channel analyzer, semi quantitative information may be obtained. On the newest EDS system available at MAIC, elements down to carbon may be identified. Spatial resolution is on the order of 1E-6 M.[23]

Current Work

In previous work performed at INSPI, thorium dioxide was exposed to UF_6 at temperatures ranging from 800 to 1200 C and time periods up to 1 hour. This earlier project is described in Appendix A. The results of this and several other projects involving exposure of samples to UF_6 at high temperatures[12, Appendix A] resulted in the conclusion that UF_6 dissociated to UF_4 and fluorine and therefore future work should concentrate on UF_4. The research reported here is a continuation of this earlier work, with emphasis now focused on compatibility with UF_4 at high temperatures.

The test apparatus used in this study was ideal for studying exposures to liquid UF_4 for any duration. When applied to gas reactions however, exposure times were limited to on the order of ten minutes. Due to fogging of the quartz vessel, direct observation of the gas/solid reactions was also interrupted. Despite these difficulties, data on the two materials studied in both the gas and liquid exposures is valid in determining their utility to the UTVR. This work attempts to determine the corrosive reactions present which affect compatibility of urania and thoria with uranium tetrafluoride. Additionally, correlation of the reactions observed with the phase diagram for the UO_2-ThO_2-UF_4 system is attempted when appropriate (see Figure 1).

Thorium dioxide was chosen for study due to its position as the highest melting point oxide ceramic (3220 C).[2] Although thorium does not possess a significant thermal fission cross section, it has been used as a breeding material in both fast and thermal reactors to produce U-233[7]. The nuclear properties of thorium have therefore been extensively

characterized. Thorium dioxide is in general very stable, however it is known to react with fluorine to produce ThF_4 as follows: $ThO_2 + 2F_2 = ThF_4 + 0_2$.[9]

If UF_4 were to dissociate significantly at high temperatures with release of fluorine, corrosion of thoria to THF_4 may be expected. Since no studies have been reported which show large scale dissociation of UF_4 at high temperatures, experiments to determine the reaction between ThO_2 and UF_4 in the liquid and gas states were performed.

UO_2 also possesses a very high melting temperature (2880 C).[2] In addition UO_2 is attractive for use in the gas core reactor since its enrichment in U-235 may be optimized for use as a driver fuel of fixed reactivity worth in various sections of the reactor vessel. The performance under irradiation of UO_2 is very well known. This should allow a fairly confident prediction of the length of irradiation a UO_2 lining could experience in the UTVR before failure.

Due to the extremely high potential value of urania and thoria to the UTVR, liquid exposures were conducted although their stability was expected to be better in UF_4 vapor. Based on the previous work with UF_6, ThO_2 was known to form a solution with UF_4 starting at around 1000 C, an observation confirmed by the equilibrium thermodynamic analysis using F*A*C*T. Uranium dioxide was reported to be infinitely miscible with UF_4 at 1100 C (Figure 1) although the rate of dissolution of UO_2 in UF_4 was unknown. For both materials, exposure to liquid UF_4 was conducted at 1100 C in order to allow direct comparison to the work of Fonteneau and Lucas while providing data applicable to their exposure in liquid and two phase regions of the UTVR.

Gas exposures were conducted using the same experimental apparatus. Samples were suspended over the reaction vessel which was heated to roughly 1450 C to vaporize the UF_4

and pass it over the sample. Attempting to go to higher temperatures was impractical due to the much more rapid expulsion of UF_4 from the vessel making it impossible to determine exposure duration. If results from these short exposures were encouraging, subsequent work should involve exposures in a system designed to maintain a UF_4 vapor atmosphere at higher temperatures and longer durations.

Subsequent to each exposure the system was allowed to cool before 20 taking a sample of the residual gases for analysis with the gas chromatograph. This analysis indicated that, particularly during vapor phase exposures, the quartz and graphite vessels were reacting with the UF_4. However this reaction has not been shown to have seriously influenced any of the experiments.

After removal from the exposure system, samples were weighed and then surface analysis was performed. Techniques used for surface analysis were optical microscopy and x-ray diffraction. In addition, 20x magnified photographs of each sample were taken for comparison of sample appearances and surface damage. Scanning electron microscopy and microprobe analysis were performed on representative samples for each reacting system and temperature studied in order to determine surface topology and qualitatively determine elements present at the reaction surface.

EXPERIMENTAL DESCRIPTION

Apparatus

Uranium tetrafluoride melts at around 1310 K and boils at around 1730 K at 1 atmosphere[7]. In the evacuated chamber used for our experiments boiling was observed to begin at closer to 1670 K. For the most rigorous compatibility tests ideally separate flowing loops for liquid and vapor UF_4 would be constructed. Due to the high temperatures required,

this ideal is unattainable at a reasonable cost at this time. Therefore a static liquid test facility was constructed, in order to simply determine chemical reactions with UF_4. Please note that as a convention in this report temperatures taken from accepted references are given in degrees K while measured temperatures are given in degrees C to maintain a realistic number of significant figures.

The reaction system was based on an induction furnace. This apparatus is shown in Figures 3, 4, and 5. A graphite crucible 3 inches long served as the reaction vessel. The crucible was filled with roughly 10 grams of UF_4 powder. The crucible was then placed inside a 2 inch diameter quartz tube which was sealed at each end with 304 stainless steel plates, gasketted with vyton. A piece of mullite tube served as the crucible stand, and was centered over the vacuum port in the lower plate. The upper plate was equipped with a type S thermocouple, which fit into a hole drilled in the graphite vessel, and could be used to monitor the vessel temperature up to roughly 1350 C (maximum service temperature 1482 C). The upper plate also incorporated a steel rod which could be used to suspend and manipulate the sample being tested, and a gas sampling port for residual gas analysis. The vacuum port in the lower plate and all of the piping up to the pumping station was 1/2 inch internal diameter. The piping from the reaction vessel was assembled from Cajon fittings made of monel. The piping just below the vessel was split to a pressure transducer for monitoring vessel pressure in excess of 1 torr, and a monel valve for sealing off the reaction system from the pumping station. Past the valve, a swagelok gas inlet fitting was provided for back pressurizing the chamber with either argon or nitrogen. The pumping station consisted of a Welch duo-seal mechanical roughing pump and a water cooled oil diffusion pump.

The reaction system was ideal for liquid exposures, because it allowed visual observation of reactions in progress. Only the graphite vessel was heated, so no significant damage or exposure would occur to the elements of the system. This same system was also used for gas phase UF_4 exposures, however these experiments caused some problems. The UF_4 vapor produced would react not only with the sample, but with the quartz tube and the ends of the vessel. This made observation of the reaction considerably more difficult, as well as complicating the chemistry of the reaction, by introducing corrosion products from the quartz and graphite and possibly the vyton into the vessel atmosphere. In the case of ThO_2 and UO_2 these added elements are not thought to have adversely affected the results of the experiments however.

At temperatures in excess of the allowed range for the type S thermocouple, temperature could be monitored using a Maxline/Ircon type MX MR04 optical pyrometer which was coupled to the inductive power supply digital control unit, to facilitate feedback temperature control. The pyrometer head available will only operate at temperatures in excess of 1327 C so there was a narrow range where temperature could not be accurately monitored. Additionally, at temperatures in excess of roughly 1400 C, the quartz tube would rapidly become clouded by UF_4 and assorted corrosion products ejected from the reaction vessel, rendering the pyrometer useless. This problem was overcome by constructing calibration curves for each graphite vessel. Curves were obtained by heating the vessel in the evacuated chamber, with no UF4, from zero to 80 % power. Temperature was recorded at intervals of 1 to 5% power, allowing sufficient time between power changes for temperatures to approach equilibrium. This data was plotted to obtain a temperature versus per cent power curve.

During an actual experiment, data at the same points was taken to determine deviation from the curve, and to estimate temperature when it could not be measured.

Procedure

Prior to each exposure, the reaction vessel and sample were each weighed on a Sartorius analytic balance sensitive to 10 micrograms. The reaction vessel was then filled with pure UF_4 and reweighed. For liquid exposures, a sufficient quantity of UF_4 had to be packed into the reaction vessel that the surface of the melt would be visible during the experiment. Due to the roughly 50% change in volume from the powder to solid UF_4, this could only be achieved by filling the vessel, heating it into the liquid range of UF_4, cooling and then refilling the vessel with more UF_4. When the second load of UF_4 was melted, the surface would be within 2 cm. of the surface of the vessel.

The sample was either hung from the steel rod or, for some vapor exposures, placed across the top of the reaction vessel. The reaction chamber was then assembled and sealed. The chamber was pumped down at room temperature for at least three hours with the roughing pump before the diffusion pump was turned on. The chamber was then pumped down until the ionization gauge at the pumping station was in the 0.1 millitorr range. The objective of this procedure was primarily to remove water vapor from the system, as small amounts of residual oxygen and nitrogen were not expected to play a significant role in the reactions. Once the pressure reached an acceptable level, the inductive power supply was turned on and the vessel was heated at around 300 degrees per hour up to 800 C. The heating rate was limited both to allow ample time for any entrained water vapor to evaporate, and to prevent the UF_4 from being ejected from the reaction vessel, a phenomenon observed at rapid heat rates and attributed to rapid degassing of the vessel and the powdered UF_4. In the 800 C range the

valve to the pumping station was closed, and heating continued to the target temperature at the same rate.

For liquid exposures, temperature was continuously monitored at around 1100 C using the thermocouple. Once the vessel reached the desired temperature, the sample was lowered into the melt by moving the manipulator rod. At this point changes in vessel temperature, chamber pressure, and the appearance of the melt could be directly monitored. Sample condition was monitored by occasionally removing it from the melt. Experiments were continued until it was decided that sufficient evidence had been collected to determine that a specific reaction or set of reactions was taking place (based on degree of surface damage or scale formation).

For vapor phase exposures, temperature could only be monitored continuously to the end of the operating range of the thermocouple, at which point it was removed from the vessel to avoid failure. Temperature was then estimated from the power level of the furnace. Once the UF_4 was completely melted, temperature could be raised at any rate desired, so the last 200 degrees up to 1450 C were covered in one minute. When the UF_4 started to vaporize significantly, it typically took 10 seconds to turn the quartz tube next to the vessel opaque, so no reliable temperature measurement could be obtained with the optical pyrometer. Gas phase exposures could only be maintained while UF_4 remained in the vessel to be vaporized. At around 1450 C the UF_4 would vaporize at roughly 1 gram per minute, and typical UF_4 loadings were on the order of 10 grams, therefore the maximum reliable exposure duration was 10 minutes.

Sample Description

The thoria used in this series of experiments was obtained from CERAC Inc. as a sintered disk 2.011 "diameter, 0.355" thick. The bulk density (calculated based on measurement of sample dimensions and weight) of the thoria was determined to be 76% of theoretical density. The chemical purity was reported to be 99.99%[24]. Samples were cut from the original disk using a Buhler-Isomet low speed diamond saw. A 1/8" hole to use for manipulation was then drilled in each sample using a diamond tipped drill. A photograph of a typical sample before exposure is provided in Figure 24, and SEM micrographs of another sample are provided in Figures 19 and 20.

The uranium dioxide used in this study was provided by the radiation control department at the University of Florida. It consisted of two 3/4 inch diameter disks roughly 1/4 inch thick manufactured from 99.9% pure depleted UO_2 at the materials science department at UF in the mid 1970s. This material had a measured bulk density of 96% of theoretical density (mean value of 3 samples, determined by measuring surface area to calculate volume and using dry weights). A photograph of one sample is provided in Figure 6 and SEM micrographs are provided in Figures 8 and 9. Due to the somewhat unknown history of these particular samples, purity was cross checked using x-ray diffraction and EDS. No impurities were detected (at a reported LLD of roughly 0.1%)

Post Exposure Analysis

Post exposure analysis consisted of a combination of chemical, crystallographic, and surface techniques. In all cases, a sample of the reaction product gases ranging from 0.1 to 0.5 cc, was taken from the reaction vessel at room temperature, and analyzed for constituent gases using the gas chromatograph. The reaction vessel was then opened and the sample and reaction crucible were weighed separately, in order to determine the amount of loss or buildup

of material on the sample, and to determine the amount of UF_4 used in the exposure. The complete sample was then photographed at 20X magnification, in order to allow coarse comparison of sample appearance before and after exposure. X-ray diffraction samples were then prepared by powdering a small piece of the original bulk sample or surface scale. X-ray diffraction analysis was provided by MAIC at the University of Florida. Finally, representative samples from each type of exposure (ThO_2 or U02, UF_4 as liquid or vapor) were mounted on purified graphite, coated with carbon, and examined under the SEM at MAiC. Both photomicrographs and EDS analysis were produced using the SEM.

RESULTS

Four major types of experiments were carried out:

1) Exposure of solid uranium dioxide to uranium tetrafluoride liquid at approximately 1100 C.

This experiment was conducted one time. The sample of uranium dioxide is shown in Figures 6 and 7 before and after the experiment. The lower third of the sample shown in Figure 6 was submerged in liquid UF_4 for two minutes. When the sample was removed from the melt the submerged portion was observed to have completely dissolved in the UF_4 as can be seen in Figure 7. This confirms the miscibility of UO_2 in UF_4 at this temperature, shown in Figure 1. X-ray diffraction was not carried out in this case due to the minimal reaction surface available for sample preparation. XRD of the UF_4 used in this experiment was performed however no UO_2 or any compounds other than UF_4 was detected. This is not particularly surprising since dissolution of roughly 0.5 g of UO_2 in 20 g of UF_4 represents a UO_2 concentration near the minimum sensitivity of powder XRD. SEM micrographs of the unexposed and exposed surfaces of this sample are shown in Figures 8, 9 and 10. The

spherules on the surface of the exposed sample, seen in Figures 10 and 11, were identified as a mixture of uranium and oxygen using EDS. No fluorine was identified on the surface of this sample, indicating that the dissolving surface was at a composition very close to the uranium dioxide. The very rapid dissolution of high density UO_2 clearly eliminates this material for use in exposure to liquid UF_4. Consequently no further experiments were carried out.

2) Exposure of solid uranium dioxide to uranium tetrafluoride vaporized at approximately 1450 C.

In this case semicircular samples cut from the original disks of UO_2 were placed across the top of the graphite reaction vessel. The vessel was then heated to approximately 1450 C (correlated with 50% power on the inductive heating power supply). The UF_4 was vaporized in the vessel passed out over the uranium dioxide sample, and condensed on the quartz wall of the exposure system. Two experiments were carried out in this sequence, one for 5 minutes and another for 10 minutes. Exposures in excess of roughly 10 minutes were impractical due to the complete expulsion of all UF_4 from the reaction vessel. Figure 11 is a photo of the sample used in the 5 minute exposure. Figure 12 shows the sample from the 5 minute exposure immediately after removal from the system, still stuck to the reaction vessel by the reaction product scale. Figure 13 shows the sample from the 10 minute exposure. In both cases a significant amount of material was deposited on the upper surface of the sample while the lower edge was observed to decrease in thickness. This resulted in a net increase in weight during the 5 minute exposure but a slight net decrease in the 10 minute exposure, which suggests that most of the actual reaction involved dissolution of the lower edge of the sample, possibly by condensed UF_4, followed by extensive redeposition of material at the upper edge.

Figure 14 shows the result of the x-ray diffraction analysis of this product scale. Apparently it consists of a solution of uranium dioxide and uranium tetrafluoride. No other possible species were identified by the automated powder diffraction phase identification routine. Figures 15 and 16 are SEM micrographs of the reaction product scale at 1500 and 10000X, these should be compared to Figures 8 and 9. The original sample surface consisting of mixed grains with minor open porosity is completely covered with a more uniform sized granular surface with greater apparent porosity. A small amount of carbon was identified on this scale using EDS however this was attributed to the carbon coating used for the SEM rather than contribution of the graphite reaction vessel to the system. These results are in complete agreement with the results of the F*A*C*T - EQUILIB analysis at 1800 K for the system UF_4 + UO_2 summarized in Appendix B. Since these experiments were conducted with the UO_2 at a temperature where condensation of UF_4 could occur, it is possible that less damage would be observed at higher testing temperatures which were unattainable using this apparatus.

3) Reaction of solid thorium dioxide with uranium tetrafluoride liquid at approximately 1100 C.

In this experiment a single sample of ThO_2 was submerged in the UF_4 melt for 5 minutes. The sample was pulled from the melt for 10 seconds at 2 and 4 minutes in order to evaluate the presence of destructive reaction. At five minutes the exposure was terminated due to the submerged portion of the sample being reduced to about half of its original thickness. The reaction product scale was dark gray with a metallic sheen, suggesting a surface was formed which was considerably smoother than the original sample surface, yet was nonetheless unstable in liquid UF_4. After cooling the sample was removed from the reaction system and placed in a nalgene beaker. During subsequent handling of the beaker, the sample fractured,

suggesting that the reaction product film was brittle and possibly contained significant residual stress as fracture of the original thoria samples was very uncommon. Figure 17 is a photograph of this sample, which may be compared to Figure 22, a typical thoria sample before exposure to UF4 vapor. X-ray diffraction analysis of this sample indicated that the scale was primarily a mixture of $(UTh)O_2$ and $Th_{.25}U_{.75}0_{2.06}$. The diffraction pattern for this sample and schematics of the JCPDS data for the above two compounds and thoria, are presented in Figure 18.[28,29,30] Figures 19 and 20 are SEM micrographs of an unexposed specimen at 1500 and 10000x showing the very fine, even particle size of the original material along with significant open porosity. Figures 21 and 22 are SEM micrographs of the exposed sample surface at 1000 and 10000x, showing a slightly liner grain structure than the original sample with some major surface cracking. An EDS pattern produced from this sample is shown in Figure 23, indicating that the surface is a uranium rich mixture of uranium and thorium with small amounts of oxygen and fluorine present. The surface apparently represents a reaction toward the ThO_2 corner of the phase diagram shown in Figure 1. The UF_4 reacts with the solid ThO_2 to form a mixture of thorium oxyfluorides and uraniumthorium oxides which gradually dissolve in the excess liquid UF_4 resulting in the loss of the sample surface to the melt. This reaction proceeds more slowly than the direct dissolution of uranium dioxide due to the intervening chemical reactions, however still rapidly enough to eliminate ThO_2 from consideration for use with liquid UF_4.

4) Reaction of solid thorium dioxide with uranium tetrafluoride vaporized at approximately 1450 C.

In this case the thoria samples were suspended above the UF_4 in the reaction vessel on a graphite rod passed through two holes drilled in the crucible. The power level of the

inductive heating system was then raised to 50% to obtain a vessel temperature of approximately 1450 C. This experiment was repeated for exposure durations of 3, 4, and 5 minutes. Photographs of a typical unexposed sample and the samples from each of these exposures are reproduced in Figures 24, 25, 26, and 27. Note that by the 5 minute exposure, sufficient disintegration of the sample had occurred to cause it to become detached from the graphite rod which held it in place in the crucible.

X-ray diffraction analysis of each of these samples gave essentially identical results. Species identified were $Th0_2$, (substrate material), $(UTh)O_2$, and $Th_{.25}U_{.75}0_{2.06}$. A typical diffraction pattern for one of these samples is reproduced in Figure 28. Additionally a diffraction pattern produced from the UF_4 and corrosion products deposited on the quartz tube is included in Figure 29. The primary compounds identified in this mixture were UF_4 and carbon from the reaction vessel. Traces of USi_3 and UO_2 may also be present however they were poorly resolved.[31,32,33]

Analysis of the deposits on the tube was prompted by the presence of considerable quantities of CO and SiF_4 identified in the corrosion product gases using the gas chromatograph. The presence of these gases indicates that extensive reaction of either UF_4 or possibly free fluorine with the quartz tube was occurring. Since no lower fluorides (particularly UF_3) were identified in significant quantities on the vessel wall, direct reaction of UF_4 with the wall cannot be shown and therefore the release of fluorine by reaction of UF_4 with ThO_2 is suggested. The presence of CO in the product gases also indicates that extensive reaction of oxygen (released from either the ThO_2 sample or the SiO_2 in the tube) with the graphite reaction vessel was occurring. Although these side reactions were occurring, there is

however no compelling evidence to indicate that they qualitatively affected the results of these experiments.

Under the SEM, the surface of these samples appeared very similar to the liquid reaction samples. One difference however was the presence of small lumps on the surface of the samples. An SEM micrograph of one of these lumps is presented in Figure 30. EDS spectra for the lump and the lower sample surface are shown in Figures 31 and 32. The large peak for carbon at the edge of Figure 31 (the lump) indicates that this is a deposit of graphite from the reaction vessel. Apparently the small deposits of graphite acted to protect the underlying thoria, resulting in the raised lumps seen on these samples. This graphite was probably spalled from the crucible due to the ongoing combination of thermal shock and pore saturation by UF_4 which generally resulted in fracture of the crucible after three to five experiments.

CONCLUSIONS

This project set out to investigate the reactions which occur between urania or thoria in liquid and gaseous UF_4 environments in order to ascertain their applicability to a uranium tetrafluoride fueled reactor. Urania and thoria were independently chosen for research due to their high temperature stability and well characterized nuclear properties. A joint study was conducted due to their forming well known solid solutions. These materials also possess among the highest melting points for oxide ceramics and have been extensively used in reactor fuels. Reactions were studied using a combination of chemical thermodynamic analysis and surface analysis consisting of x-ray diffraction, scanning electron microscopy, energy dispersive x-ray spectroscopy, and direct visual observation of reactions in progress. Surface analysis was performed in order to determine the compounds present in the reaction surface which could

then be correlated with the predictions of the equilibrium thermodynamic analysis and the available phase diagram for the system ThO_2 - UO_2 - UF_4 at 1100 C.

In liquid UF_4, the UO_2 dissolved very rapidly, confirming the miscibility of UO_2 in UF_4 as expected based on the phase diagram of Figure 1. The thoria was also shown to be incompatible with liquid UF_4, although the kinetics of dissolution were retarded by chemical reaction of thoria to uranium-thorium oxyfluorides, once again in agreement with Figure 1. SEM and EDS of the surfaces of samples exposed to liquid UF_4 tend to support this conclusion, with the surfaces composed of a fine regular structure composed primarily of uranium or uranium and thorium, and oxygen, which was in the process of dissolving in UF_4 when the reactions were stopped.

In UF_4 vapor, the reactions and reaction products were essentially the same however the kinetics of reaction and the effect on the structure of the samples was considerably different. The UO_2 once again exhibited little or no chemical reaction with UF_4. In this case the primary effect appeared to be ablation of the sample at the edge closest to the UF_4 source, accompanied by redeposition of UO_2 on the cooler upper reaches of the sample. Condensation of vaporized UF_4 on the cooler UO_2 sample may have played a significant role in damage to these samples, therefore urania should be considered for higher temperature testing with UF_4. The thoria samples on the other hand exhibited a combination of chemical and physical effects. Thoria apparently reacted with UF_4 to form the non-stoichiometric compound $Th_{.25}U_{.75}0_{2.06}$ and $(UTh)O_2$. These compounds were not predicted by the F*A*C*T analysis, primarily because thermodynamic data for them did not appear in the database used for analysis. At any rate the reaction product solution formed on the surface of the thoria sample was non-protective, samples being essentially completely destroyed after 5 minutes at 1450 C. SEM and EDS of

the sample surfaces confirmed these reactions, as well as showing that fragments of the disintegrating graphite crucible were responsible for the uneven surface of the thoria samples. Excess fluorine and oxygen released by the reaction of UF_4 and ThO_2 apparently reacted with the crucible and the quartz wall to form CO and SiF_4, based on the results of gas chromatography of the reaction product gases.

All of the results discussed above lead to the conclusion that neither UO_2 nor ThO_2 are suitable for use as structural or lining materials in exposure to pure UF_4 in either the liquid or gas phase. However these results do prove the applicability of the phase diagram produced by Fonteneau and Lucas to the liquid phase reactions of these compounds, as well as proving the assumption that at the temperatures of interest in this study, corrosive reactions will proceed to equilibrium so rapidly as to make reaction kinetics relatively unimportant.

Two other materials partially investigated during this study should be considered in further research. Although the graphite crucibles did generally fail after a few exposures, the graphite used was a relatively low strength, low density material chosen primarily for machineability and chemical purity. A graphite chosen for strength and high temperature durability could be expected to perform considerably better. Additionally, starting with the F*A*C*T analysis and the literature search, a parallel investigation into the compatibility of uranium nitride (UN) with UF_4 has been conducted. Some initial UN samples have been provided by Dr. Donald Czechowicz of Los Alamos National Lab. These samples were of low density and poor strength however better samples are expected during the fall of 1990.

REFERENCES

1) N.J. Diaz "Preface--Gaseous Core Reactors," Nuclear Technology., 69, 129-133 (1985).

2) CRC Handbook of Chemistry and Physics, 67th edition, 1986.

3) E.D. Whitney, D.J. Kim, D.S. Tucker, "A Study of Corrosion-Resistant Materials for Pulsed Gas Core Nuclear Systems," Nuclear Technology, 69,154-160 (1985).

4) S. Wang, C. Collins, S. Anghaie, "Ultrahigh Temperature Materials for Uranium Fluoride Based Gas Core Reactor Systems Part I: An Overview", Innovative Nuclear Space Power Institute, Report INSPI-UF-M-01 (1988).

5) N.J. Diaz, S. Anghaie, E.T. Dugan, I. Maya, "Ultrahigh Temperature Reactor and Energy Conversion System" (proposal), Innovative Nuclear Space Power Institute, October 1988.

6) Blanchere, J.R., Pettit, F.S., High Temperature Corrosion of Ceramics, Noyes Data Corporation, 1989, p6-9, 33.

7) Benedict, M., Pigford, T., Levi, H.W., Nuclear Chemical Engineering, 2nd edition, McGraw-Hill Book Company, 1981.

8) Seaborg, G.T., Katz, J.J., The Actinide Elements, 1st edition, McGraw-Hill Book Company, 1954.

9) Gmelin Handbuch Der Anorganischen Chemie, "Volume Th C.1. Compounds of Thorium With Oxygen", Springer-Verlag 1979. P176-183.

10) Gmelin Handbuch Der Anorganischen Chemie, "Volume U C.8., Compounds of Uranium with Fluorine", Springer-Verlag 1980. P1516, 27-28, 215.

11) Gmelin Handbuch Der Anorganischen Chemie, "Volume U C.1. Compounds of Uranium with Oxygen", Springer-Verlag 1980. p144-169.

12) Collins, C. "Reaction Between Zirconium Oxide and Uranium Hexafluoride at Elevated Temperatures", masters thesis, University of Florida, 1989.

13) Arthur G. Hepworth M.A., "Ceramic Materials for Magnetoplasmadynamics (MPD) Power Generation". Magnetoplasmadynamics electric power generation, Rept. Syrup. Kings Coil., Univ. Durham, New Castle upon Tyne, England, 1962, 52-56 (1963). (Summarized in Chemical Abstracts, 1964, p5333).

14) Nagahiro, A. et. al. "Refractory materials for the MHD electric power generation. I. "Preparation and test of insulating wall materials for generating ducts." Asahi Garasu Kenkyu Hokoku 16 61-76 (1966) (summarized in Chemical Abstracts, Vol 67, 35985k).

15) O'Driscoll, W.G., Tee, P.A., "The magnesium reduction of uranium tetrafluoride. Thermodynamic considerations in the choice of lining materials.", U.K. Atomic Energy Authority, Ind. Grp. Hdq. R&DB(C)TN-2 3 p3 (1952) (summarized in chem abstracts, vol 53, 16664).

16) Wathen, T. British patent No. 806 031, December 17, 1958. (summarized in Chemical Abstracts, Vol 53, 1172d).

17) Latta, R.E., Duderstadt, E.C., Fryxell, R.E., "Solidus and Liquidus Temperatures In the UO_2 - ThO_2 System", Journal of Nuclear Materials Vol. 35-3, p347-9 (1970).

18) Fonteneau, G., Lucas, J. "Etude De Systemes Oxyfluorides De Thorium et D'Uranium - IV", Journal of Inorganic Nuclear Chemistry 33(12), 4061-7 (1971).

19) Roth, R.S., Negas, T., Cook, L.P., Phase Diagrams for Ceramists, vol. 5, plate 6027. ACERS, 1975.

20) Greenfield, B.F., Hyde, K.R. "Solubility of UO_2 in UF_4 melt." Report 1983~ AERE-6463 from HMSO, 20pp. (summarized in chemical abstracts, vol 100, 164250r).

21) Cullity, B.D. Elements of X-Ray Diffraction, Addison-Wesley publishing Co., 1978, p421-444.

22) Jeffery, P.G., Kipping, P.J. Gas Analysis By~ Gas Chromatography, Pergamon Press, 1964. p23-31.

23) ALLTECH Associates, catalog number 200, pill, 145.

24) Goldstein, J.i. et al. Scanninq Electron Microscopy and X-Ray Microanalysis, Plenum Press, 1984, p123-203,275-299.

25) Tagawa, H. "The Reaction of Uranium Tetrafluoride With Uranium Mononitride", Journal of Inorganic Nuclear Chemistry, vol. 37,731-3 (1975).

26) Barrington, A.E. High Vacuum Engineering, Prentice-Hall Inc. 1963, P 13.

27) Thompson, W.T., Eriksson, G., Bale, C.W., Pelton, A.D. F*A*C*T Guide to Operations, Thermfact Ltd., 1988.

28) Joint Committee On Powder Diffraction Standards (JCPDS), Card number 37-1367 (Th2.5UO.7502.06).

29) JCPDS card number 5-549 $(UTh)O_2$.

30) JCPDS card number 4-556 ($Th0_2$).

31) JCPDS card number 9-293 (USi_3).

APPENDIX A

SUMMARY OF THE INVESTIGATION OF COMPATIBILITY OF THORIUM DIOXIDE WITH URANIUM HEXAFLUORIDE AT HIGH TEMPERATURES

INTRODUCTION

One of the key obstacles to high temperature gas-core reactors utilizing UF6 as the working fluid is finding suitable materials to use for the lining of the reactor vessel. The INSPI UTVR design postulates wall temperatures in the neighborhood of 3000 K exposed to a mixture of roughly 95% LiF, 5% UF6 and assorted gaseous and solid fission products. The philosophy of this investigation is to identify potential materials on the basis of melting temperature, neutron economy, and compatibility with UF6. The assumption is made that UF6 is the most corrosive component of the fuel mixture. Therefore potential materials are exposed to pure UF6 at progressively higher temperatures in order to determine their range of compatibility. Of specific interest in this investigation are materials used as fissile or fertile components of reactor fuels. If these materials prove to be compatible with UF6 they would be extremely valuable as lining material since the lining would then also be part of the fissile inventory and thereby reduce the fraction of the critical mass in the gas phase. The nuclear properties, irradiation performance, and fabrication of these materials is well known therefore the key parameter of interest in this investigation is the range of compatibility with UF_6. Thorium Dioxide is the highest melting point oxide ceramic (3500 K) used as a fuel material. Thoria is also relatively non-toxic and easily obtained in high purity sintered form making experiments fairly straightforward. This report therefore details the procedures utilized and results obtained in investigating the suitability of thoria as a potential vessel material for the UTVR.

EXPERIMENTAL PROCEDURE

For this series of experiments a disk of thoria 1 centimeter thick and 5 centimeter diameter was purchased from CERAC incorporated. The density of this material was measured as 7.57 g/cc versus 9.86 g/cc theoretical density of thoria or roughly 77% of theoretical density. Samples were cut using a low speed diamond saw to the desired size, roughly 1 x 1 x 2.5 cm. The surface area of each sample was measured using a micrometer in order to determine the area of the reaction surface. Each sample was then weighed on a digital balance sensitive to .01 milligrams.

The exposure system incorporated the UF_6 handling system, reaction chamber, and waste collection vessel in a single closed path. The handling system was constructed entirely of 1/2 inch i.d. Monel tubing, valves, and Cajon fittings. The reaction vessel consisted of an alumina tube, bonded to monel inserts at the ends, and placed inside of a 24 inch tube furnace operable to 1200 C. Samples were placed in an alumina boat and slid to the center of the furnace. The vessel was then closed by connecting the Cajon fittings at each end. The entire system was evacuated using a conventional pumping station incorporating a roughing pump and diffusion pump attached to the end of the system through a 1/8 inch i.d. fitting. By pumping overnight with the furnace held at 200 C essentially all of the moisture was removed from the system, leaving a residual system pressure estimated at about 5 militorr based on the average mean free path of air at this temperature.[26] The furnace was then raised to the reaction temperature at about 200 C per hour. Upon reaching the reaction temperature the valve to the pumping station was closed and the UF_6 supply cylinder, heated to 60 C using heating tape, was opened. Pressure was monitored at two transducers, mounted immediately above the supply and waste cylinders. Every effort was made to keep reaction pressures and temperatures consistent however no provision was made for measuring or calculating the flow

rate of the UF_6 during the experiment. At the conclusion of each experiment the UF_6 supply was shut off and the furnace turned off. All of the condensable species in the system were collected in the waste cylinder, which acted as a cold trap. Non-condensable gases, primarily 0_2 and F2, were not removed from the system until it had cooled.

Immediately following removal from the reaction vessel each sample was weighed to determine net weight change for the reaction. Samples were then examined using an optical microscope in order to evaluate the condition of any surface scale formed. 20 X magnification photographs of the samples were then taken. Samples of the scale and the bulk material were then removed and prepared for X-ray diffraction analysis. X-ray diffraction was performed by the Major Analytic Instrumentation Center (MAIC) of the University of Florida.

Equilibrium thermodynamic analysis was performed using the Facility for Analytic Chemical Thermodynamics (F*A*C*T) (Appendix B.). Specifically the equilibrium products for the reaction of ThO_2 with UF_6 at 1000, 1200, and 1400 K were calculated. In all cases the predominant products were ThF_4, UO_2F_2, and UF_6. In addition, previous work by Collins[12] using this same experimental apparatus for ZrO_2 as well as work by Whitney et. al.[3] had shown that in the presence of other materials, particularly oxides, UF_6 begins rapidly decomposing to UF_4 and Fluorine at temperatures above 1000 K. Therefore it was decided to conduct exposures of ThO_2 starting at 800 C and proceeding to higher temperatures in 100 degree increments.

RESULTS

- 800 C: Sample exposed for 1 hour at 800 C, light brown scale developed on surface, probably UO_x too small for detection in X-ray diffraction. Essentially zero weight change.

- 900 C: Sample exposed for 1 hour at 900 C, darker scale formed on surface, determined to be UO_3. Weight increased 1.82 %.
- 1000 C: Sample exposed for 1 hour at 1000 C could not be retrieved, reaction vessel almost completely filled with UF_4. Experiment repeated for 17 minutes. Sample retrieved was roughly half gone and completely coated with UF_4. Subsequent X-ray diffraction analysis indicated that essentially the entire sample had become mixed fluorides.
- 1100 C: Sample exposed for 1 hour could not be retrieved, reaction vessel was plugged with UF_4. Experiment repeated for 10 and 20 minute intervals. In both of these cases the sample was retrieved embedded in UF_4 which had formed in and around the alumina boat, apparently as a liquid. X-ray diffraction analysis of the sample showed $U0_3$, $Th0_2$, and AlF_3, indicating that the alumina was an important part of the reacting system.
- 1200 C: Sample exposed for 10 minutes was retrieved largely intact, completely coated in a loose black scale which proved to be U_30_8. Analysis of the bulk sample revealed ThOF and UO_3 showing that although the sample appeared to be structurally intact, the reaction had proceeded well into the material. The U_30_8 scale was clearly not protective. The end of the reaction vessel close to the UF_6 supply cylinder was filled with loose UF_4 indicating that the majority of the UF_6 had dissociated to UF_4 and fluorine in the cooler regions of the vessel, before reaching the sample. This experiment could then best be correlated to the exposure of ThO_2 to fluorine mixed with a relatively small fraction of UF_4 and lower fluorides.

APPENDIX B

PREDICTION OF EQUILIBRIUM REACTION PRODUCTS USING F*A*C*T

F*A*C*T is the acronym for the Facility for Analysis of Chemical Thermodynamics. F*A*C*T is essentially a computer system incorporating a database of over 4000 inorganic stoichiometric compounds and several code modules which may be used to calculate thermochemical data. Of particular interest to the work performed at INSPI is the EQUILIB program. EQUILIB performs heterogeneous equilibrium calculations on systems containing up to 12 elements and 20 compounds. At the temperatures envisioned or the UTVR, chemical reactions may be expected to proceed so rapidly that the equilibrium reaction products can be taken to represent the steady-state condition of the system. The only significant limitation discovered using EQUILIB in this investigation is the lack of non-stoichiometric compounds in the data base. Although it is possible to include data in the calculations from a private data base, this requires foreseeing which compounds to include as well as providing accurate thermodynamic data for some rather obscure compounds.[27]

Uranium dioxide and thorium dioxide were analyzed independently to determine equilibrium reaction products with UF_4. The results may be summarized as follows:

1) Reaction of uranium dioxide with uranium tetrafluoride.

   At all temperatures from 1200 to 2600 K, the predominant equilibrium species were UF_4 in the liquid or gas phase, and UO_2 as a solid. The solubility of uranium dioxide in uranium tetrafluoride was apparently not included in the F*A*C*T database, since at no temperature was a liquid solution of UO_2 and UF_4 predicted. The important result here however, is that no significant chemical reaction of UO_2 with UF_4 was predicted at any temperature. This led to the conclusion that UO_2 should be investigated for compatibility with UF_4 in the gas phase.

2) Reaction of thorium dioxide with uranium tetrafluoride.

In this case the predicted reaction products varied somewhat with temperature. At 1273 K, the liquid phase was predicted to be ThF_4 and the solid phase UO_2. This result is not consistent with the experiments conducted at 1100 C due to the exclusion of nonstoichiometric compounds from the F*A*C*T database. Note that this does however predict a reaction which would completely destroy the thoria, as occurred in the actual experiments. At 1473 K, a liquid solution of ThF_4, UF_4, and ThO_2 is predicted to be in equilibrium with a solid solution of UO_2 and $ThOF_2$. This prediction once again proved to be inaccurate, due to both the exclusion of non-stoichiometric compounds and the solubility of UO_2 in UF_4. At temperatures where UF_4 is a gas, reaction is still predicted, however the equilibrium solid solution is now a mixture of UO_2 and $Th0_2$, with the ThO_2/UO_2 ratio increasing with temperature. This result was taken to suggest that although ThO_2 was expected to react with UF_4, at very high temperatures where UF_4 was in the gas phase, a stable solid solution of ThO_2 and UO_2 might form.

UF_4-ThO_2-UO_2

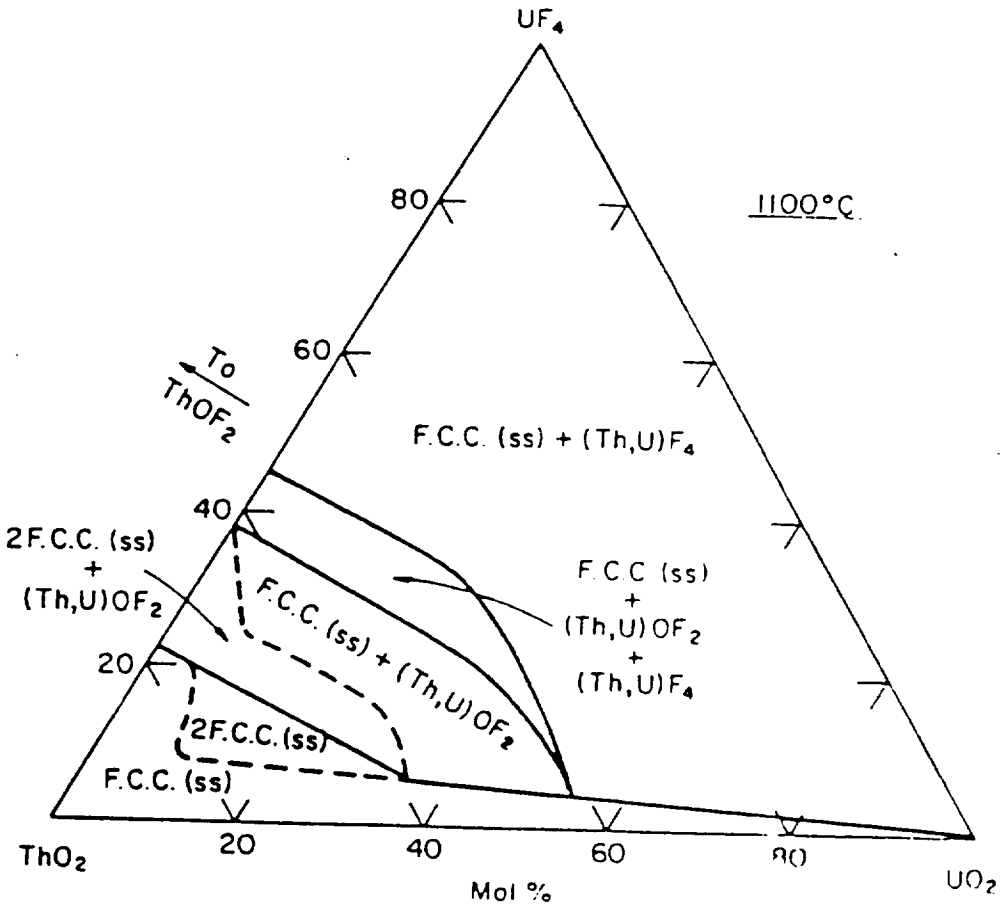

Figure 1. Ternary phase diagram for the system UF_4 - ThO_2 - UO_2 at 1100 C. Taken from Phase Diagrams For Ceramists [19] and based on the work of Fonteneau and Lucas [18].

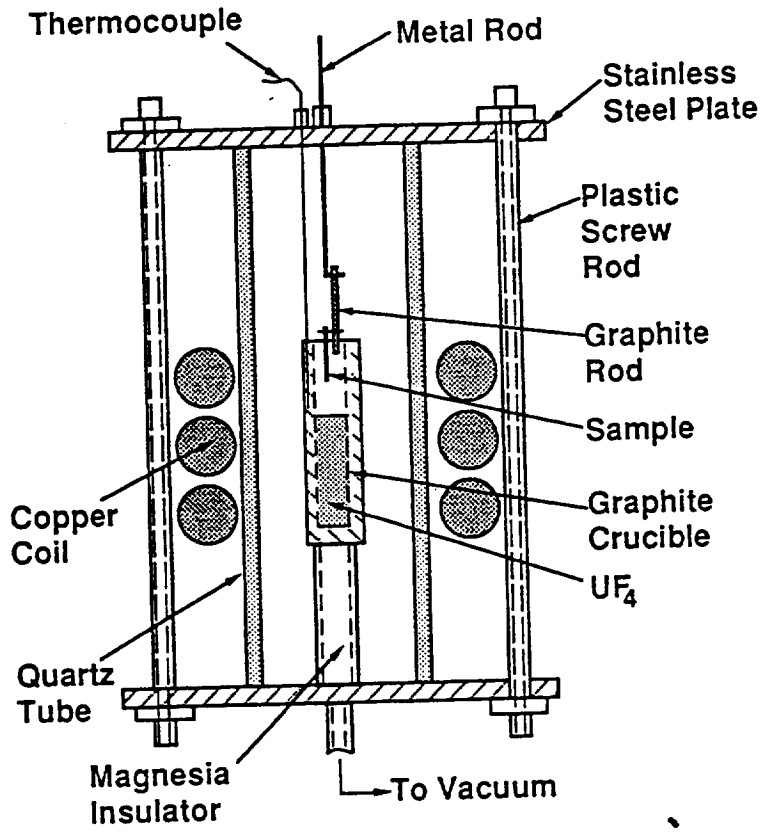

Figure 2. Schematic of reaction vessel used for liquid and vapor phase UF_4 materials testing

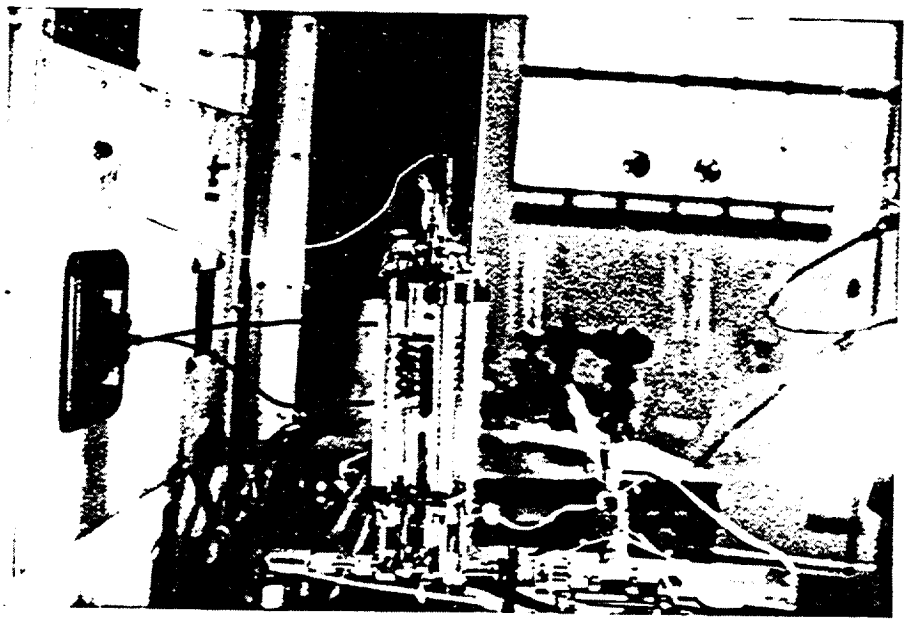

Figure 3. Photograph of system used for liquid and vapor phase UF_4 materials testing.

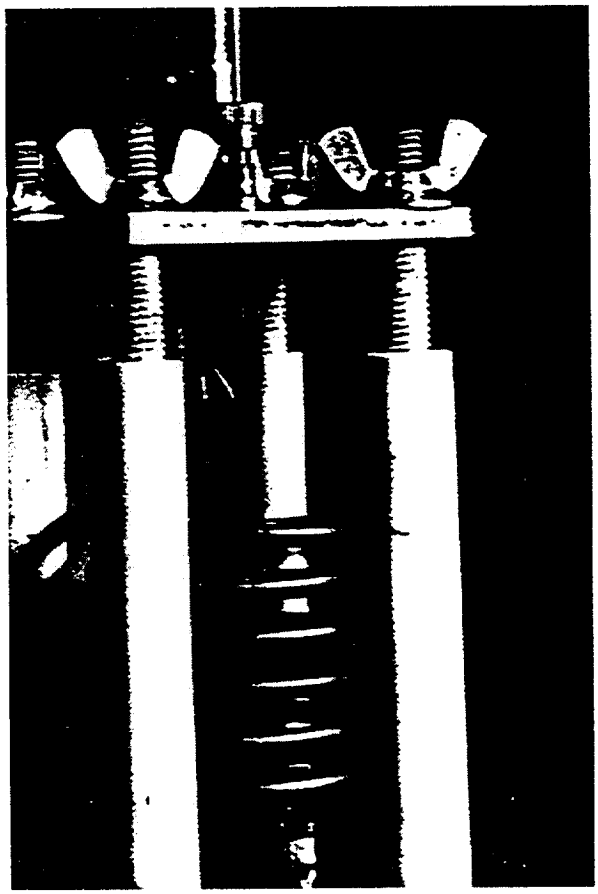

Figure 4. Close up of reaction system showing quartz tube, upper closure plate, graphite reaction vessel, and sample before exposure to liquid UF_4.

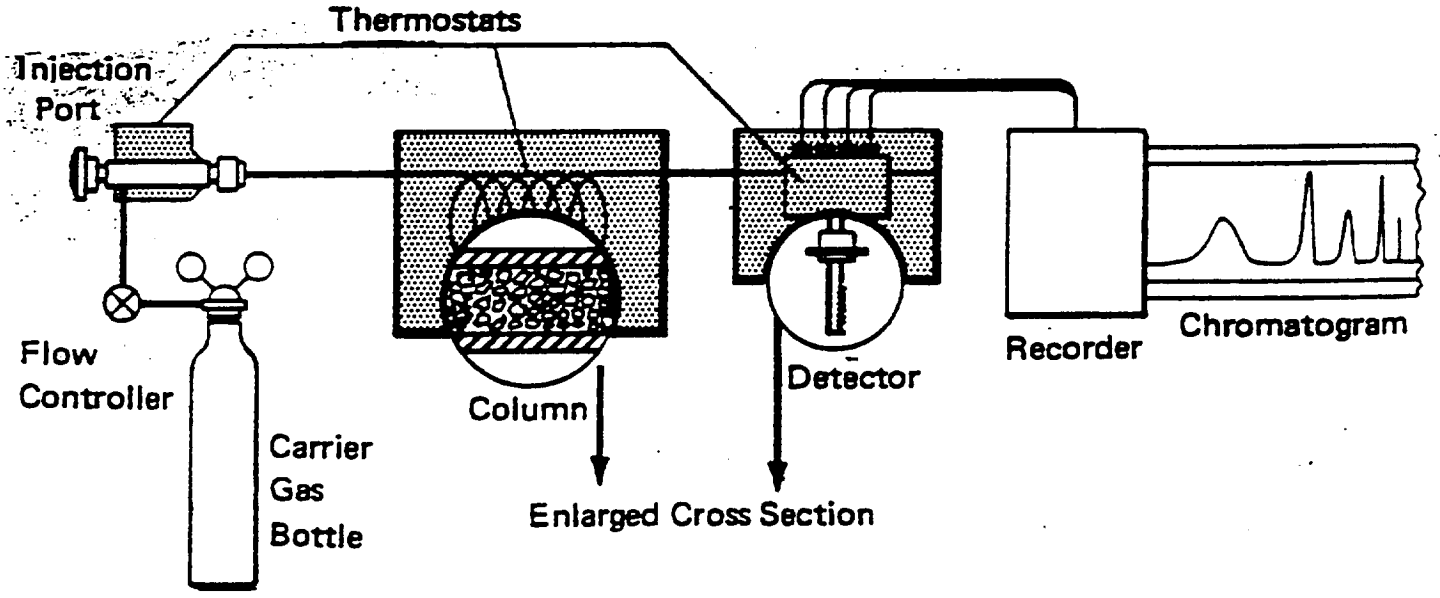

Figure 5. Schematic diagram of a gas chromatograph. [22]

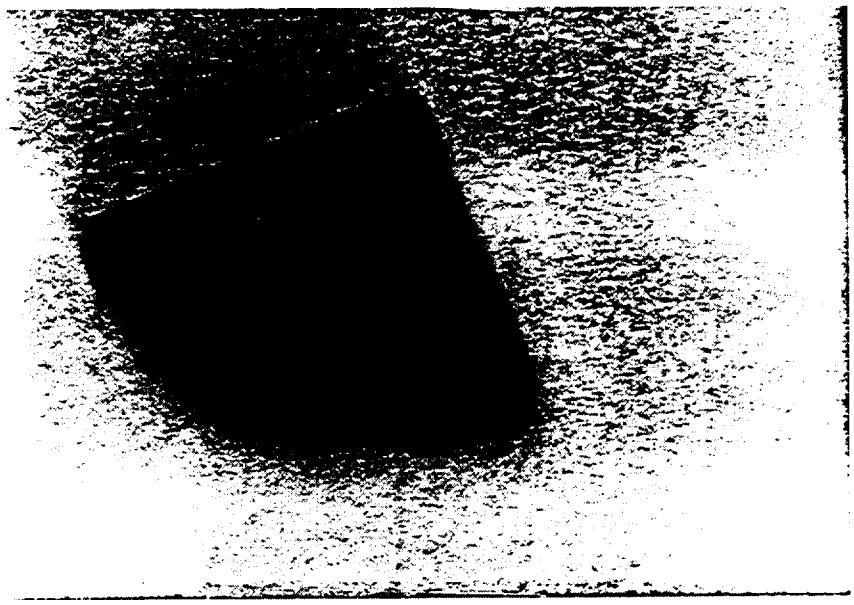

Figure 6. Uranium dioxide sample for liquid UF_4 at 1100 C exposure, before exposure. 2.5 X magnification.

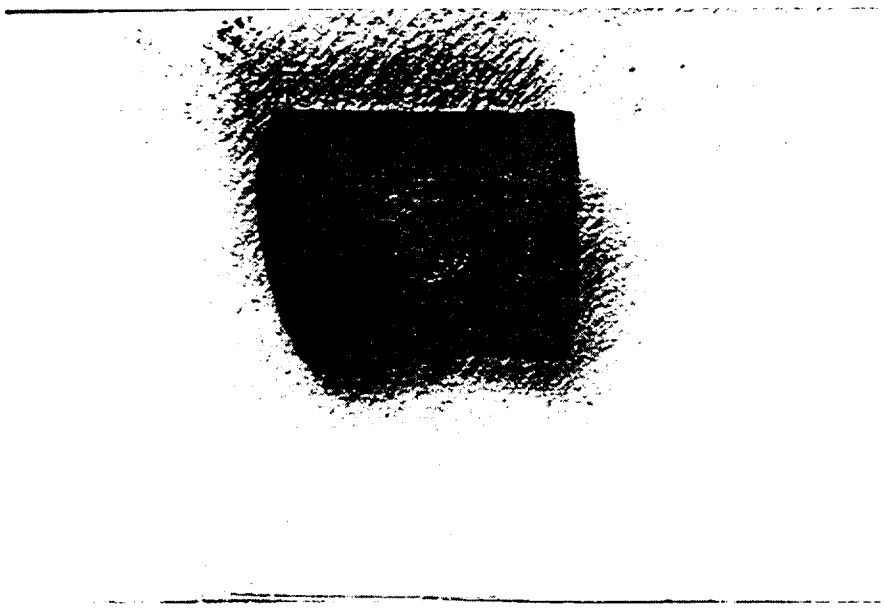

Figure 7. Uranium dioxide sample after lower third was submerged in liquid UF_4 at 1100 C for two minutes. 2.5 X magnification.

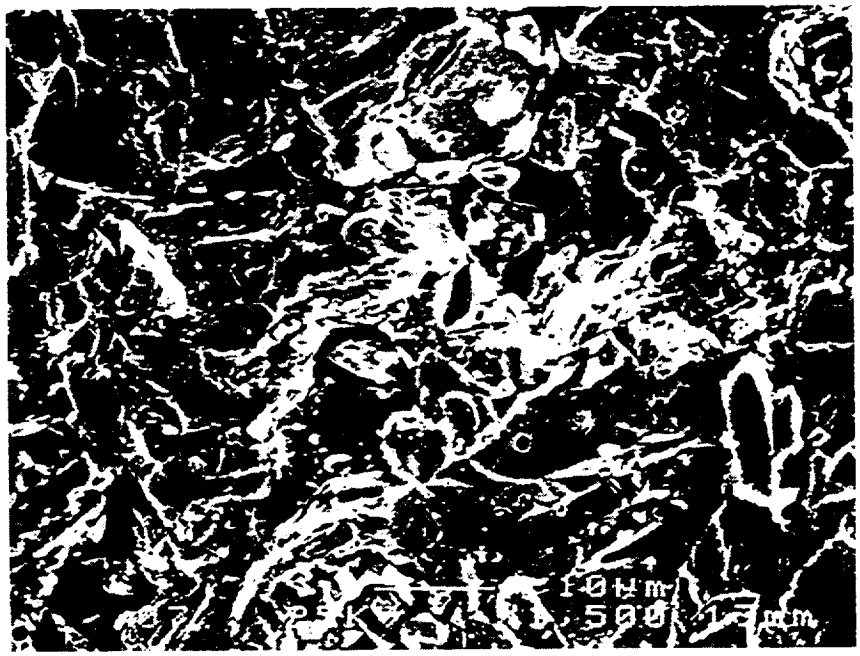

Figure 8. SEM micrograph of unexposed uranium dioxide sample, 1500x magnification.

Figure 9. SEM micrograph of unexposed uranium dioxide sample, 10000x magnification.

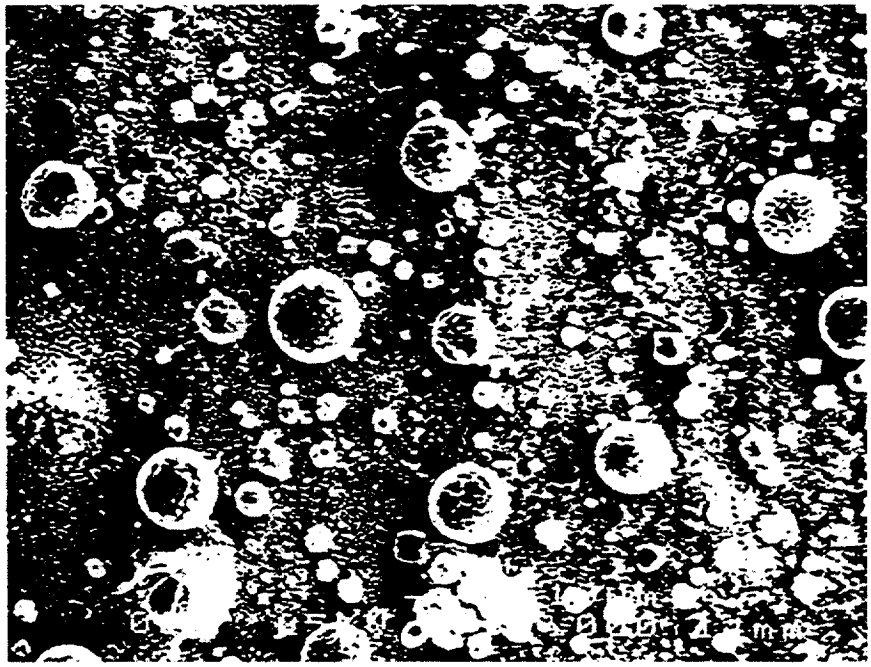

Figure 10. SEM micrograph of uranium dioxide sample exposed to UF_4 liquid at 1100 C, 1000X magnification.

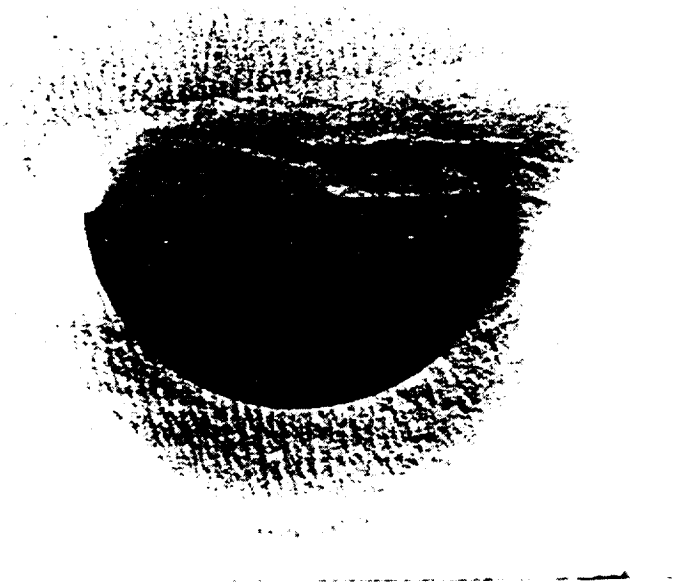

Figure 11. Uranium dioxide sample before exposure to uranium tetrafluoride vaporized at approximately 1450 C. 2.5 X magnification.

Figure 12. Uranium dioxide sample after five minute exposure to uranium tetrafluoride vaporized at approximately 1450 C. Sample was stuck to reaction vessel by build-up of corrosion products later identified as a mixture of uranium dioxide and uranium tetrafluoride. 2.5 X magnification.

Figure 13. Uranium dioxide sample after 10 minute exposure to uranium tetrafluoride vaporized at approximately 1450 C. 2.5 X magnification.

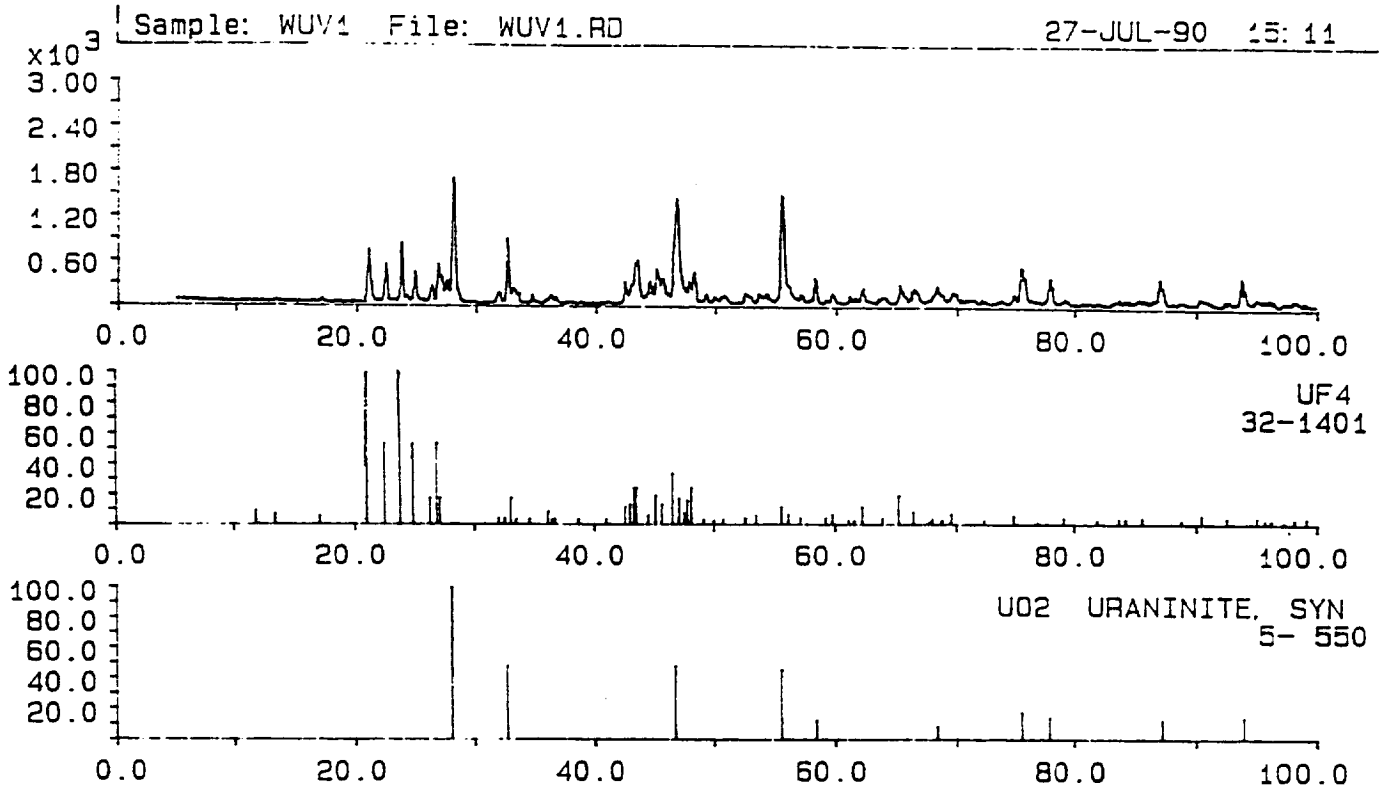

Figure 14. X-ray diffraction pattern produced by powder sample of corrosion products from exposure of uranium dioxide to uranium tetrafluoride vapor.

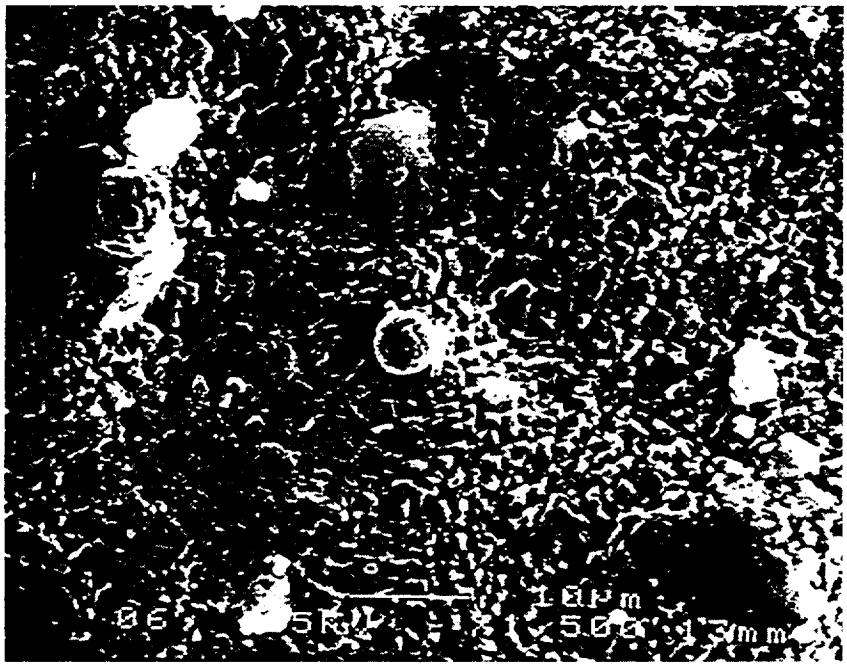

Figure 15. SEM micrograph of uranium dioxide sample exposed to uranium tetrafluoride vapor at approximately 1450 C. 1500 X magnification.

Figure 16. SEM micrograph of uranium dioxide sample exposed to uranium tetrafluoride vapor at approximately 1450 C. 10000X magnification.

Figure 17. Thoria sample after five minute exposure to uranium tetrafluoride liquid at 1100 C, sample subsequently fractured during handling. 2.5 X magnification.

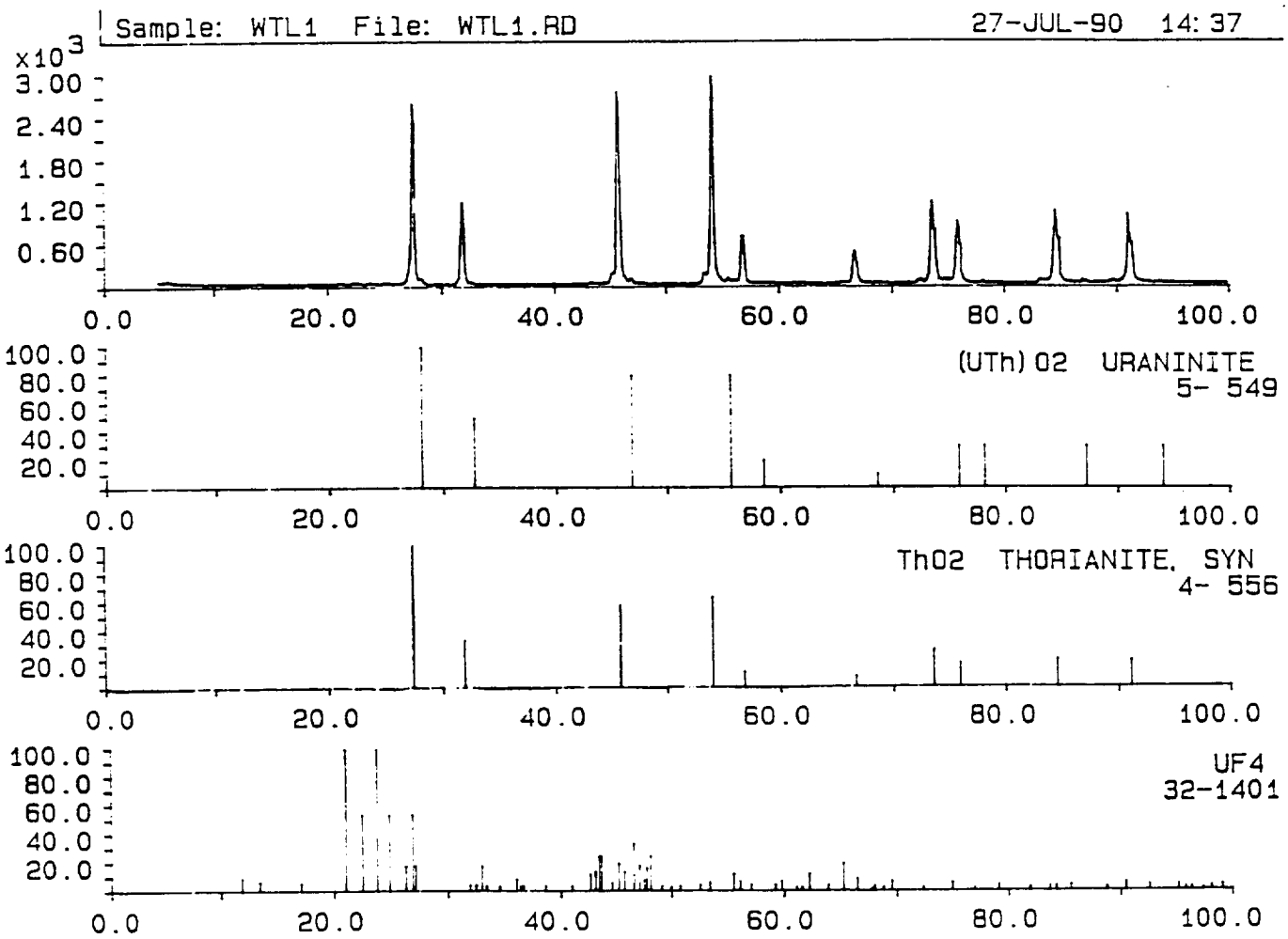

Figure 18. X-ray diffraction pattern produced from thoria sample exposed to liquid uranium tetrafluoride at 1100 C.

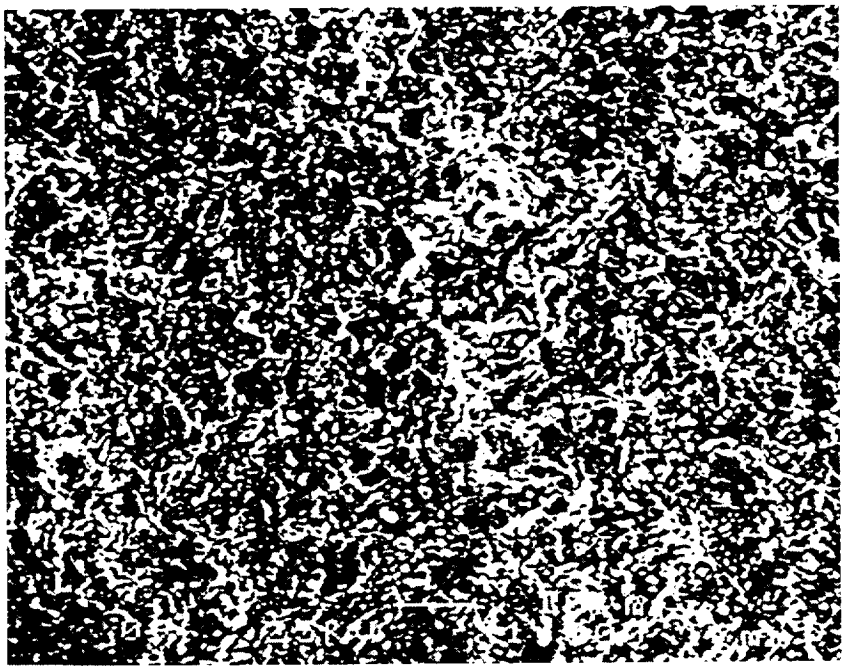

Figure 19. SEM micrograph of unexposed thoria sample, 1500X magnification.

Figure 20. SEM micrograph of unexposed thoria sample. 10000X magnification.

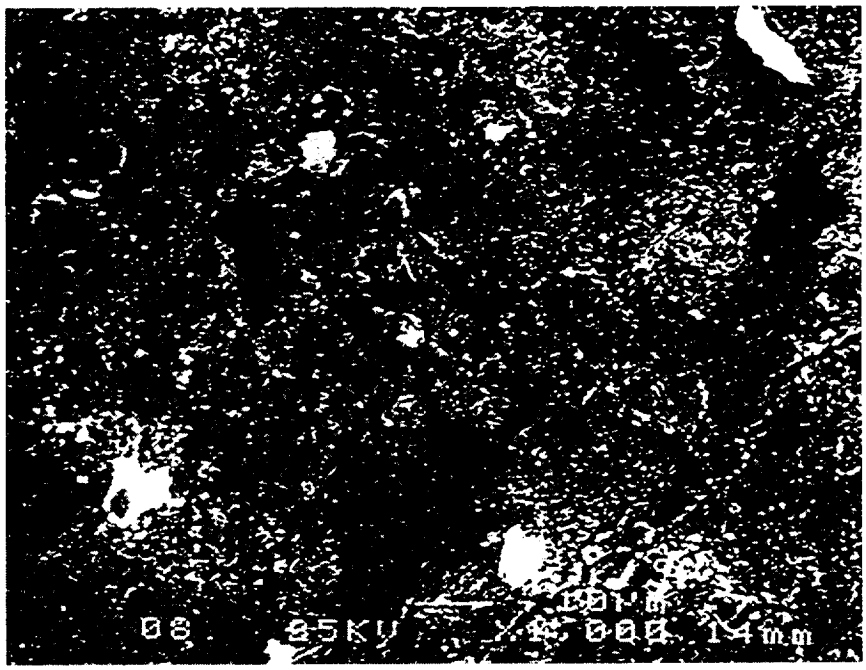

Figure 21. SEM micrograph of thoria sample exposed to liquid uranium tetrafluoride at 1100 C for two minutes. 1000X magnification.

FIgure 22. SEM micrograph of thoria sample exposed to uranium tetrafluoride liquid at 1100 C for five minutes. 10000X magnification.

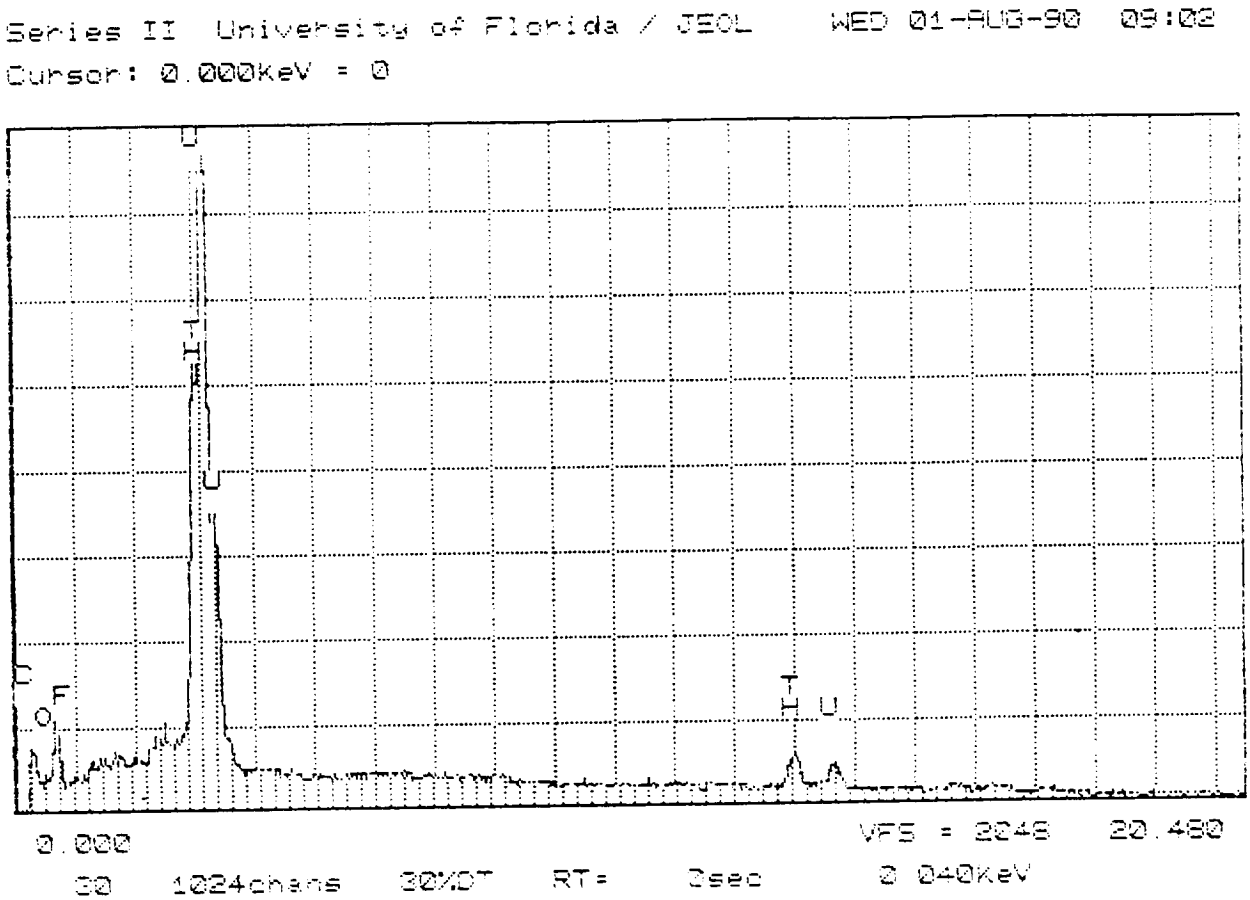

Figure 23. EDS spectrum obtained from surface of thoria sample exposed to uranium tetrafluoride liquid at 1100 C, showing that the surface layer is composed primarily of uranium oxyfluorides.

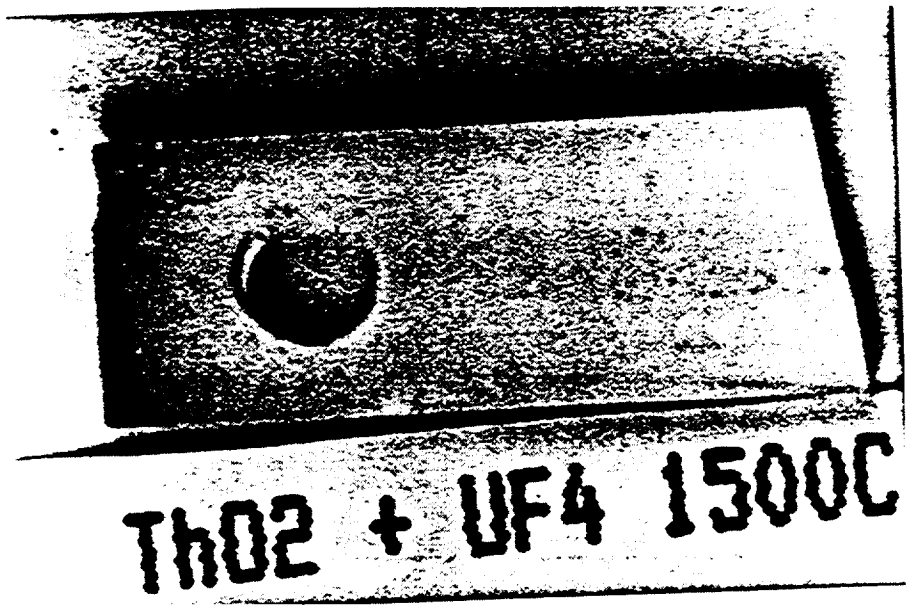

Figure 24. Typical unexposed thoria sample prepared for reaction with uranium tetrafluoride at approximately 1450 C. 2.5 X magnification.

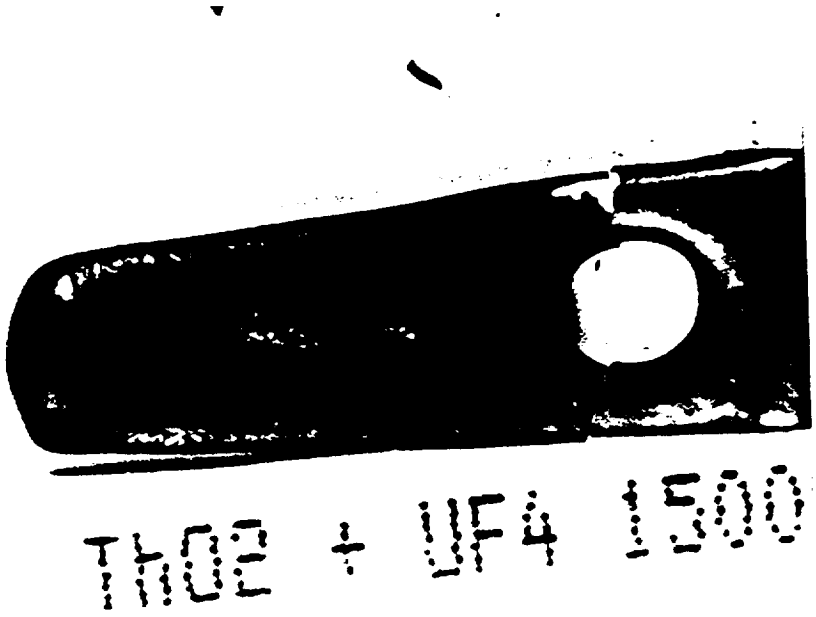

Figure 25. Thoria sample exposed to uranium tetrafluoride vapor at approximately 1450 C for 2 minutes. 2.5 X magnification.

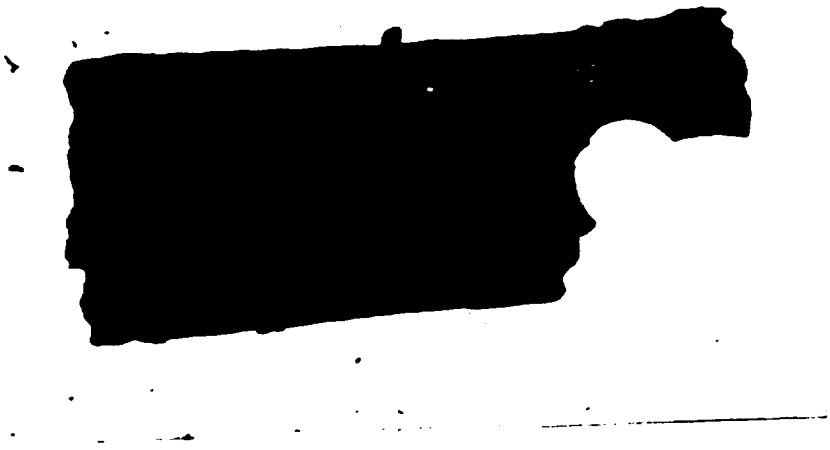

Figure 26. Thoria sample exposed to uranium tetrafluoride vaporized at approximately 1450 C for three minutes. 2.5 X magnification.

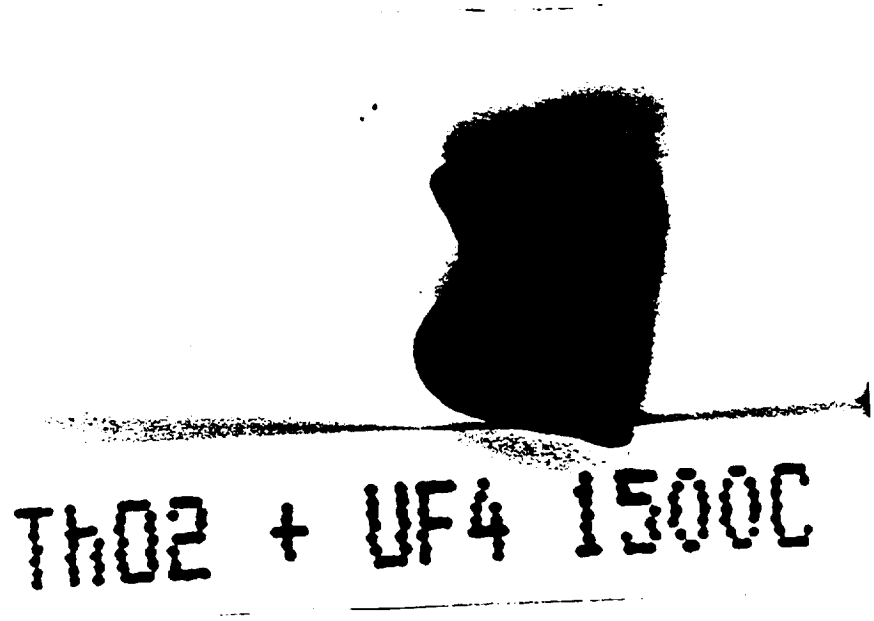

Figure 27. Thoria sample exposed to uranium tetrafluoride vaporized at approximately 1450 C for 5 minutes. 2.5 X magnification.
/

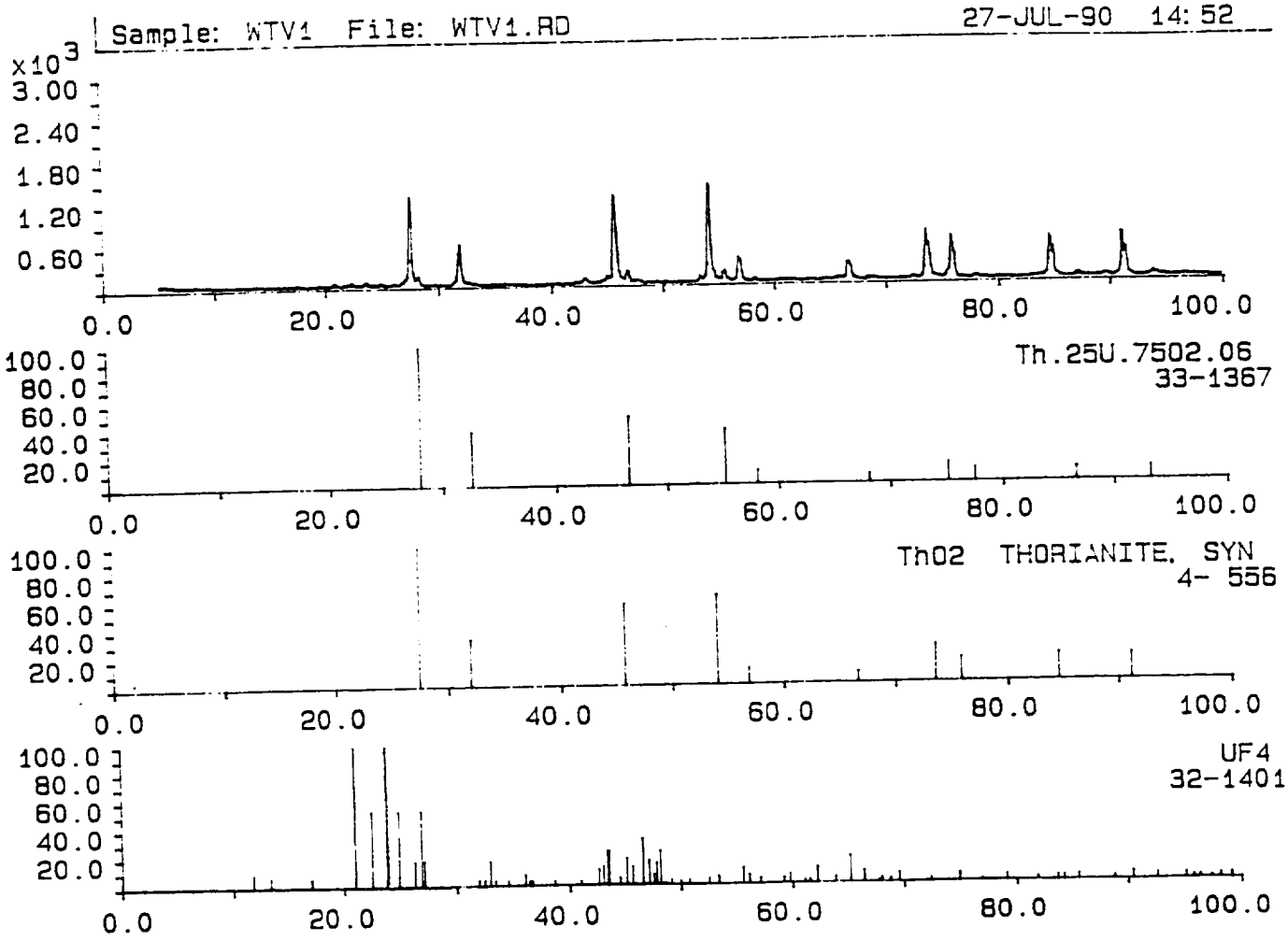

Figure 28. X-ray diffraction pattern produced from thorium dioxide sample exposed to uranium tetrafluoride vapor.

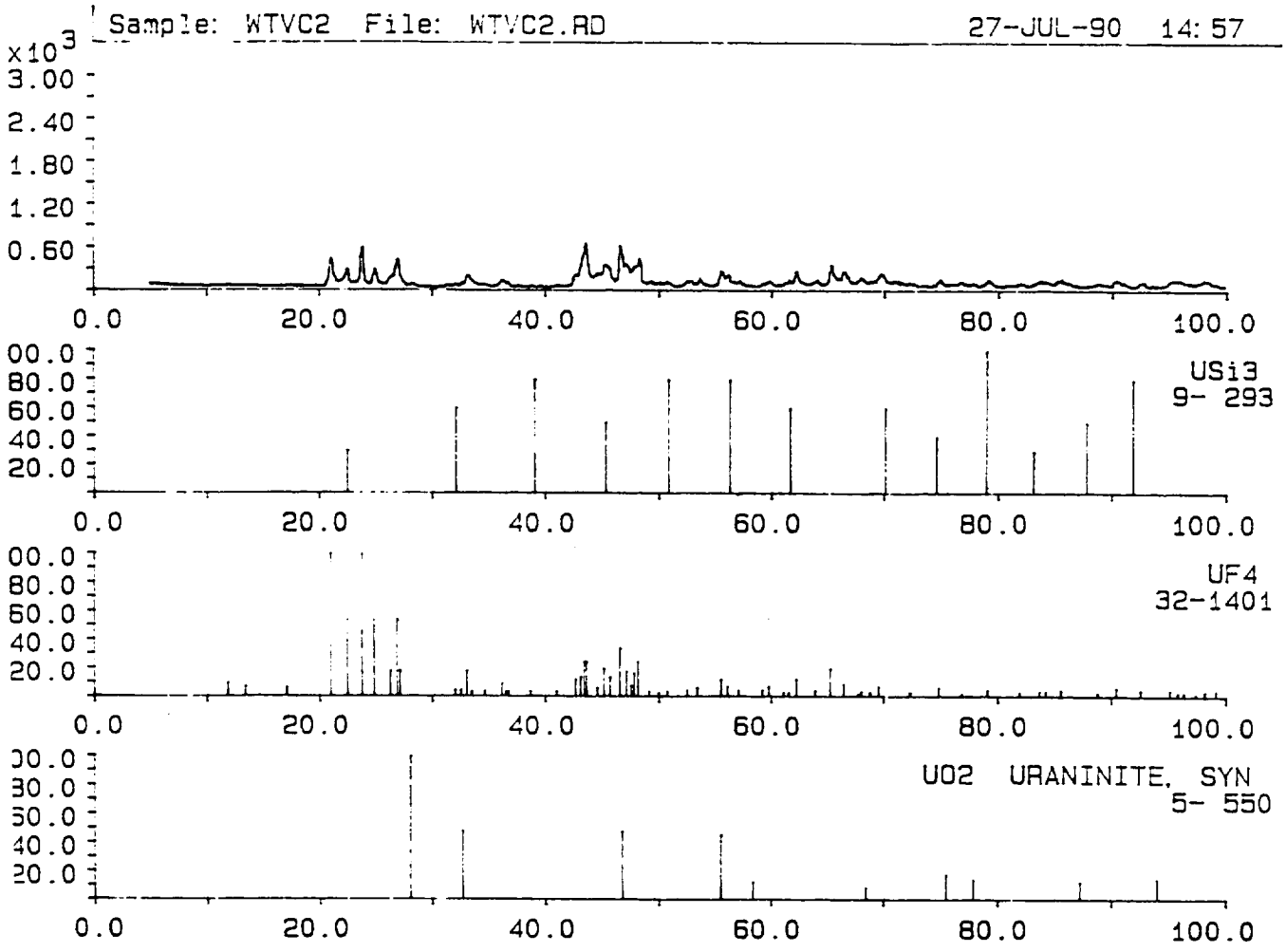

Figure 29. X-ray diffraction pattern produced by materials condensed on the wall of the reaction vessel during exposure of thoria to uranium tetrafluoride vapor.

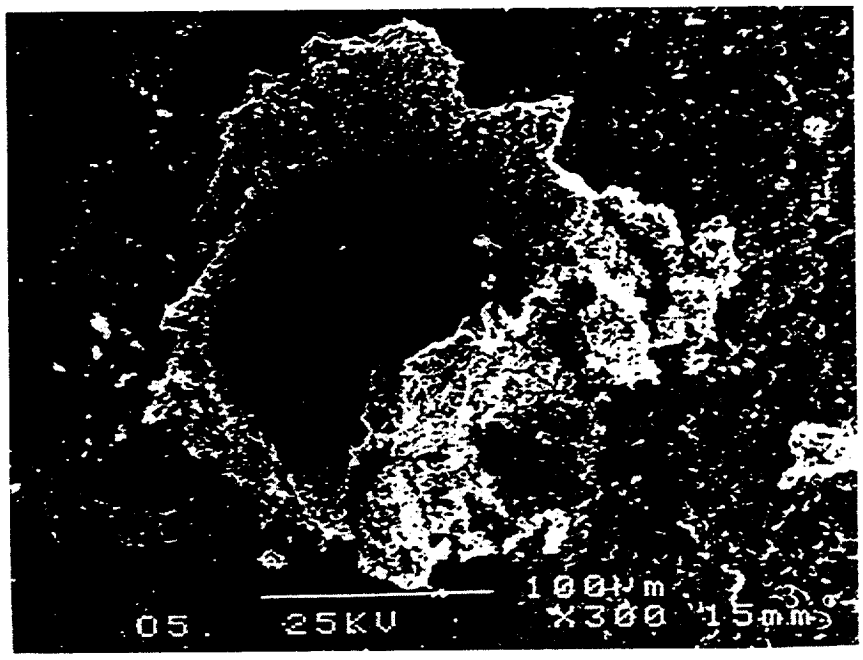

Figure 30. SEM micrograph of thoria sample exposed to uranium tetrafluoride vapor for 3 minutes. 300 X magnification.

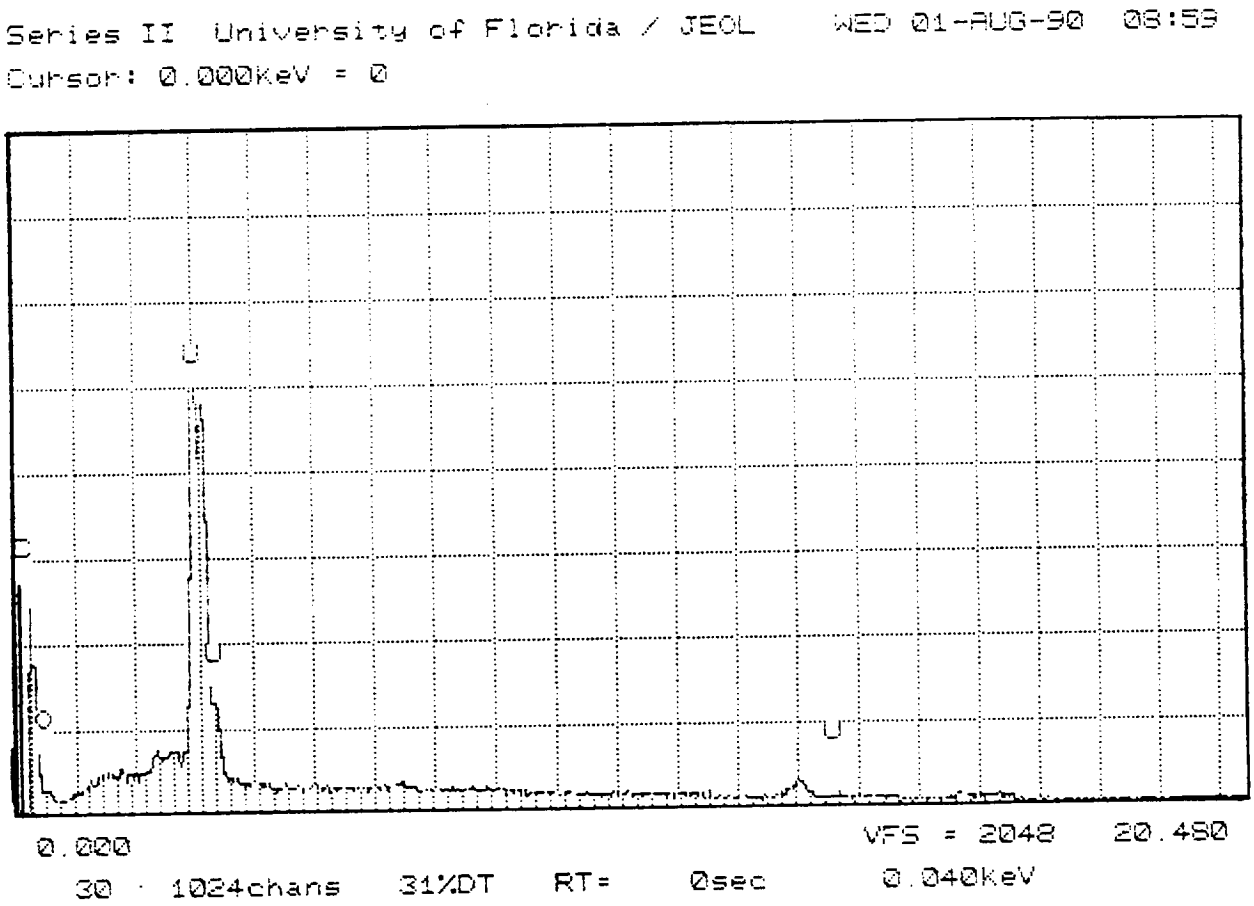

Figure 31. EDS pattern produced from surface of lump in figure 30, showing large concentration of carbon.

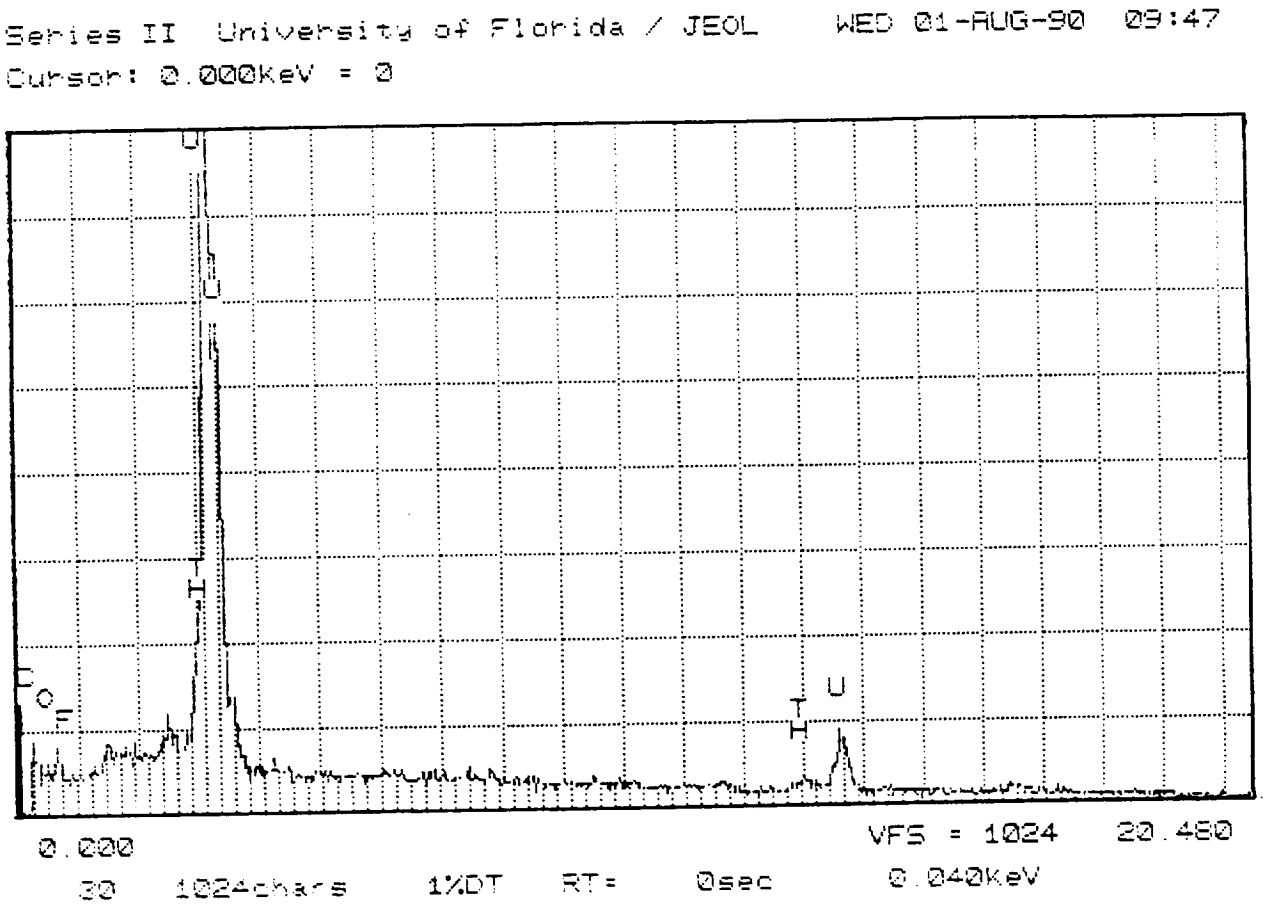

Figure 32. EDS spectrum produced from the smooth surface of thoria sample exposed to uranium tetrafluoride vapor shown in figure 30.

PART II

Interaction of Uranium Tetrafluoride and Uranium Hexafluoride with Yittria and Molybdenum

ABSTRACT

The reaction of yttria with UF_6 and UF_4, and the compatibility of molybdenum with the liquid and gaseous phases of UF_4 were investigated. High-density samples of yttria were processed using sintering and hot-pressing techniques. Yttria reacted extensively with UF_6 gas at 1173 K and formed two reaction layers. These layers were found to be composed of YF_3, UO_2, and U_3O_8. The reaction of yttria with gaseous UF_4 caused the formation of three consecutive reaction layers which were labeled as outer, center, and inner layer. The crystallization of dendrites and formation of a peritectic and a eutectic region occurred during cooling of the liquid outer layer. It was found that the outer layer included YU_xF_y (eutectic and peritectic regions) and UO_2 dendrites. The center layer was composed of hypostoichiometric UO_2, while the inner layer contained a mixture of YF_3, Y_2O_3, and YOF. A reaction model was developed to explain the formation of these layers. The solid state diffusion analysis was performed based on the defect chemistry of the UO_2 layer, and the solidification scheme was drawn from the analysis of the microstructures. Fick's second law with the reacting boundary conditions was applied to the UO_2 layer and the analytical solution was derived using experimental data. The theoretical models for multicomponent, multiphase diffusion also was reviewed. A semi-quantitative model of diffusion in one dimension was developed and the flux-velocity relationship was derived for local equilibrium conditions at the interfaces for the existing components. According to the model, the calculated diffusion coefficients of the oxygen and uranium ions in UO_2 were compared with their experimental values.

Molybdenum metal also was tested at temperatures ranging from 1390 K to 1470 K and 1740 K to 2273 K in the liquid and gaseous phases of UF_4, respectively. Electron Microprobe analysis performed on the cross section and Energy Dispersive Spectroscopy on the surface of the samples showed no trace of uranium or fluorine diffusion. After the complete elimination of the oxygen from the reaction chamber, it was found that the molybdenum did not react with the media during the exposure testing.

TABLE OF CONTENTS

LIST OF TABLES

LIST OF FIGURES
(Figures Located at end of Part II)

Figure

CHAPTER 1
INTRODUCTION

The interaction of UF_4 with the candidate wall materials at temperatures above 1273 K is the main emphasis of the second part of this report. From this perspective, several materials have been tested in UF_4 environment at the Innovative Nuclear Space Power and Propulsion Institute (INSPI) laboratories.

Exposure testings have been performed at different temperatures and testing intervals. Uranium tetrafluoride (UF_4) is an intermediate product in the conversion of uranium ore to uranium hexafluoride (UF_6) and it is also used in the manufacture of $U0_2$ and uranium metal fuels.[1,2,3,4] When mixed with various other metal fluorides (LiF, NaF, and KF), UF_4 proved to be the most suitable fuel for the molten salt reactor.[3,5] Uranium tetrafluoride is a green color powder with monoclinic structure. At room temperature, it is nonvolatile, insoluble in water, and relatively stable in air. It has a melting point of 1309 K and a boiling point 1715 K under one atmosphere. Its density is 6.7 g/cm^3 at solid phase and drops nearly to 6.36 g/cm^3 in liquid phase between 1340 and 1630 K[3].

Uranium (U) and fluorine (F) diffusion can determine the behavior of the candidate materials at high temperatures or under the influence of various external conditions. High temperature diffusional creep, coagulation of finely dispersed precipitates in heat-resistant alloys, appearance of different types of defects in diffusion, and migration of atoms in crystal lattices are only a few examples of the effects of diffusion on the properties of metals and alloys. Under these conditions, diffusion mobility of atoms is one of the decisive factors that determines the duration of the effectiveness of the materials.

Various methods are employed for determining the diffusion coefficients in solids. In the case of ceramic oxides, diffusion takes place with the chemical reaction in which the speed of the reaction can be assumed equal to the diffusion rate of the species[6]. From this standpoint, this research is intended to investigate the diffusion behavior of U and F atoms in molybdenum (Mo) and yttria (Y_20_3). Uranium hexafluorite (UF_6) gas has been used to test yttria alone, and UF_4 for testing molybdenum and yttria in both liquid and gas phases. Due to its similarity with the problem of heat flow, the subject of atomic diffusion has been treated in many texts in conjunction with heat conduction, under the broad designation of transport phenomena. However, it should be emphasized that even in the simplest case of one-dimensional diffusion, in a three component system, the system of equations could not be rigorously solved when the diffusion coefficients were independent of composition and the Kirkendall effect, which is the displacement of markers, initially located at the interface of two interdiffusing metals, was neglected. In the opening remarks of his work on the theory of heat, Fourier indicated a basic dilemma that although the primary causes are unknown, they are subject to simple and constant laws. These laws may be discovered by observation, and the study of them is the subject of natural philosophy.

In Chapter 2, sample processing techniques and, the experimental system are described and discussed in detail. In this research, some samples are prepared using sintering, hotpressing, and metallographic techniques, while some of them are directly obtained from outside suppliers. Results of postexperiment analysis are discussed in Chapter 3. In this chapter, results of surface and bulk analyses such as scanning electron microscopy (SEM), x-ray diffraction (XRD) analysis and electron microprobe (EMP) analysis are provided. The

EMP analysis is done for Mo samples exposed to UF_4 and yttria samples exposed to UF_6 and UF_4. In addition, the calculation of the reaction rate constant (k) is explained, referring to gravimetric and metallographic analysis.

In Chapter 4, evolution of the multilayer structure with the chemical reactions, solid state diffusion of ions through the $U0_2$ layer, and formation of different phases following the solidification are explained plausibly.

The study of ceramic oxides and metals in UF_6 and UF_4 gases began in the 1960s. Detailed discussion of the mathematical modeling and the theoretical development of the mass diffusion and thermodynamics of corrosion can be found in References 8 through 28. The preliminary study of the reaction of UF_6 with metals was done by Hale, Barber, and Berhardt.[29] In their experiments, samples of nickel were exposed to static UF_6 at 1255 K for 24 hours. The results proved that intergranular corrosion occurs above 1000 K. In 1978, Florin[30] studied a variety of materials exposed to UF_6 at temperatures between 373 K-973 K. Materials tested were precious metals, common metals, ceramics, and polymers. Among them, aluminum oxide was the most resistant material up to 973 K. In 1985 Whitney, Kim, and Tucker[31] tested alumina, yttria, magnesia, and pyrophyllite $[Al_2(Si_20_5)_2(OH)_2]$ which were exposed to UF_6 at 973 K at 87 Torr for one hour. In that experiment, the fluoride compounds showed high film failure temperatures at 1233 and 1323 K for alumina and magnesia, respectively. The highest film failure temperature of fluoride was 1423 K in the yttria sample. Another UF_6 corrosion study involving $Zr0_2$ with UF_6 gas was performed by Collins.[32] In his study, Collins reported rates of reaction measured at 873, 973, and 1073 K using a discontinuous gravimetric technique. It was found that the reaction products were composed

of ZrF_4, CaF_2, $U0_3$, U_30_8, UO_2F_2, UF_4, and zirconium oxyfluorides. At 1073 K, ZrO_2 samples were completely reacted after one hour. A recent study on the UF_6 reaction with alumina (Al_20_3) was reported by Wang, Anghaie, Whitney, and Collins.[33] In their work, sapphire and polycrystal alpha alumina were tested and it was found that the maximum service temperature of alumina in a UF_6 environment was 1273 K. Chapter 6 will contain a conclusion addressing yttria and molybdenum results separately.

An original example of a multiphase, multicomponent diffusion system was investigated in this research. The microstructure and morphology of the samples after the tests were thoroughly observed. The analytical and the phenomenological modelling of the problem was given with some assumptions.

CHAPTER 2

EXPERIMENTS

In this chapter, the experimental procedure for exposure testing of yttria and molybdenum samples to the UF_6 and UF_4 gases will be explained.

2.1 Exposure of Yttria to UF_6 and UF_4 Gas

2.1.1 Sample Preparation

2.1.1.1 Sintering

Yttria powder, approximately 1 micron in size and 98% purity,[†] was used as a raw material. The yttria powder was compressed manually by dry pressing to 170 MPa pressure for 10 to 15 minutes (min). The diameter and thickness of processed disks were approximately 2.54 cm and 0.20 cm, respectively. The green yttria disks were then mounted on a mullite plate. Some yttria powder was added between the plate and the disks to prevent contamination of the sample by the mullite substrate. The sample set was then placed in an electric furnace.[††] Samples were heated gradually up to 1973 Kelvin (K) at 473 K per hour (K/h) heating rate under atmospheric pressure in air. Then, they were kept for 1 hour at 1973 K and subsequently cooled to room temperature in 25 hours[34,35,36]. The Archimedes method was used to measure the density of the samples[37,38] according to ASTM C20-80a standards. Sample densities following sintering were approximately 85% of the theoretical density. These samples were labeled Ytt85. For convenience, samples obtained through this process are called Ytt85.

2.1.1.2 Hot Pressing

Yttria powder was pressed to 170 MPa in order to form green compact disks. A high-strength graphite die having a compression strength of 117 MPa was used to prepare yttria

disks samples in the hot press†. The inner wall of the graphite die was spray coated with boron nitride in order to reduce carbon diffusion through the samples.

After the graphite die containing the green disk was placed in the hot press, the temperature was increased slowly by induction heating to about 773 K at a rate of 5-6°C/min under argon atmosphere. The samples were held at this temperature for about 1 hour. Then the temperature was raised to 1873 K, and a pressure ranging from 30 to 45 MPa was applied to a series of samples. They were kept at this pressure and temperature for up to 1.5 hours. Finally, the furnace was turned off to allow a cooling period of 8 hours, and the samples were left to cool down slowly. At the end of the hot-pressing process, it was observed that the color of all yttria samples had changed from white to black. In order to eliminate this problem, yttria disks were placed in an electric furnace and heated to 1473 K in air for 3 hours. After heat treatment, sample color changed from black to white. Three samples listed in Table 3.2 of Chapter 3 were hot pressed: the sample with 88.2% of theoretical density was prepared applying lower pressure and shorter time, while the high-density samples (98% and 99.5% of theoretical density) were processed at 40 MPa about 40 minutes. Hot-pressed and sintered samples are presented in Figure 2.1.

For convenience, samples with densities higher than 99% were labeled Ytt99. Next, a diamond saw was used to cut both high-density and low-density samples.

2.1.1.3 Density Measurements

The densities of Ytt99 and Ytt85 were measured following the Archimedes method recommended by ASTM standards.[37,38] Essentially, three measurements are necessary to obtain the density. These include

1. Saturated weight (Sat w): the weight measured after boiling the sample for two hours.
2. Suspended weight (Sus w): the weight measured in the water.
3. Dry weight (Dry w).

$$\text{Volume} = [(\text{Sat w})-(\text{Sus w})][\rho H_2O\ (T)] \quad [39] \qquad [2\text{-}1]$$

$$\text{Bulk density} = (\text{Dry w/Volume}] \qquad [2\text{-}2]$$

ρH_2O = Density of water at T(°C)

The results of density measurements for sintered and hotpressed samples are given in Chapter 3.

2.1.2 UF_6 and UF_4 Characteristics

Uranium hexafluoride (UF_6) is the only uranium compound that is stable and gaseous at relatively low temperatures.[4] It is the intermediate stage in the separation of uranium isotopes. Uranium hexafluoride is prepared exclusively by the action of elemental fluorine on uranium tetrafluoride:

$$UF_4 + F_2 \rightarrow UF_6 \qquad [2\text{-}3]$$
$$\Delta H_{298} = -59\ \text{kcal/mol}$$

A scheme explaining the use of uranium fluorides in the nuclear fuel cycle is presented in Figure 2.2.[4]

The UF_6 is a colorless, crystalline (monoclinic), and deliquescent solid at room temperature (25°C). Its density is 4.68 g/cm^3, and its melting and sublimation points are 64.6 and 56.2 °C, respectively.[39] As mentioned earlier, UF_4 is an intermediate product in the

conversion of uranium ore to UF_6. It also is used in the manufacture of $U0_2$ and uranium metal fuels.[2,3,4]

When mixed with various other metal fluorides such as LiF, NaF, and KF, UF_4 was proved to be the most suitable fuel for the molten salt reactor.[3,5] Uranium tetrafluoride (UF_4) is a green powder with a monoclinic structure. It is nonvolatile, insoluble in water, and relatively stable in air at room temperature. It has a melting point of 1309 K and a boiling point of 1715 K under one atmosphere. Its density is 6.7 g/cm^3 in the solid phase and drops to nearly 6.36 g/cm^3 in the liquid phase. This occurs between 1340 and 1630 K.[3] The choice of this fluoride over chloride is necessary for its superior physical properties: stability, volatility, and purity. The industrial production of UF_4 is carried out almost everywhere in the world, following dry processing techniques. With the use of uranium dioxide treated at 500 °C to 700 °C by both gaseous and anhydrous hydrofluoric acid, UF_4 was obtained according to the following reaction:

$$UO_2 + 4HF \rightarrow UF_4 + 2H_2O \qquad [2-4]$$

The quality of the UF_4 is very important. The eventual presence of untransformed $U0_2$ or of uranyl fluoride (UO_2F_2), resulting from an incomplete reduction of U^{6+} to U^{4+}, interferes in later stages of the reaction (fluorination to UF_6 or reduction to metal). Generally, the products are of excellent quality and contain more than 97-98% UF_4.[4] In this research, 98% purity UF_4† was used.

2.1.3 Exposure of Yttria to UF_6 Gas

The corrosion test of yttria by UF_6 gas was carried out in a flowing test unit. A schematic diagram of the unit is shown in Figure 2.3. After measurement of the weight and the surface area, samples were put in an alumina boat and inserted into an alumina reaction tube for exposure testing. The alumina tube was placed at the center of a 1500 K horizontal furnace. Two Monel cylinders, one for UF_6 supply and one used as a cold trap, were installed in the system. The test system was evacuated to vacuum of 10^{-5} Torr with the aid of a diffusion pump. Connection tubes and joints were wrapped with heating tapes and heated to about 420 K to keep UF_6 in gas phase. The furnace temperature was increased to 1173 K at a rate of 423 K/h prior to UF_6 flow.

During the experiment, two pressure transducers were used to monitor the gas flow. Typical pressures being measured were 3.76×10^4 Pa at the inlet and 3.65×10^4 Pa at the outlet of the reaction tube. At the end of the test, UF_6 flow was stopped by turning off the valve of the supply tank, and the furnace was shut down to make the system cool down naturally. A decontaminant recovery pump was connected to remove the residual gas which could exist in the monel tubes. After cooling was achieved, the alumina reaction vessel was removed and the samples were taken out. Residual weights of the exposed samples were measured using an electronic balance† upon removal from the reaction tube.

Preliminary exposure of yttria was performed at 1073 K for 90 min. No apparent reaction was observed on the surface of the sample after exposure at this temperature. However, a test conducted for 90 min at 1173 K resulted in complete decomposition to the point that no solid piece from the samples was left in the reaction vessel. Hence, it was

necessary to reduce the exposure time to a maximum of 25 min in order to observe the corrosion of yttria at 1173 K.

2.1.4 Exposure of Yttria to UF_4

2.1.4.1 Experimental System

The experimental system was composed basically of four components:

1. a stainless steel reaction chamber,
2. two optical pyrometers attached to a DCU (digital controller unit),
3. a 20 kw 450 kHz induction power supply, and
4. a diffusion pump connected to a mechanical pump (Figure 2.4).

The reaction chamber has two sapphire (Al_2O_3) windows, one for visual inspection, and the other for temperature measurement and control with optical pyrometers during the experiment. As seen in Figure 2.5, this system consists of a sensor and an indicator/DCU linked by a signal cable. The pyrometers measure the infrared radiance generated from the Mo tube. The intensity or brightness of this radiance varies with the temperature, which stimulates the detector to produce an electrical signal proportional to the radiant intensity and therefore analogous to the temperature being observed. Then, the pyrometer sends this signal to the indicator, which provides a digital display of the temperature on the front panel. The MR04 indicator has two channel operations which require the use of two different pyrometers. The measured temperature range for channel one lies between 1000 and 1755 K, and for channel 2, between 1640 and 3866 K. The temperature signals are digitized to provide data inputs for DCU. They also are linearized and scaled to the range of the instrument. The DCU monitors

accuracy and periodically initiates a series of sensor tests and calibration checks in background mode without interrupting the ongoing measurements.

An ideal infrared radiator, called a blackbody, emits the maximum amount of infrared energy possible at each given temperature. It also has an emissivity (ε) of 1.0. As can be seen from Figure 2.6, the targets, in practice, are nonblackbodies.

The formula describing the physical situation can be given as follows: $E + T + R = 1$ in which E is the emissivity, R reflectivity, and T transmission factors. The difference in emissivities between the actual and the blackbody radiation was compensated by adjusting the E factor on the indicator, since the amount of radiance at a given temperature depends on the type and also on the surface characteristics of the material. In order to obtain a true measurement of temperature, E factor must be settled to match the E factor of the material under measurement. In the present system, the emissivity slope of polished molybdenum (Mo) tube is given as 1.06; hence, the indicator was adjusted before starting the experiment. As seen in Figure 2.6, the more times reflected radiation bounces on a surface, the less reflective the target. This is due to the fact that the surface absorbs more of the radiation at each bounce, leaving less and less radiation to be reflected away from the surface. Since targets that are less reflective have higher emissivities, the rough surface and the cavity represent increasingly high emissivity values even though they are made from the same material as the polished sample. During the experiment, the constant operating temperature was achieved by switching to auto-control mode, which starts a feedback system to stabilize the temperature. The reaction chamber was surrounded by copper tubes in which water circulated in order to cool the chamber walls during the test.

Circular rings of copper-nickel alloy were used to prevent leakage along the junctions during the vacuuming period. Fittings provided necessary insulation of the power supply coils at the entrance of the chamber. The pressure of the chamber was recorded with two different gauges. The ion gauge was used to measure very low pressures under high vacuum, and the regular gauge was used to measure the argon pressure during the test. The induction power supply was a thermionic 20 KW power capacity generator which could produce a maximum potential of 460 volts, a current of 61 amperes, and a frequency of 450 KHZ. The induction furnace was used to provide the necessary thermal energy in order to melt, boil and superheat UF_4. As shown in Figure 2.7, the high alternating current of the helical copper coils created an alternating magnetic field on the crucible which in turn was heated by the resistance against the eddy currents formed on its surface. Finally, the pumping system was used sequentially in order to obtain high vacuum of the order of 10^{-6} Torr.

2.1.4.2 Temperature Measurement of the Molybdenum Crucible and the Wall

To measure the temperature differences between the inner and the outer wall of the Mo tube, a series of experiments under vacuum and under argon atmosphere were performed. The test scheme is described in Figure 2.7. For this reason the molybdenum tube was cut longitudinally and a rectangular piece was taken out. It then became possible to observe the radiance of the crucible and the tube simultaneously during the experiment. Initially, the temperature was stabilized at the maximum power (100%) for about 15 minutes. After the first recording, power level was decreased gradually (in 5 percent steps), and the corresponding temperatures were read from the pyrometer. The results are presented in Figure 2.8.

The temperature difference was observed to be 87°C in average under vacuum and 188.4°C under argon atmosphere. Although the crucible temperature did not change significantly, the outer tube temperature increased when argon gas was used close to the atmospheric pressure. These results showed that there was a significant amount of heat loss due to the radiative heat transfer under vacuum. It was found that there was a linear relationship between the crucible and tube temperature, as shown in Figure 2.9. Therefore, the test temperatures were corrected using the equation derived from the results.

2.1.4.3 Experimental Procedure

The procedure can be explained as follows: Samples of yttria (Figure 2.10), in nearly equal dimensions (about 2 cm^2 total surface area), were prepared using a diamond saw and a diamond drill. Then, 10 g UF_4 was put delicately into a Mo crucible maintained on top of a graphite pedestal as seen in Figure 2.11. In between the pedestal and crucible, a thin sheet of Mo was placed in order to prevent carbon from contaminating the crucible.

A Mo tube of 2.6 cm diameter was placed then on the top of the pedestal. A thin Mo pin crossing the tube and the pedestal at the bottom provided fixture. This system of tube, crucible, and pedestal then was placed in the reaction chamber at the center of the copper-nickel helical coils. A vacuum range of 10^{-3} Torr first was reached by using a mechanical pump which was connected to a diffusion pump. Subsequently, 10^{-5} Torr was achieved using the diffusion pump. The induction furnace was used to provide the heat necessary to melt UF_4. The copper helical coils and the reaction chamber were cooled by water circulation. In the beginning, a relatively low power rate (20-25%) was used to heat the system to a level such that undesirable residues such as humidity, grease, and oils could be eliminated by

evaporation. Then the diffusion pump was disconnected from the system, the reaction chamber was filled with argon until about 600 Torr pressure was reached, and the power was raised to reach the operation temperature. Argon was used for three reasons: (a) to suppress early vaporization of UF_4 due to the drop of its boiling point under high vacuum, (b) to prevent electrons sparking between poles, and (c) to produce a back pressure against outside pressure, hence preventing possible air leakage. In this case, since the boiling point of UF_4 was 1715 K at one atmosphere (atm), the testing temperature was held at 1650 K and 1740 K at about 0.8 arm pressure for two different sets of experiments.

As a first step, the argon pressure was measured with equal time intervals at the operating temperature without the presence of UF_4 and the sample. As a second step, UF_4 was placed in the reaction chamber, and the pressure of argon and vaporizing pressure of UF_4 was recorded. This pressure was established as the reference pressure. The third step was to record the inner pressure, which consisted basically of the partial pressures of argon, UF_4, and gases during the reaction. The difference between reference and reaction pressures provided the partial pressure of the reaction gases. The test sample was squeezed between two parallel thin sheets of Mo that were attached to a moveable handlebar. The sheets were doubly wrapped at the side of the sample in order to keep the sample firmly in place without damage (Figure 2.12) This method of adjustment pictured in Figure 2.12 facilitated the removal of the tested sample and the insertion of the new one for the following test. During the experiment, after the initial vacuum (10^{-5} Torr) was reached, temperature was increased in two steps. In the first step, a certain time was allowed (about 1/2 hour) for UF_4 to melt at about 300°C over its melting point. During this soak period, due to the gas expansion, the inner chamber pressure

was increased. The second step was to raise the temperature above the boiling point of UF_4. After the testing temperature was reached, the inner pressure was adjusted to equal the initial reference pressure. Then the yttria sample, which was initially held far above the surface of the UF_4, was placed 0.312 inches above the boiling liquid where the vaporizing UF_4 was flaring its surface. At the end of the exposure, the sample was pulled back and the output power was turned off. In order for the sample to receive the same amount of gas flux, it was important that the same distance over the boiling liquid be maintained in each experiment. However, since UF_4 reacted with the sample or was condensed on the Mo wall, there were losses which increased the actual distance between the sample and the liquid after each experiment. At the end of the test, it was observed that the UF_4 level was below the maximum heating zone. This zone was identified as the shiny white zone on the Mo tube located at the center of the helical heating coils (Figure 2.13). Reacting UF_4 with yttria showed more experimental accuracy and data control than UF_6 exposure. This was due to the compactness of the testing system and the easy manipulation of the sample before and after testing. At the end of the test, it was observed that the bottom portion of the sample was ellipsoidal in shape, while the upper portion more or less retained its original form (Figure 2.14). It was concluded that this was due primarily to the surface tension and gravitational forces acting on the sample. Another reason could have been that the bottom portion received more UF_4 vapor flux than the sides. In order to eliminate this situation, smaller samples were prepared. They were attached to a Mo wire hanging over the liquid during the experiment. At the end of a series of tests, it was again observed that the samples formed a product layer of ellipsoidal shape in the form of a droplet. This proved our initial assumption.

In order to expose the sample to liquid or gaseous UF_4, the handlebar of the chamber could move vertically along the tube without affecting the vacuum during the experiment. Both the chamber and its cover were made of stainless steel, and copper-nickel circular seals were used to join them.

During the experiment, UF_4 vapors were condensed on the walls of the molybdenum tube. Liquid droplets descended to the bottom due to gravity and vaporized again, providing a continuous circulation. Because of the immediate condensation on the walls, very small amounts of uranium tetrafluoride contaminated the chamber walls outside of the Mo tube. The sample weights were measured before and after both liquid and gas phase testing, using a digital microbalance.

2.2 Exposure of Molybdenum to UF_4

Thermodynamical data of the chemical reactions between UF_4 and different materials were obtained using a computer code for analysis of chemical thermodynamics, FACT.[40] According to the computational analysis, Mo showed good compatibility under the operating conditions; in addition, due to its high melting point (2610 K) and low neutron absorption cross section (0.20 barn), Mo was thought to be one of the candidate materials for space power and propulsion applications.

During the first set of experiments, the operational temperatures in the crucible were held at 1390 and 1480 K over the melting point of UF_4 (1109 K). In the second set, it was held at 1740, 1825, and 1910 K over its boiling point (1715 K). The corresponding tube temperatures were 1500, 1600 K for liquid phase and 1900, 2000, 2100 K for gaseous phase, respectively. The melting of UF_4 was accomplished in about 1/2 hour at 1480 K. While UF_4

was melting, it shrank significantly; hence, reloading the crucible two or three times was necessary in order to completely fill it with UF_4.

The Mo sample was then attached similarly between the Mo sheets, which in turn was fixed to the end of the moveable handlebar. Following the initial pressure recording, the sample was slowly immersed into liquid UF_4. Sparking and short-circuit can happen if the sample comes in close contact with the wall of the Mo container or if there is not enough inert gas pressure in the chamber. During the exposure at this temperature, the increase in the chamber pressure was recorded with equal time intervals from the transducer. The test procedure was basically the same as the yttria case.

CHAPTER 3

POSTTEST ANALYSIS AND RESULTS

Characterization of the reaction layers was performed using analytical instrumentation techniques such as scanning electron microscopy (SEM), electron microprobe (EMP) analysis, and x-rays diffraction (XRD) analysis, and the results were evaluated phenomenologically.

3.1 Sample Preparation

3.1.1 For SEM and EMP Analysis

After the experiments, prior to the surface preparation, yttria and Mo samples were mounted in cylindrical shaped molds nearly 1 inch in diameter. Two different types of mounting material were used: for Mo samples, 2 parts of powder epoxy resin was mixed with 1 part of acrylic plastic liquid ingredient obtained from Fisher, Inc.† The mixture was mixed about 2 minutes until the solution became homogeneous and viscous enough to fill the edges of the sample. Exothermic reactions occur at this stage, and heat evolution accompanies the solidification.

Yttria samples, due to their fragile reaction product layers, required more care than the Mo samples. Relatively lower viscosity epoxy resin was used to mount the samples. From Fisher, Inc., low-viscosity 5cc methyl methacrylate (CH_2:$C(CH_3)COOCH_3$) was mixed with 9 mg 2,2-Azobis [2-methylpropionitrile] ($(CH_3)_2C(CN)N$:$NC(CN)$ $(CH_3)_2$). The sample was placed in a glass container and then the epoxy was poured into it. Next, containers were held in the electrical furnace at 65°C for about 7-8 hours.

In order to observe and analyze the microstructure, reacted samples must be sectioned, ground, and polished to make the surface flat and clean. Grinding was performed using 60,

120, 240, 320, 400, and 600 grades abrasive paper in sequence. Then, with vibrators, polishing was accomplished down to 1 micron using diamond powder. Prior to the SEM analysis, ceramic samples were carbon coated in order to make them conductive.

3.1.2 For XRD Analysis

X-rays diffraction analysis used a powder diffraction technique in which the samples were ground under 30 μ size. Characteristic X-rays generated from a copper target (Cu K) were collimated onto the powder, where they were diffracted at specific angles from the crystal planes of the samples. Computer analysis provided the diffraction angles, corresponding interplane spacings and relative intensities, and a list of possible compounds. For this reason, yttria samples were ground into powder after the exposure and then were stuck on a piece of slit with the aid of amyl acetate.

3.2 Characterization of the Reaction Layers After UF_6 Testing

3.2.1. Weight Change Analysis

Table 3.1 shows the results of weight change analysis of yttria samples after being exposed to UF_6 at 1173 K. Table 3.2 gives the hot press results for different temperature, pressure, and time conditions. The weight change of the samples was measured before and after the test using a digital micro-balance with an accuracy of 5 decimal points. In general, a weight increase was observed for both ytt85 and ytt99 samples for different testing times at 1173 K.

Table 3.1 UF_6 Reacting with Yttria at 1173 K

DENSITY %	TEST TIME (Min)	WEIGHT BEFORE (g)	WEIGHT AFTER (g)	W. CHANGE (g/cm^2)
85	5	0.3023	0.3794	0.0194
85	10	0.4694	0.5020	0.0181
85	15	0.2470	0.2700	0.0228
85	20	0.2184	0.2823	0.0600
85	25	0.2654	0.3494	0.0690
99	20	0.3487	0.5146	0.1120
99	25	0.5235	0.7709	0.1250

Table 3.2 Hot Press Results of Yttria Samples

TEMPERATURE C	PRESSURE MPa	TIME Min	THEO. DENSITY %
1700	30	10	88.30
1600	45	40	98.14
1600	40	90	99.45

The dissociation of UF_6 to F_2 and other lower compounds such as UF_4 over 1000 K and 760 Torr conditions[1] suggested that the extensive corrosion was due to the reaction of multitype gas molecules rather than a single specie UF_6. The results of the weight change analysis (Figure 3.1) were used in the parabolic rate law formula derived for oxidation in order to obtain an approximate value of the rate constant of the yttria reaction with UF_6. Parabolic rate law formula is given as follows:

$$(\Delta w^*)^2 = kT \qquad [3-1]$$

where ΔW^*, $= \Delta W/(W_i/A)$, ΔW^*, = Dimensionless quantity

and ΔW = Weight change/A, Wi = Initial weight (g),

A = Surface area (cm^2), t = time (min)

From the slope of the line in Figure 3.1, rate constant K was found to be 0.00562 (min^{-1}). The sharp weight increase at 20 and 25 min and the complete decomposition of the sample for testing times greater than 1 hour showed that the film failure temperature of yttria was below 1423 K which is reported in a previous work.[31] This might be due to the higher UF_6 pressures and to the flowing UF_6 rather than stagnant low pressure UF_6 (87 Torr) which was used in the past experiments.[31] In addition, nearly 15% porosity might have some effect in the accelerated failure of the samples. For exposure less than 15 min, samples maintained their shape, and a relatively thin black product layer formed on the surface. After 20 and 25 min exposures, samples were almost decomposed following cracking and spallation (Figure 3.2). The sharp weight increase was probably due to the initiation of the cracks allowing the gas insert and react further with the sample.

3.2.2. SEM-EMP Analysis

At the end of the SEM analysis, it was observed that a soft, porous scale was formed followed by an inner layer (Figure 3.3). The EMP analysis was completed after scanning the sample for a total of 100 micrometers, with 20 equal steps. The measured elemental concentration profiles are plotted with reference to their micrographs as shown in Figures 3.4, 3.5, and 3.6.

The elemental analysis by EMP established the formation of two layers of reaction products with different chemical constituents. As shown in Figures 3.4 to 3.6, the outer layer consisted of yttrium, fluorine, and uranium atoms, whereas the inner contained yttrium and fluorine atoms. The thickness of the inner layer was determined between the end points of uranium concentration at the outer interface (the interface of the inner and outer layers) and

the fluorine concentration at the inner interface (the interface of substrate and the inner layer). It was found that the thickness of the inner layer decreased from about 90 to 55 micrometers as exposure time increased from 5 to 20 minutes (Figures 3.4 to 3.6).

3.2.3 XRD Analysis

X-ray analysis identified YF_3, $U0_2$, a small amount of U_30_8, and Y_20_3 as the reaction products. Similar XRD results were obtained for different exposure times. In Figure 3.7, and Table 3.3, the diffraction pattern for a 15 min exposure is given as an example. The standard patterns of the identified components (Y_20_3, YF_3, $U0_2$, and U_30_8) taken from JCPDS reference cards are also provided in Figure 3.7 and Table 3.3 for comparison with the sample pattern. The intensities between the experimental and the standard patterns were not exactly matched due to the overlapping of different compounds.

Table 3.3 X-Ray Diffraction Powder Pattern of the Yttria Sample After UF_6 Reaction

EXPER. 2Ø	I/I_0 %	YF_3 2Ø	I/I_0	UO_2 2Ø	I/I_0	U_3O7 2Ø	I/I_0
21.555	70.88	24.627	75	28.245	100	28.401	100
21.765	56.12	25.987	75	32.717	48	32.865	30
24.602	31.76	27.885	100	46.943	49	33.204	20
25.652	64.11	30.961	95	55.697	47	47.150	20
25.997	100.00	43.917	80	58.397	13	47.359	25
29.155	64.11	45.619	85	68.539	9	55.844	20
33.247	2.75	46.995	100	75.727	18	56.479	15
33.725	54.08	47.569	95	78.077	15	58.888	15
34.000	86.04	49.043	100	87.297	13	68.653	5
43.505	23.81	49.498	70	94.146	15	69.642	5
43.900	43.99	51.421	70	105.61	6	75.870	10
45.437	45.83	52.310	70	112.95	15	76.372	10
50.787	52.08	53.409	60	115.46	8	78.077	10
51.595	57.16	54.990	70	125.87	9	79.079	10
57.567	42.63	57.899	35	134.92	7		

3.2.4 Thermodynamic Analysis

The prediction of possible chemical reactions and endproducts at certain combinations of temperature and pressure was performed by the Facility for the Analysis of Chemical Thermodynamics (FACT)[40] computer data base and code package. In particular, the equilibrium program (EQUILIBR) was used to analyze the reactions of UF_6, UF_4, and F_2 with yttria at 1173 K and 278 Torr (0.365 atm) average pressure. This program determines the molar concentrations of product species when specified elements or compounds react to reach chemical equilibrium. The calculation of the equilibrium concentration is based on the minimization of the total free energy formation in the system. The EQUILIB program is designed to solve chemical equations for up to twenty reactants with a maximum of 12 elements. The reactants, reaction temperature, and total pressure (or volume) need be entered only as input data. The code automatically generates a list of all possible stoichiometric compounds found in the program data base as well as in the user's private input data. All possible compounds with a concentration larger than 10^{-5} mole are considered in the equilibrium calculation. The program then predicts the combination of reaction products which is most stable at the specified temperature and pressure. At 1173 K and 0.365 atm. pressures, FACT analysis showed that UF_6 was favored to react with Y_20_3 at the given conditions to form YF_3, U_30_8, $U0_2$ in solid phase and 0_2 in gas phase. Similarly, UF_4 reacting with yttria forms YF_3, $U0_2$, Y_20_3 in solid phase, and F_2 reaction with yttria releases YF_3, Y_20_3 in solid phase and 0_2 in gas phase. Results are presented in Table 3.4.

Table 3.4 Thermodynamic Results of UF_6 Reaction with Y_20_3 at 1173 K and 0.365 atm Pressure

REACTANTS MOLE	PRODUCTS	STATE	CONCENTRATION MOLE
UF_4 (1) Y_2O_3 (1)	UO_2 YF_3 Y_2O_3	Solid Liquid Solid	1. 1.3333 0.3333
F_2 (1) Y_2O_3 (1)	YF_3 O_2 Y_2O_3	Liguid Gas Solid	0.66667 0.99986 0.66667
UF_6 (1) Y_2O_3 (1)	O_2 YF_3 U_3O_8.	Gas Solid Solid	1. 2. 0.33333

According to the X-ray and thermodynamic results, the chemical reactions occurring are as follows:

at the inner-outer interface,

$$3UF_6(g) + 3Y_2O_3 \rightarrow 6YF_{3(s)} + U_3O_{8(s)} + 0.5\ O_2(g) \qquad [3-2]$$

$$3UF_4(g) + 2Y_2O_3 \rightarrow 3UO_{2(s)} + 4YF_{3(s)}, \qquad [3-3]$$

also, a possible reaction according to literature[32,41]

$$F_2 + O_2 + 4UO_{2(s)} \rightarrow UO_2F_{2(s)} + U_3O_{8(s)}, \qquad [3-4]$$

and at the inner layer-substrate interface,

$$3F_{2(g)} + Y_2O_3 \rightarrow 2YF_{3(s)} + \frac{3}{2}\ O_2(g)\ . \qquad [3-5]$$

3.3 Characterization of the Reaction Layers After UF_4 Test

The Y_20_3 sample (85%) which was exposed to the liquid UF_4 at 1220 K showed O.167(g/cm^2) weight change in 1 minute. This value is much higher than the data obtained from the exposure of gaseous UF_6. Also, a small piece of yttria crystal which was 100% close to theoretical density was tested in liquid UF_4 at 1480 K. It was observed that the sample reacted completely, after 5 min.

In the gas phase of UF_4, two set of experiments, one at 1650 K and the other at 1740 K at nearly 84.6 KPa (635 Torr, 0.835 atm), were performed from 5 to 40 min.

3.3.1 Weight Change Analysis

The results of these experiments are given in Figure 3.8. In both cases, the weight change by time showed an increase in 5, 10, and 15 minutes, while it decreased for longer times. Eventually, samples were lost completely. The samples used at operating temperatures 1650 and 1740 K were originally different in size. Hence, a small difference in weight gain was found between the two experiments. However, Figure 3.8 reveals the similar trend of the weight gain for both temperatures. The argon pressure during the experiments is given in Figure 3.9. It was observed that no significant rise in pressure was recorded due to the chemical reactions during the experiments. The pressure increased due to the expansion of the argon gas while the temperature was rising. The curves which had nearly equal initial pressures were almost overlapped as expected.

3.3.2. SEM Analysis

In general, the formation of three consecutive layers has been observed with SEM[††]: a) outer layer b) center layer, and c) inner layer. Below, Figure 3.10 shows the polished

cross section of the yttria sample at 50 times magnification exposed to gaseous UF_4 at 1740 K for 40 min.

A primary dendritic phase formation, a secondary phase surrounding the primary phase, and a eutectic phase were observed in the outer layer. Figure 3.11 taken in backscattering mode shows that the center layer and the primary dendrites have the same degree of contrast, whereas the eutectic phase is barely distinguishable. A picture taken at 650 magnification on the broken cross section shows the granular structure of the center layer (Figure 3.12-a). The finely dispersed eutectic phase and secondary dendrites are clearly visible in Figure 3.12-b taken at 500 mag.

3.3.3 Optical Microscope Analysis

Observations made using a Zeiss optical microscope showed that the reaction layers grew thicker as the exposure time increased. Figure 3.13 shows a four consecutive sample exposed for 10, 15, 20, and 30 min at 1650 K. Figure 3.14 shows a scheme of the moving reaction boundaries. The distances were measured using a micrometer connected to the optical microscope. It was observed that for most of the samples the reaction boundaries moved outward and the sample increased in volume. From the scheme, the approximate interface velocities were found to be 0.6μ/min for UO_2-Liquid interface and 100μ/min for the Liquid-Vapor interface. The growth rate measurements are given in Figure 3.15a-b. The inner layer grows faster than the center layer at both temperatures.

At 1650 K (or 1800 K, which is measured tube temperature), the center layer growth is parabolic, which explains that the growth is diffusion controlled. The almost exponential growth of the inner layer is due to the easy exchange of oxygen and fluorine ions in the

lattice during the diffusion; then the inner layer forms and grows with further diffusion and reaction of fluorine with the yttria matrix. The rate constant k of the inner layer is found to be about 10 times larger than the center layer at 1740 K.

$$K_{inner} = 6.45x10^{-4} \frac{cm}{sec} \text{ and } K_{center} = 8x10^{-5} \frac{cm}{sec}$$

3.3.4 EMP Analysis

EMP analysis† was performed on the reaction layers after samples were polished down to 1μ size. The result of a scan across the outer, center, and inner layers of a sample exposed to UF_4 at 1740 K for 20 min is presented in Figure 3.16. The spikes seen were due to the presence of mixed phases in the outer layer and also partly due to the porous nature of the sample. It was found that the eutectic phase was composed of a mixture of dark and gray plate-like layers. The composition of dark regions were $Y_{11}U_{7.8}F_{80}$ or nearly $YU_{1-x}F_8$, and gray regions were composed of $YU_{3.5}F_{12}$ or nearly YUF_7.[3,41] The peritectic region surrounding the secondary dendrites was formed by gray layer with identical composition (YUF_7). The dendrites and the center layer were hypostoichiometric UO_2 where O/U = 1.922. Finally the composition of the inner layer was found to be $Y_{.34}O_{.33}F_{.33}$ or YOF. Some uranium diffusion through a crack across the inner layer is seen close to the upper edge of Figure 3.16. This suggests that UF_4 gas was inserted through the existing crack in the beginning of the reaction.

3.3.5 XRD Analysis

Similarly, X-rays diffraction analysis†† was performed to the yttria samples after the reaction with UF_4. For the sample tested in UF_4 at 1740 K for 15 min, XRD patterns

showed the presence of YOF, Y_20_3, UO_{s2}. For the sample tested at 1740 K for 40 min, the results were YOF, Y_20_3, $U0_2$. The x-ray powder patterns are provided in Figure 3.17, Table 3.5.

3.3.6 Thermodynamic Analysis

FACT analysis showed the presence of YF_3 and $U0_2$ at 1740 K and 0.004 atm pressure. Since the presence of YF_3 (yttrium fluoride) does not match with x-ray results (YOF was detected in this case), data sources in this program are questionable. Thermodynamic results of the Y_2O_3 reaction with UF_4 gas are provided in Table 3.6.

Table 3.5 X-Ray Diffraction Powder Pattern of the Yttria Sample after UF_4 Reaction

EXPER. 2Ø	I/I_0 %	YOF_3 2Ø	I/I_0	UO_2 2Ø	I/I_0	U_3O_7 2Ø	I/I_0
28.280	87.31	28.776	100	28.245	100	28.401	100
28.797	81.62	33.280	50	32.717	48	32.865	30
29.205	100.00	47.969	100	46.943	49	33.204	20
32.757	18.48	56.860	90	55.697	47	47.150	20
33.227	22.42	59.642	30	58.397	13	47.359	25
33.827	30.06	69.820	50	68.539	9	55.844	20
43.275	26.10	77.400	65	75.727	18	56.479	15
43.485	28.38	79.870	45	78.077	15	58.888	15
46.977	58.25	89.103	75	87.297	13	68.653	5
47.425	50.45	96.313	65	94.146	15	69.642	5
47.922	57.31	108.69	45	105.61	6	75.870	10
48.575	63.11	116.06	80	112.95	15	76.372	10
55.695	39.60	118.78	45	115.46	8	78.077	10
57.615	45.28	130.27	75	125.87	9	79.079	10
69.682	17.95	140.48	60	134.92	7		

Table 3.6 Thermodynamic Results of UF_4 Reaction with Y_2O_3 at 1740 K at 0.004 atm Pressure

REACTANTS MOLE	PRODUCTS	STATE	CONCENTRATION MOLE
Y_2O_3 (1)	YF3 Y_2O_3	Liquid Solid	1.3333 0.33333
UF_4 (1)	UO_2	Solid	1.

3.4 Analysis Results of Molybdenum Exposed to UF_4

According to FACT analysis,[40] Mo showed good thermodynamical compatibility with both liquid and gaseous UF_4 at a temperature range of 1000-2300 K. A set of experiments with pure Mo exposed to gas and liquid UF_4 was performed for different time exposures in order to investigate whether any diffusion or dissolution occurred after the reaction. The experiment settings were exactly the same as in the yttria case.

3.4.1 Weight Change Analysis

The weight change of these experiments was given in Table 3.7. In the gravimetric analysis of Mo samples at 1480 K in liquid UF_4, an insignificant amount of weight change was observed after the exposure testing. The experiment was repeated for 45 min exposure in order to check the reproducibility of the results. Then, the samples were annealed at 1500 K for 1 hour under argon atmosphere at 600 Torr pressure. The weights of the annealed samples were found to be the same as the original samples (Table 3.7).

Table 3.7 Weight Change Results of Mo Tested in Liquid UF_4

TIME Min	W_i g	W_a g	W_{an} g	Size cm^2	Vacuum Torr	Argon Torr	W_a-W_i/s g/cm^2
15	.22778	.23384	.22743	.924	$2x10^{-5}$	720	.00656
30	.24336	.26309	.24337	.979	$2x10^{-5}$	734	.02015
45	.22520	.22929		.905	$2x10^{-5}$	730	.00451
45	.21688	.22450	.21680	.897	$2x10^{-5}$	742	.00849
60	.21318	.21992	.21276	.88	$2x10^{-5}$	776	.00766
75	19955	.20830	.19953	.803	$1x10^{-5}$	767	.01089

This fact proved that, at 1480 K, for short exposure times such as 15 to 75 min, no reaction of U, F, or UF_4 occurred through the Mo sample. The weight analysis after testing at 1800 K, 2000 K, and 2200 K with gaseous UF_4 showed much less deposition on the samples with respect to the liquid phase tests; in the vapor phase the deposition rate seemed to decrease by time (Figure 3.18).

3.4.2 SEM Analysis

During SEM analysis, it was observed that the grain size varied throughout the crosssection and the grain growth occurred in samples exposed at 1480 K (Figure 3.19 a-b). The flow lines in the as-received sample disappeared after the test, and the grains recrystallized upon heating, having an average size of nearly 20 μm. At the end of the exposures at 2000 and 2200 K, it was found that there was some particle deposition on the surface of the samples (Figure 3.20 a-b). These particles were identified as being as U, F, 0 with Energy Dispersive Spectroscopy† (EDS).

3.4.3 EMP Analysis

After the exposure testings, samples were cut by a diamond saw and prepared for post-test analysis. After being mounted in epoxy resin, they were ground and polished as previously done for the yttria case. During sample preparation, distilled water was used and samples were polished separately in order to prevent any contamination effects. The EMP was done across the cross section from one edge to the other with equal scanning steps. The result was that the U and F concentrations were very low and discontinuous. Results in both line scanning and spot scanning cases were almost the same, and no significant diffusion of U or F was found on the cross sections (Figure 3.21).

For each time interval at 1480 K, the uranium K ratio stayed within the limits of 0.0025/1 and fluorine K ratio was within 0.001/1. These limits were in the statistical fluctuation range

of the instrument being used. In addition, in order to see the long term effect of the liquid and gaseous UF_4 to the Mo, two small pieces of the Mo crucible, one from the upper side, the other from the bottom side, were cut after many experiments were performed using the same crucible. The EMP analysis was performed along the crosssections of these samples; no significant U and F atoms were detected for an average testing temperature of 1730 K and an average testing time of 9 hours. The results of the long exposure test were given in Table 3.8.

Table 3.8 Atomic Concentration of U and F in Mo Sample Exposed to UF_4 for 9 Hours at 1730 K

	UPPER CRUCIBLE			BOTTOM CRUCIBLE		
POINTS	MICRONS	U-M	F-K	MICRONS	U-M	F-K
1	0.0	0.00	0.00	0.0	0.00	0.00
2	94.4	0.00	0.00	83.6	0.00	1.58
3	188.9	0.03	0.61	167.1	0.00	0.00
4	283.3	0.02	1.98	250.6	0.04	0.00
5	377.8	0.00	0.87	334.2	0.00	0.36
6	472.2	0.00	0.51	417.7	0.00	0.77
7	566.6	0.04	0.00	501.3	0.02	0.00
8	661.1	0.00	0.10	584.9	0.02	0.47
9	755.5	0.00	0.00	668.4	0.02	0.05
10	850.0	0.00	0.00	752.0	0.14	0.00

CHAPTER 4

THE EVOLUTION OF THE REACTIONS AND SOLIDIFICATION

In this chapter, the mechanism of the chemical reactions at the interfaces, the solid state diffusion mechanism of the ions, and the formation of various phases following the solidification are explained using a phenomenological approach.

4.1 Reactions and Diffusion of the Components

When UF_4 first came in contact with the yttria wall, it reacted with yttria and exchange reaction occurred between oxygen and fluorine. At the early stages of the reaction (approximately the first 10 minutes), a solid wall of UO_2 (experimental ratio of O/U is 1.922) was formed on the surface of the sample while YF_3 was released in gas phase as a second reaction product at the operating temperature, which was 1380 and 1468°C. The reactions [4-1] and [4-2] explain the formation of the center layer and are in good agreement with both theoretical and experimental results.

$$2Y_2O_{3\ (s)} + UF_{4\ (g)} \rightarrow 4YF_{3\ (g)} + 3UO_{2\ (s)} \qquad [4-1]$$

$$YF_{3(g)} + Y_2O_3 \rightarrow 3YOF_{\ (s)} \quad (Y_{1+x}OF_{2+y}) \qquad [4-2]$$

Then, the gaseous YF_3 advanced through interconnected porosity and reacted rapidly with yttria matrix according to the reactions given above; hence, the inner layer formed as a different phase following the reactions (Figure 4.7). Since we observed experimentally the presence of both yttrium and oxygen atoms in the outer layer after the formation of the UO_2 wall, it was concluded that these elements diffused through the center layer during the reaction at temperatures about 1460 °C. During the reactions, it is also assumed that no oxygen remained in the chamber after high vacuum was achieved. The diffusion of those elements was mainly due to the higher chemical potential of the substrate with respect to the layers. At the

operating temperature ranges, UO_2 can behave intrinsically where the point defects, primarily vacancies, could appear by thermal effects. The defect reactions can be presented as follows:

$$\begin{aligned} UO_2 &\rightarrow Null \rightarrow V_u'''' + 2\,V_o^{\cdot\cdot} \\ O_o &\rightarrow O_i'' + V_o^{\cdot\cdot} \\ U_u &\rightarrow U_i^{\cdot\cdot\cdot\cdot} + V_u'''' \end{aligned} \qquad [4\text{-}3]$$

in which 0_o and U_u stand for one oxygen atom placed in oxygen site and uranium atom locating in uranium site, and O_i" is the oxygen interstitial carrying two negative charges and $V_o^{\cdot\cdot}$ is the oxygen vacancy carrying two positive charges. Similarly, $Ui^{\cdot\cdot\cdot\cdot}$ stands for a uranium interstitial carrying four positive charges and Vu'''' a uranium vacancy with 4 negative charges. Experiments showed that the $U0_2$ wall was found to be almost stoichiometric (O/U = 1.922).

Knowledge of the atomic structure of the nonstoichiometric phases is important in interpreting the thermodynamic behavior of the material and the dependence of transport properties, such as electrical conductivity and diffusivity, upon the O/M ratio. According to the literature,[41] among the 40 different oxides, more than one oxide phase might be in equilibrium at room temperatures such as $U0_2$ with alpha U_40_9 between 2-2.23 range and gamma $U0_3$ in equilibrium with alpha U_30_{8+x} over 2.6 of U/O ratio. In addition, each oxide phase might be present with various crystalline modifications. It is significant that the lattices of most phases may be derived with only minor modifications from a few basic structures. Thus, the fluoride lattice of the most stable oxide of tetravalent uranium, $U0_2$, offers the opportunity for the formation of many discrete oxides by the acceptance of various amounts and by different positioning of the oxygen atoms at interstitial sites and/or slight lattice distortions. Such properties are critically dependent upon the positions of the excess oxygen atoms in the crystal structure. Stoichiometric $U0_2$ crystallizes in the fluoride structure, which is shown in Figure 4.1. Deviations of uranium from exact stoichiometry are permissible since

it has many valence states in which U^{4+}, U^{5+}, and U^{6+} states tend to be the most stable. The different phase regions with respect to O/U ratio and temperature are presented in Figure 4.2. When the oxygen atoms are removed (vacancies) or added (interstitials) to the lattice of the stoichiometric UO_2, in order to hold the electrical neutrality, U^{4+} ions are converted to U^{+5} or U^{+6} in hyperstoichiometric UO_{2+x} or they are converted to U^{2+} in hypostoichiometric UO_{2-x} crystal. The largest open spaces in this lattice are the centers of the cubes formed by the eight oxygen ions in the simple cubic sublattice. In UO_2, half of these cubes are occupied by uranium ions, but the other half are empty. Figure 4.3 shows the empty cube formed by eight normal oxygen ions with the locations of the two types of interstitials sites for oxygen: type 1 and type 2. The type 1 sites lie along each of the six diagonals in [110] directions half way between the cube center and the midpoints of the cube edges. There are 12 type 1 sites in each empty oxygen cube. Since there are four such cubes in the fluoride unit cell, the unit cell contains 48 type 1 oxygen interstitial sites, or 12 for each uranium ion in the lattice. The Type 2 interstitials sites are located midway from the cube center to the cube corners in [111] directions. There are 16 type 2 sites in each UO_2 unit cell, or 4 per uranium ion. In total, 64 sites are available for excess oxygen to diffuse through the UO_2 unit cell. For small values of x, an occasional unit cell of the fluoride lattice is presented in Figure 4.4. The defect complex consists of two type 1 oxygen interstitials, two type 2 oxygen interstitials, two vacant oxygen sites, and four U^{5+} ions on nearby normal cation sites. To maintain charge neutrality, four U^{4+} ions nearest to the type 1 oxygen ions are converted to U^{5+} ions. Because of the coulombic repulsion the two oxygen ions nearest to the pair of the extra oxygen ions relax outward along the possible [111] direction, leaving their anion sites vacant.[42] The mechanism of this substitution can be described as follows:

$$2UO_2 + O^{--} \rightarrow 2U_u^{\wedge} + 4O_o + O_i'' \qquad [4-4]$$

This equation describes the two uranium ions in stoichiometric UO_2 which were converted from +4 to +5 valence state by forming a hole in its uranium site, thus preserving the charge neutrality. Also the mass balance on both sides of the equation was preserved. Equation [4-4] provides an explanation for oxygen ions to diffuse from the oxygen rich yttria site through the UO_2 center layer into the outer layer via migration of oxygen interstitials. As mentioned earlier yttrium ionic diffusion must occur to some extent through solid UO_2 wall. This can be explained by the following reaction:

$$\{2Y^{+3}, 3^{O-2}\} + V_U^{+4} + 2V_O^{-2} \text{ -in } UO_2 \rightarrow Y_u' + 2O_o + O_i' \qquad [4-5]$$

For the oxygen ions coming from yttria, two of them are located in the vacant oxygen site of the UO_2 empty cell, while the other ion occupies an interstitial site carrying -2 negative charge. In this way, both charge balance and atomic balance were held in the equation. Again, due to the chemical potential, the diffusion of oxygen and yttrium species might occur via migration of interstitials through vacancies at high temperatures from high concentration to the low concentration side.

When those species come in contact with UF_4 molecules, the probable reaction which forms the liquid can be expressed as follows:

$$\{y_i^{\wedge\wedge\wedge}, O_i''\} + UF_{4(g)} \rightarrow UO_{2(s)} + \{Y^{+3}, U^{+4}, F^-, O^{--}\}_{(L)} + \{F^-\}_{(Diff)} \qquad [4-6]$$

According to the reaction [4-1], UO_2 must form in the outer interface of the center layer, thus contributing to the increase in thickness of the center layer. The curvature of the outer interface is probably due to the divergence of the diffusing fluxes of yttrium and oxygen ions (Figure 4.5). Fluorine and some uranium diffusion must also occur simultaneously through the

center layer, since the inner layer grows with time. Its mechanism can be explained similarly by the following reaction:

$$2V_u^{+4} + 4V_o^{-2} + \{U^{+4}, 4F^-\}\text{--in } UO_2 \rightarrow U_u + V_u'''' + 4F_o^{\cdot} \qquad [4\text{-}7]$$

In this case, the diffusion of fluorine and uranium ions proceeds via a vacancy mechanism at high temperatures. The rate of the diffusion also depends on the thickness of the UO_2 wall. This can be seen easily in Figure 4.5, in which the inner (dark) layer is thicker at places, where the wall is thinner. As mentioned earlier, cation diffusion (U^{+4}) is slower than anion diffusion. Uranium diffusion via a vacancy mechanism was investigated by Lidiard.[43] He assumed that the uranium diffused by means of uranium vacancies in UO_{2+x} and interstitial cations U^{4+}. Figure 4.6 shows the experimental diffusivities of uranium and oxygen.[44] This prediction was confirmed by the results of Matzke.[44-46] In his experiments, Matzke tested UO_2 with impurities Nb_2O_5, La_2O_3, and Y_2O_3. The uranium diffusion coefficient increased in the material containing Nb_2O_5 and decreased in the presence of La_2O_3 or Y_2O_3. Since additions of Nb_2O_3 lead to an excess oxygen content in UO_2, and La_2O_3 or Y_2O_3 reduce the oxygen content ($U_{1-x}Nb_xO_{2+x/2}$ and $U_{1-x}La_xO_{2-x/2}$), this indicates that the diffusion of uranium is accelerated in material containing an excess of oxygen. The best estimate which is in agreement with most of the experimental data is found to be for 1500°C:

$$\log D = -10.85 + 1.5 \log x.$$

The most reliable data relating to the activation energy of volume diffusion of uranium is found to be 70 kcal/mol for UO_2 to 105 kcal/mol for $UO_{2.1}$.[48] Substitutional effects between YOF and Y_2O_3 molecules are also possible due to the high temperature and volumetric changes in small amounts which can cause vacancy formation.

$$2V_u^{+4} + 4V_o^{-2} + YOF \xrightarrow{in} Y_2O_3 \rightarrow Y_y + O_o + F_o^{\cdot} + V_o^{\cdot\cdot} + V_y^{'''} \qquad [4\text{-}8]$$

Substitution

The yttrium and oxygen vacancies become the sinks for a backward ionic oxygen and yttrium migration in the system. Figure 4.7 shows a scheme of the ionic diffusion through $U0_2$ wall. As mentioned before, at the later stage of the reaction, a liquid phase starts to appear on the outer face of the uranium oxide layer. This liquid phase is basically a eutectic mixture of U, F, O, Y which constitutes a 4-component phase system in which oxygen and yttrium ions cross the $U0_2$ wall during the reaction. During the second stage of the reaction, F ions diffuse through liquid phase continuing to react with yttria matrix, and the incoming oxygen ions react with uranium in liquid phase, contributing to the further increase of the center layer thickness.

4.2 Solidification

During cooling, at temperature T_2, primary dentrites within the eutectic composition start to appear in liquid phase L_1, hence changing L_1 to L_2 as described below:

$$A_{(s)} + L_1 \rightarrow A_{(s)} + A'_{(s)} + L_2 \qquad [4\text{-}9]$$

where $A_{(s)} = UO_2$ in solid phase

$A'_{(s)}$ = Primary dentrites (UO_2) in solid phase.

At T_3, a peritectic reaction[47] occurs in which A' phase reacts with L_2 to give $B_{(s)}$ which is YUF_7. The fluorine-rich, yttrium uranium fluoride phase (YUF_7) encircles A' and prevents further reaction of the liquid with the dentrites (A'). Consequently, L_2 changes to L_3.

$$A_{(s)} + A'_{(s)} + L_2 \rightarrow A_{(s)} + A'_{(s)} + B_{(s)} + L_3 \qquad [4\text{-}10]$$

where $B = YUF_7$

Finally at T_4, L_3 crystallizes to give lamellar type eutectic

where $B = YUF_7$ and $C = YU_{10}F_{3-x}$ forms the eutectic phase.

$$A_{(s)} + A'_{(s)} + B + L_3 \rightarrow A_{(s)} + A'_{(s)} + B_{(s)} + (B+C)_{(s)} \qquad [4\text{-}11]$$

The directions of the primary dendrites indicate the direction of the heat flow. The lamellar formation suggests that the rate of cooling was moderate.[49] As seen from the micrograph (Figure 3.13), wall thickness increases toward the bottom end; this is due to the fact that the reaction rate is faster because of the higher influx of UF_4 which first strikes the bottom portion of the sample. The droplet shape at the bottom end of the sample is due to the surface tension of the liquid coupled with gravitational force.

Basically, three layers were formed during the reaction. The concentration of the components through the layers was almost constant and time independent.

CHAPTER 5

SUMMARY AND CONCLUSION

A detailed analysis of yttria reacting with UF_6 and UF_4 was performed in this research. The compatibility of Mo with UF_4 in liquid and gas phases was also tested.

Samples of yttria were prepared using sintering and hotpressing techniques. Disk shaped samples first were prepared by compressing the yttrium oxide powder, then sintering was performed at 1973 K in an electrical furnace and about 85% of the theoretical density was reached after this process. For hot-pressing, a high strength graphite die was used in which the precompressed sample was placed between two tungsten disks. Three samples were pressed at 1873 K under pressures ranging from 30 to 45 MPa pressure in argon atmosphere. Densities reaching above 99% of the theoretical density of yttria were obtained after hot-pressing. Due to color changes of the samples, partial transparency was observed; however, following an annealing period of 3 hours at 1473 K this contamination problem was removed and fully white samples were obtained. Uranium hexafluoride gas at 1173 K was used first to test the yttria samples in a flowing loop system. This provided a more realistic approach to gas core conditions and decreased UF_6 losses due to oxygen reactions and dissociation to lower fluorine compounds.

Extensive corrosion of yttria was observed after the experiments for short periods of time (5 to 20 min). For longer exposure times, samples fully reacted and dispersed in the reaction chamber. Products from UF_6, mainly free fluorine and UF_4, caused the breakdown of the high temperature ceramic material. The multilayer formation following the chemical reactions was observed with SEM technique. The observed reaction layers were named as outer, center, and inner layers. Following the XRD and EMP analyses, it was found that the outer layer was a mixture of UO_2, U_3O_8 and YF_3 while the inner layer was only composed of yttrium and fluorine

without the presence of uranium atoms. It was concluded that UF_6 gas reacted with yttria following a complex chemical reaction scheme and at least two simultaneous chemical reactions formed two moving reaction boundaries in the samples.

In the second phase of the experiments, samples of yttria and molybdenum were tested with UF_4 in a stainless steel reaction chamber. This time, oxygen contamination of the chamber due to the external factors such as the silica or alumina container tube was totally removed by placing the yttria and molybdenum samples into a molybdenum tube. The insertion of argon gas into the chamber, which was under high vacuum of approximately 10^{-5} Torr, further helped to minimize contamination. The oxidation of molybdenum and loss of UF_4 at temperatures above 1273 K was prevented in this manner. Yttria samples reacted extensively, in a manner similar to the UF_6 case, while molybdenum showed good compatibility at temperatures up to 2273 K. The reaction products with yttria at 1750 K were analyzed extensively with optical microscope, scanning electron microscopy (SEM), electron microprobe (EMP) and x-ray diffraction analysis. In this case, three reaction boundaries were formed. The UF_6 caused only two reaction boundaries in the yttria sample. The existing components in the three reaction boundaries were found to be UO_2, YOF, YF_3, and U_3O_{7-8}. Uranium oxide (UO_2) formed a solid wall between the liquid outer layer and solid inner layer at the time of the experiment. This layer did not form during the UF_6 exposures, because the lower operating temperature (1200 K) significantly decreased the diffusion of the 0 and Y ions, thus preventing the formation of a liquid eutectic mixture and the accumulation of the center UO_2 layer. The higher activity of the UF_6 gas, due to its higher fluorine concentration increased the intensity of the reactions, accelerating the corrosion of the material. The higher reactivity of fluorine compared to uranium ions showed itself in both UF_6, UF_4 cases by advancing and reacting further in the yttria matrix, thus forming the inner layer. The outer

layer showed extensive sponge-like porosity after UF_6 reaction. However, in the UF_4 case, the presence of the liquid phase and its solidification during the cooling period produced an outer layer without porosity. It was also found that the outer layer was composed of a significant amount of dendrites surrounded with a gray peritectic phase. This phase itself was followed by lamellar, finely dispersed eutectic. The dendrites were found to be composed of hypostoichiometric UO_2 while the peritectic and the eutectic layer were a mixture of uranium, yttrium and fluorine.

In the case of molybdenum, due to the presence of oxygen, formation of MoO_3 and $MoOF_4$ on the surface at temperatures over 1273 K was observed. However this problem was eliminated after modifications were done to the system. Contrary to the previous work performed with melted uranium,[25,26,27,28] molybdenum resisted the UF_4 at any temperatures below 2300 K. No significant diffusion nor reaction was detected in the samples after EMP, SEM, and EDS analyses. However, samples became more brittle after each experiment. This is due to the rapid cooling rate from temperatures over 1273 K after turning off the power.

The major conclusions derived from this research are:

a. The complex multilayer structure of the yttrium oxide ceramic containing different phases, after being exposed to UF_4 and UF_6 gases at temperatures between 1173 and 1750 K, was analyzed and a semi-quantitative model describing the process was developed. The experimental and predicted diffusion coefficients of uranium and fluorine atoms in UO_2 is compared according to the model developed.

b. High purity molybdenum was found to be resistant to liquid and gas phase UF_4 at ranges 1273-2273 K. Molybdenum was found to be a promising material for the corrosive environments of the proposed gas core reactors.

LIST OF REFERENCES

1. Dugan E.T., Welch G.E., Kahook S., in: Proc.of the 24th Energy Conversion Engineering Conference, Ed. W.D. Jackson, IECEC-89, Washington, DC (Aug. 6-11, 1989).

2. Cochran R.G., Tsoulfanidis N., The Nuclear Fuel Cycle: Analysis and Management, American Nuclear Society (ANS), La Grange Park, IL (1990).

3. Bacher W., Karlsruhe K., Jakob E., 'Uran' in: Gmelin Handbuch der Anorganischen Chemie, Ed. Keller C., Kerntechnik S.F., Karlsruhe K., C8, Springer-Verlag, Berlin (1980).
4. Hagenmuller P., Inorganic Solid Fluorides. Chemistry and Physics, Academic Press, Orlando, FL (1985).

5. El-Wakil M.M., Nuclear Energy Conversion, ANS, La Grange Park IL (1978).

6. Fedorov G.B., Smirnov E.A., Diffusion in Reactor Materials, Trans Tech Publications, Aedeermannsdorf Switzerland (1984).

7. Assuncao F.C.R., Diffusion Study in the *Fe-Co-Ni-Au* System using the Penetration Tendency Approach, Doctoral Dissertation, University of Florida, Gainesville (1978).

8. Crank J., The Mathematics of Diffusion, Oxford University Press, Bristol, England (1975).

9. Jost, W., Diffusion in Solids, Liquids, Gases, Academic Press, New York (1960).

10. Crank J., Free and Moving Boundary Problems, Clarendon Press, Oxford (1984).

11. Hill J.M., One-Dimensional Stefan Problems. An Introduction, John Wiley & Sons, New York (1987).

12. Barrer R.M., Diffusion In and Through Solids, Cambridge University Press, London (1941).

13. Geiger G.H., Poirier D.R., Transport Phenomena in Metallurgy, Addison-Wesley, Reading, MA (1973).

14. Murch G.E., Nowick A.S., Diffusion in Crystalline Solids, Academic Press, Orlando (1984).

15. Romig A.D., Dayananda M.A., Diffusion Analysis and Applications, The Minerals, Metals & Materials Society, Chicago (1989).

16. Ozisik M.N., Mikhailov M.D., Unified Analysis and Solutions of Heat and Mass Diffusion, John Wiley & Sons, New York (19-84).

17. Szekely J., Evans J.W., Sohn H.Y., Gas-Solid Reactions, Academic Press, New York (1976).

18. Wong K.Y., Mathematical Models for Gas-Solid Reactions, Master's Thesis, University of Florida, Gainesville (1976).

19. Incropera F.P., De Witt D.P., Fundamentals of Heat and Mass Transfer, John Wiley & Sons, New York (1990).

20. Borg R.J., Dienes G.J., An Introduction to Solid State Diffusion, Academic Press Inc., San Diego (1988).

21. Wise H., Oudar J., Material Concepts in Surface Reactivity and Catalysis, Academic Press, San Diego (1990).

22. Laidler, J.K., Chemical Kinetics, Harper & Row, New York (1987).

23. Kondratiev V.N., Nikitin E.E., Gas-Phase Reactions: Kinetics and Mechanisms, Springer-Verlag, Berlin (1981).

24. Ovchinnikov A.A., Timashev S.F., Belyy A.A., Kinetics of Diffusion Controlled Chemical Processes, Nova Science Publishers, New York (1986).

25. Kuznietz M., Livne Z., Cotler C., Erez G., J. Nucl, Mater., 152, 235-245 (1988).

26. Kuznietz M., Livne Z., Cotler C., Erez G., J. Nucl, Mater., 160, 69-74 (1988).

27. Kuznietz M., Livne Z., Cotler C., Erez G., J. Nucl. Mater., 160, 196-200 (1988).

28. Lundberg L.B., J. Nucl. Mater., 167, 64-75 (1989).

29. Hale C.F., Barber E.J., Berhardt H.A., High Temperature Corrosion of Some Metals and Ceramics in Fluorinating Atmospheres, Report K-1459, Union Carbide Nuclear Co., Oak Ridge National Lab., Oak Ridge, TN (1960).

30. Florin A.E., Some Corrosion Tests of Materials in UF_6, LA-7327-MS, Los Alamos National Lab., Los Alamos, NM (1978).

31. Whitney E.D., Kim D.J., Tucker D.S., Nucl.Technol., 69, 154 (1985).

32. Collins C., Reaction Between ZrO_2 and UF_6 at Elevated Temperatures, Master's Thesis, University of Florida, Gainesville (1988).

33. Wang S.C.P., Anghaie S., Whitney D., Collins C., High Temperature Testing of Alumina and Zirconia in Uranium Hexafluoride Environment, Nucl. Technol., 93[3], 399 (1991).

34. LeRoy, Furlong R., Domingues L.P., Sintering of Yttrium Oxide, Ceramic Bulletin, 45[12], 1051 (1966).

35. Sordelet J.D., Akinc M., Sintering of Monosized, Spherical Yttria Powders, J. Am. Ceram. Soc., 71[12], 1148 (1988).

36. Alper M.A., High Temperature Oxides, Academic Press, New York (1971).

37. Aitcin P.C., Density and Porosity Measurement of Solids, J. Mater., JMLSA, 6[2], 282 (1971).

38. ASTM Standards, C20-80a, American Society for Testing and Materials, Philadelphia, PA.

39. Chemical Rubber Company (CRC), Handbook of Chemistry and Physics, 68th edition, CRC Press, Boca Raton, FL (1987-88).

40. Thompson W.T., Pelton A.D., Bale C.W., Facility for the Analysis of Chemical Thermodynamics, Ecole Polytechnique de Montreal, Montreal, Quebec (1985).

41. Bacher, W., Gmelin Handbuch der Anorganischen Chemie, U Uran, C1, Springer Verlag, Berlin, New York (1980).

42. Olander D.R., Fundamental Aspects of Nuclear Reactor Fuel Elements, Technical Information Center, U.S. Department of Energy, Washington, DC (1976).

43. Lidiard A.B., J.of Nucl. Mater., 19, 106-108 (1966).

44. Matzke H.J., Diffusion in Doped U02, Trans. Amer. Nucl. Soc., 8[5], 26-27, (1970).

45. Matzke H.J., Lattice Disorder and Metal Self-Diffusion in Non-Stoichiometric UO2 and (U,Pu)02, Journal de Physique, 34[11-12], 317 (1973).

46. Matzke H.J., On Uranium Self-Diffusion in U02 and $U02^{+}$, J of Nuclear Mater., 30[1-2], 26-35 (1969).

47. Guy A.G., Essentials of Materials Science, McGraw-Hill, New York (1976).

48. Kingery W.D., Bowen H.K., Uhlmann D.R., Introduction to Ceramic, John Wiley & Sons, New York (1976).

49. Rostoker W., Dvorak J.R., Interpretation of Metallographic Structures, Academic Press, San Diego (1990).

50. Denton E.C., Interface Stability During Isothermal. Ternary Phase Transformation, Doctoral Dissertation, McMaster University, Hamilton, ON, Canada (1970).

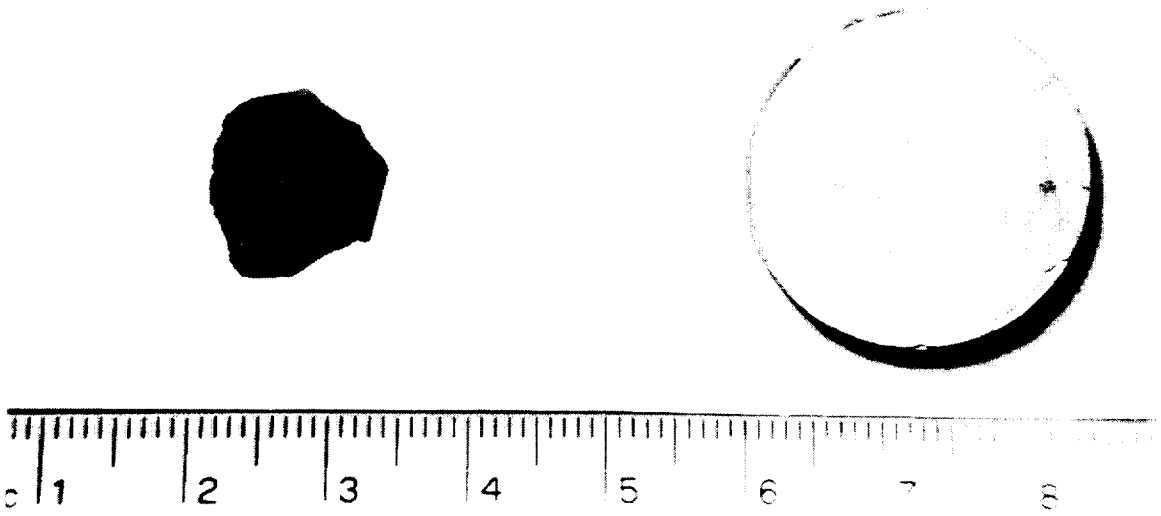

Figure 2.1 Hot-Pressed (99%) and Sintered (85%) Samples

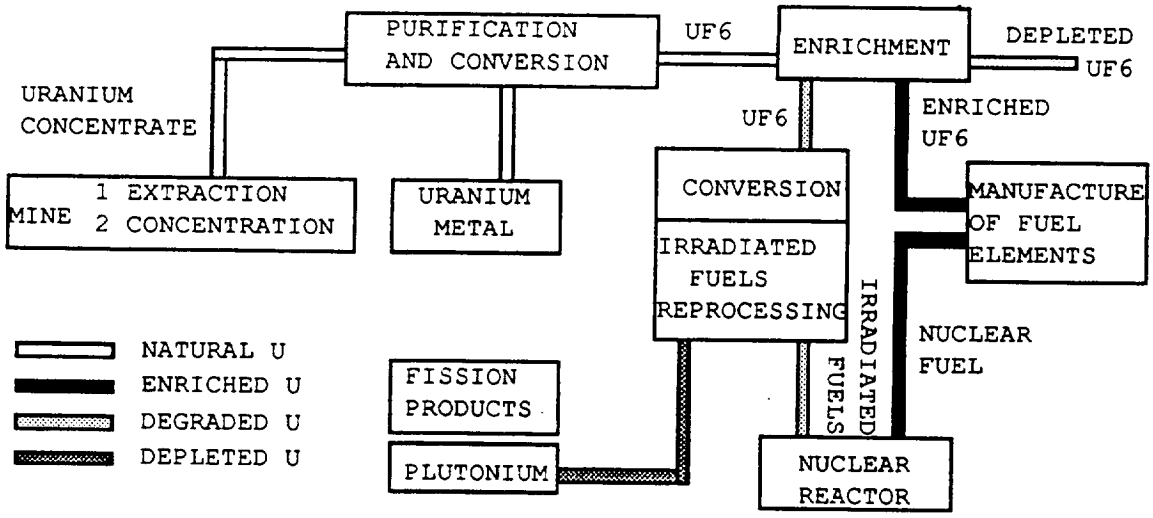

Figure 2.2 Nuclear Fuel Cycle and Fluorine Derivatives

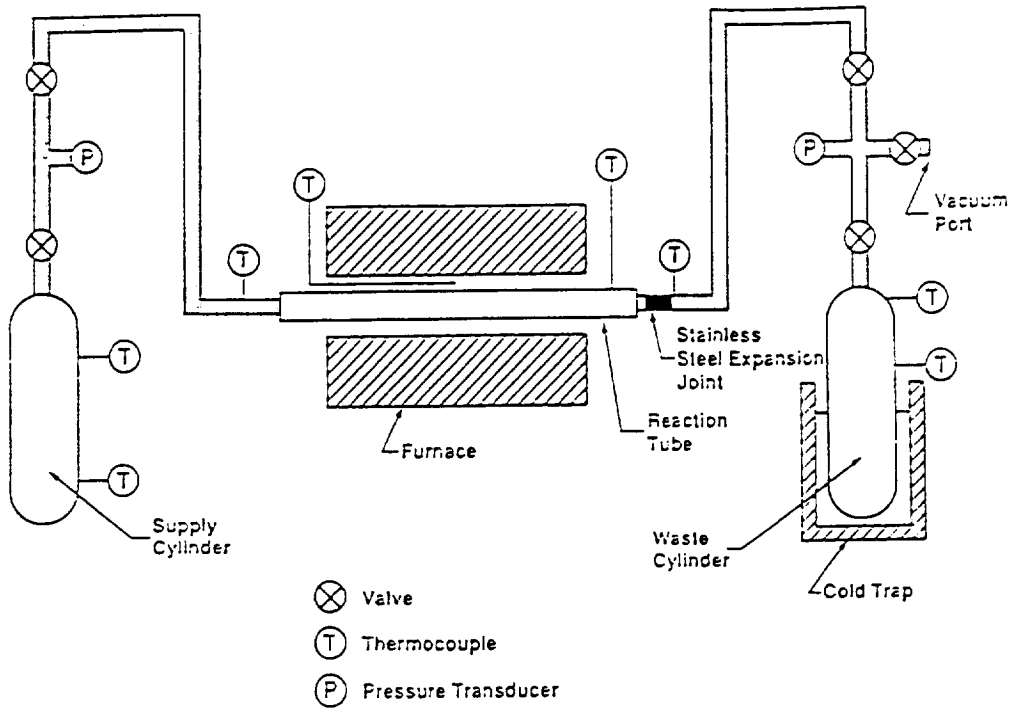

Figure 2.3 UF_6 Test Unit

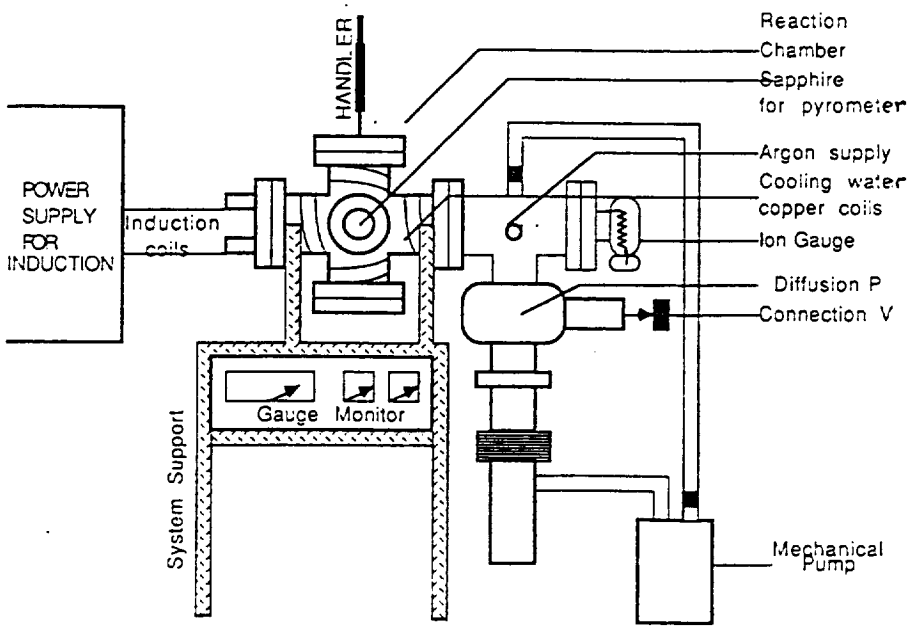

Figure 2.4 UF_4 Test Unit

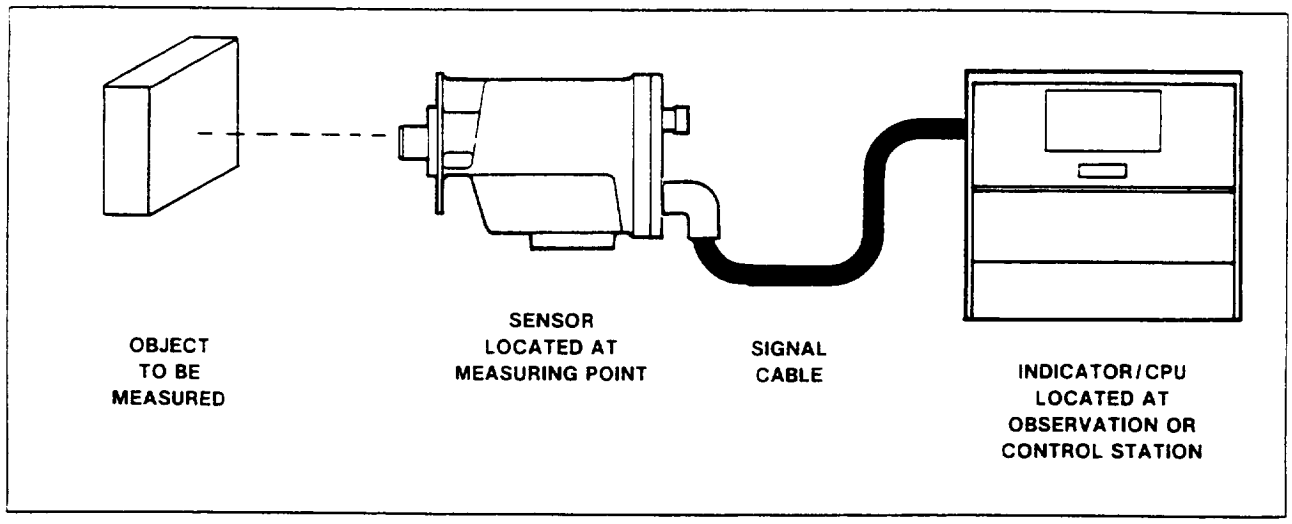

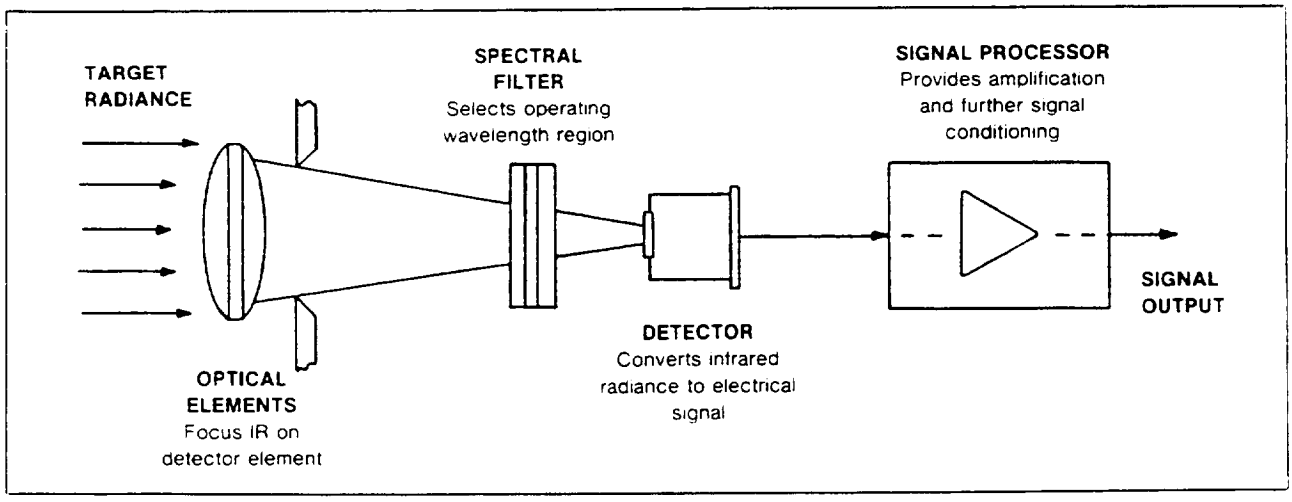

Figure 2.5 Optical Pyrometer and Its Functional Mechanism

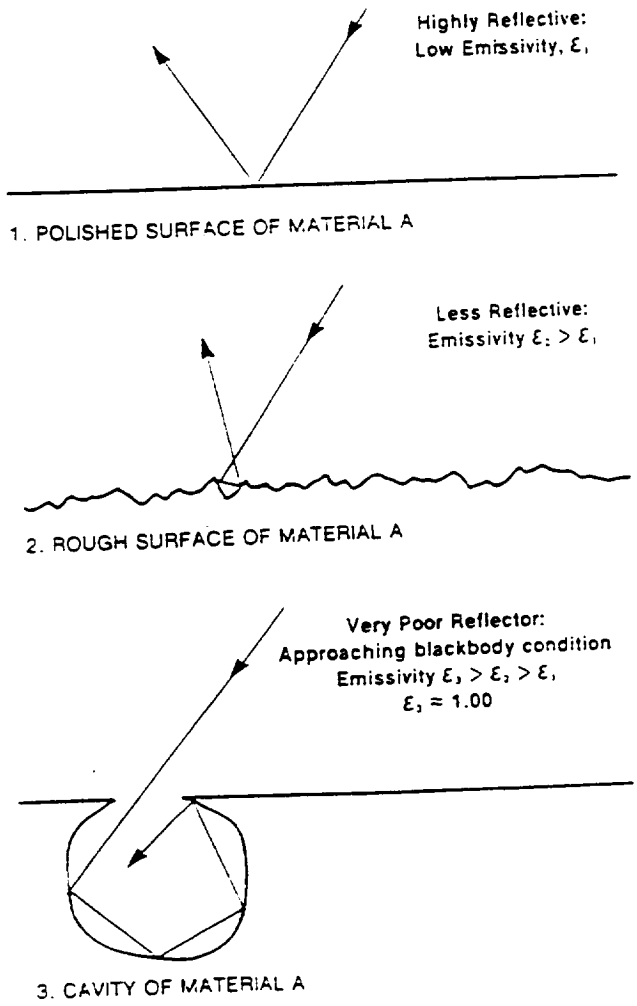

Figure 2.6 Emissivity Change Due to the Surface Conditions

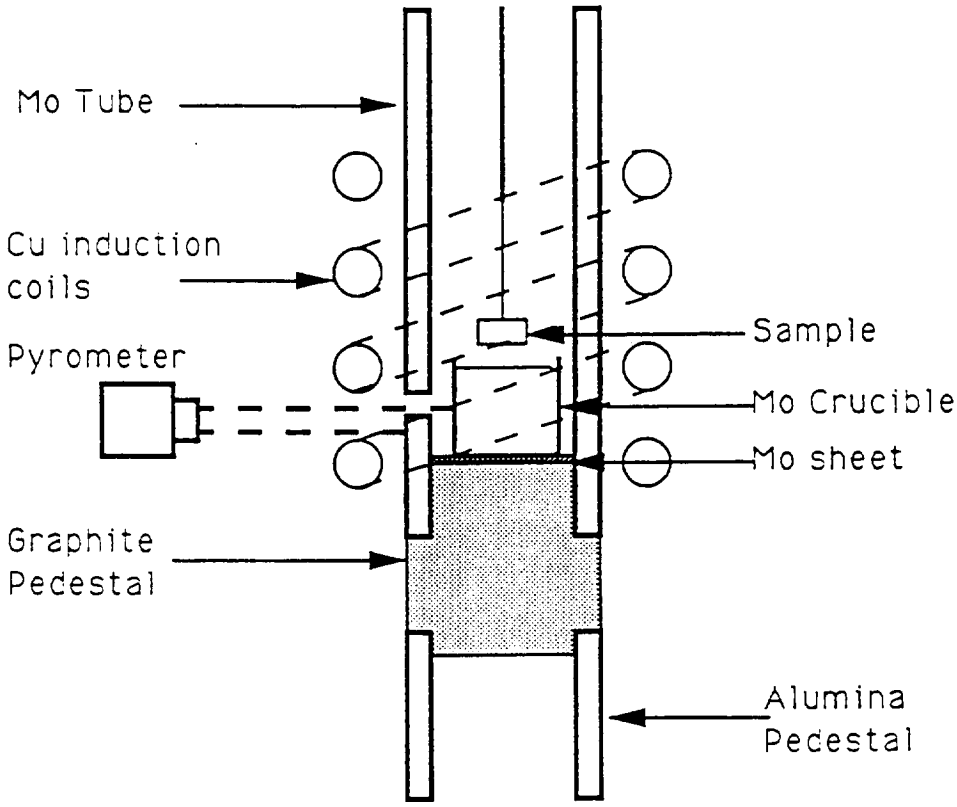

Figure 2.7 Temperature Measurement of The Inner and Outer Wall

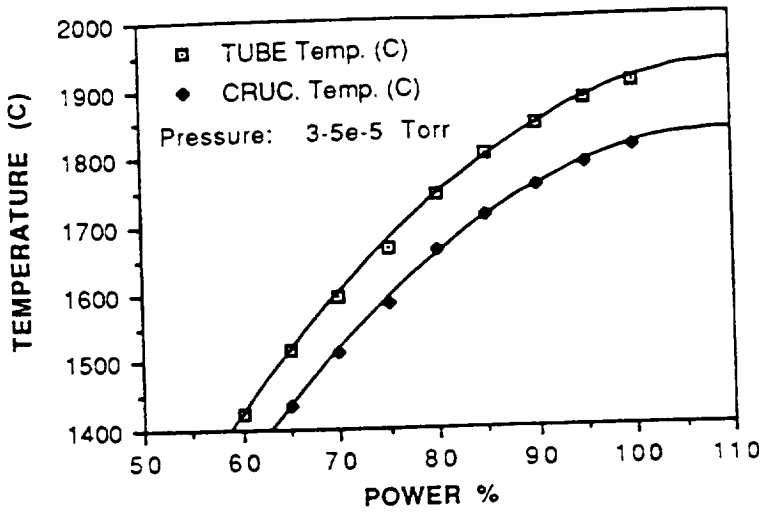

a

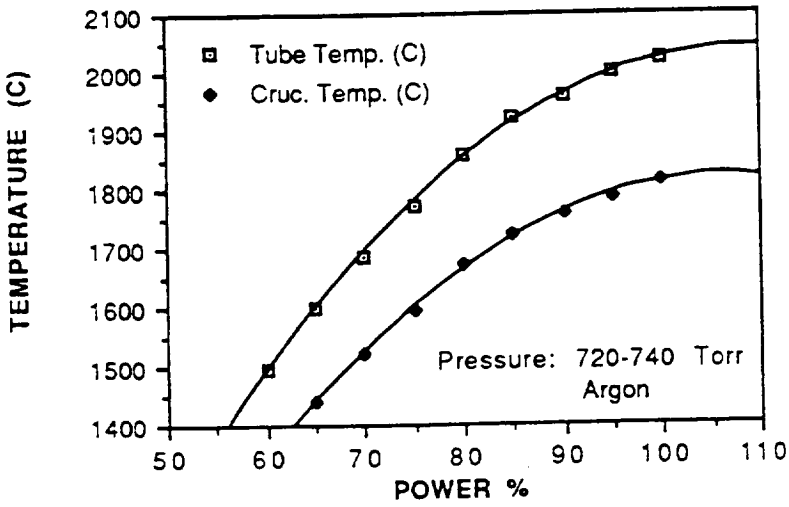

b

Figure 2.8 Temperature Corrections of Tube Crucible System a. Under Vacuum, and b. Under Argon

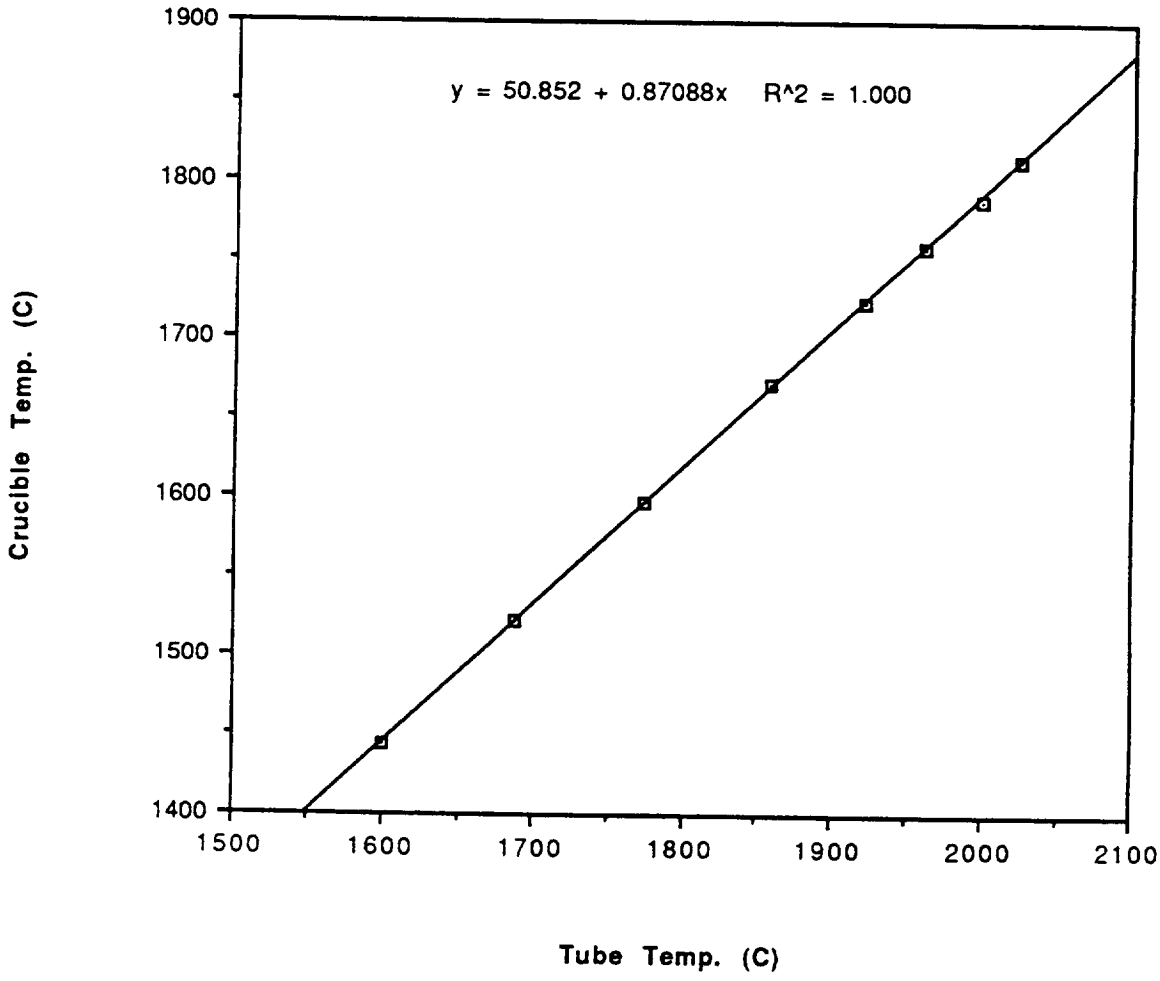

Figure 2.9 Tube and Crucible Temperature Relationship

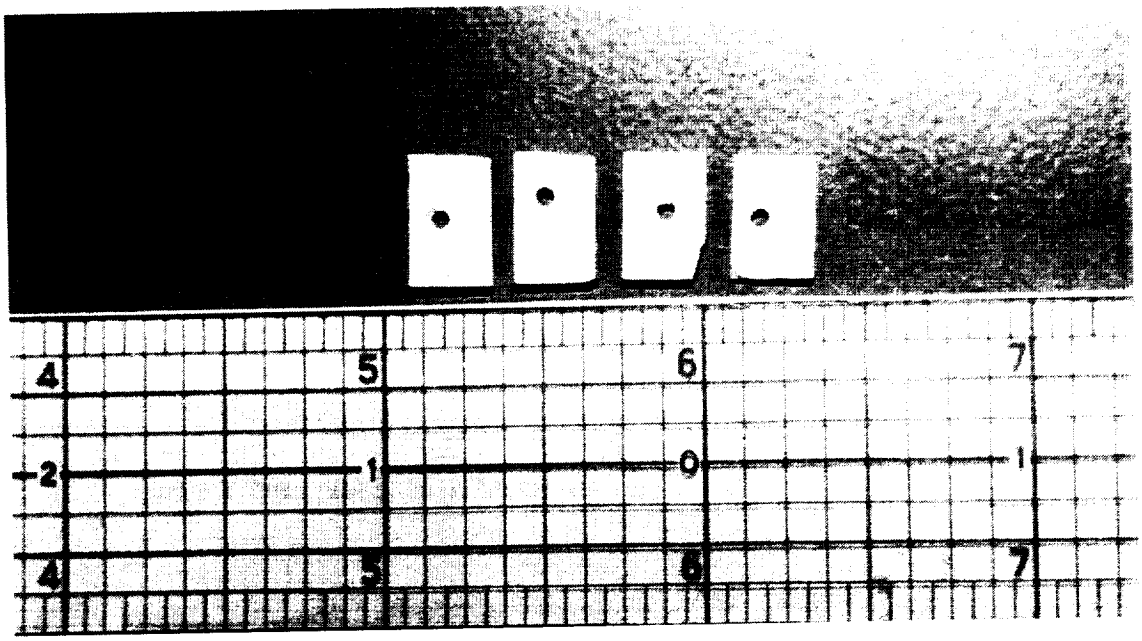

Figure 2.10 Yttria Samples Before the Exposure

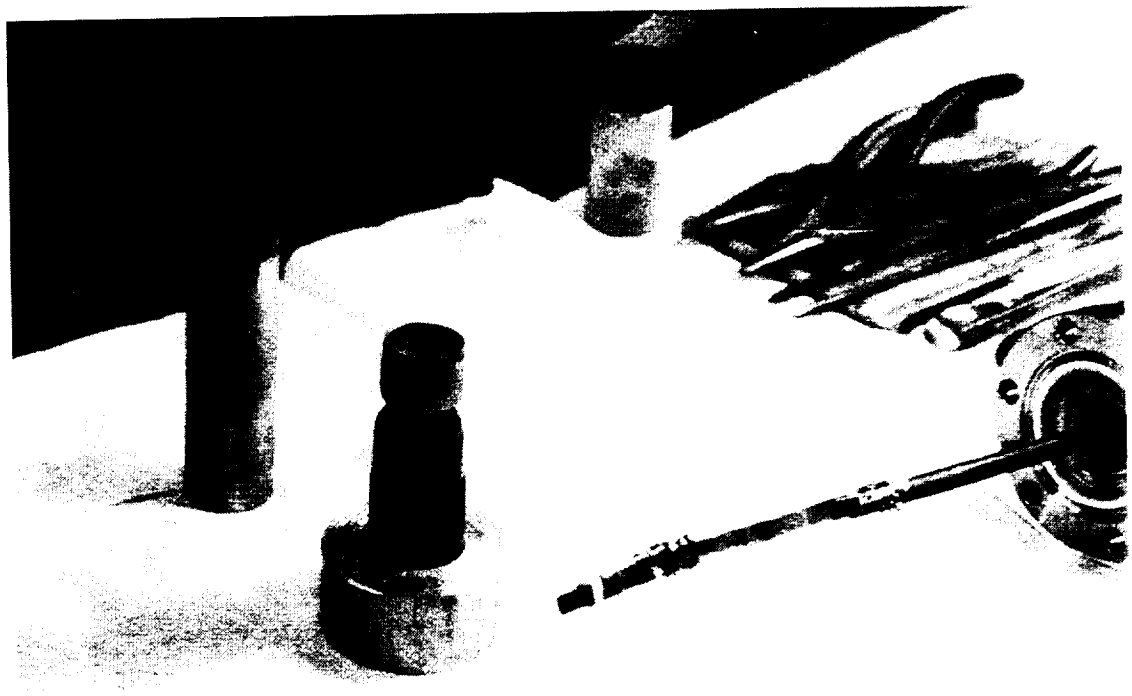

Figure 2.11 Mo Tube, Crucible, Handler and Graphite Pedestal

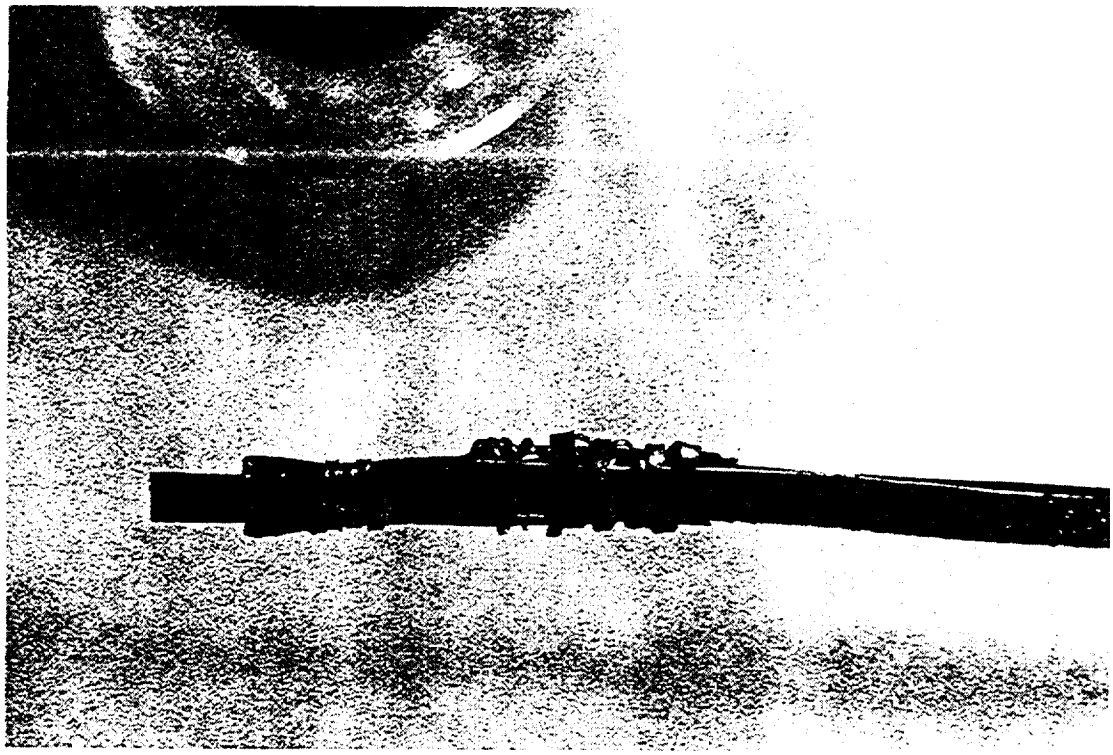

Figure 2.12 Doubly Wrapped Mo Sheets Holding the Mo Sample

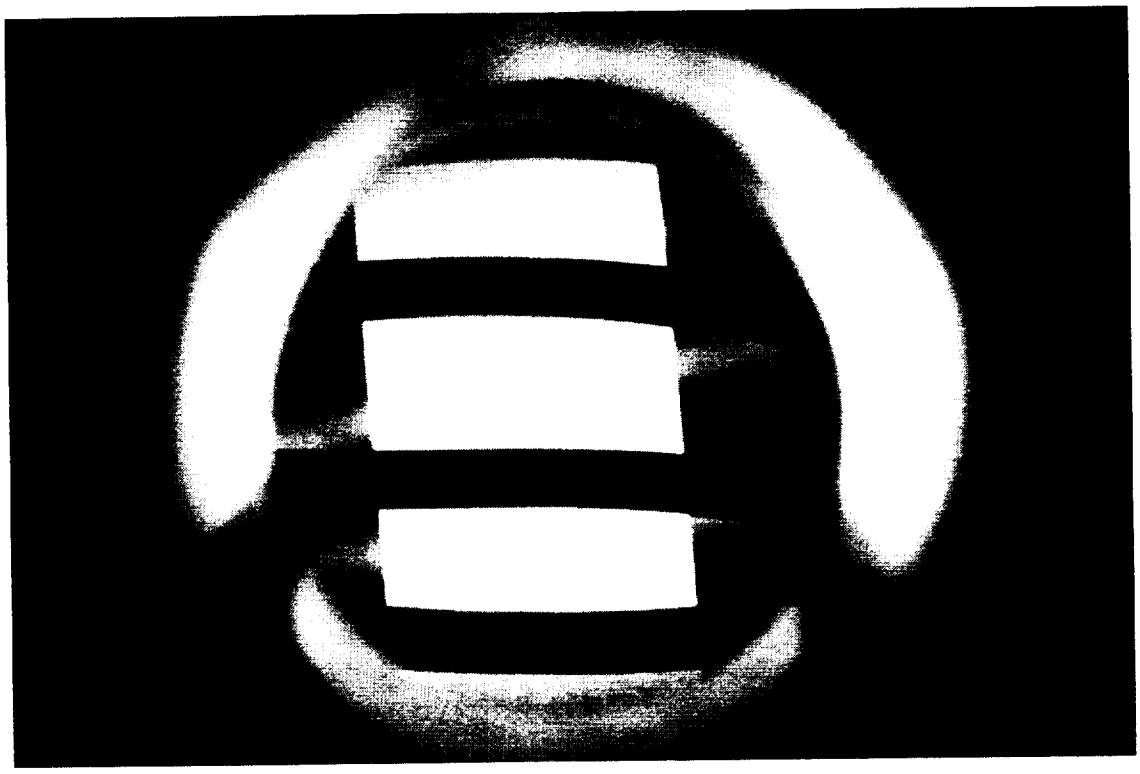

Figure 2.13 View of the Central Heating Zone

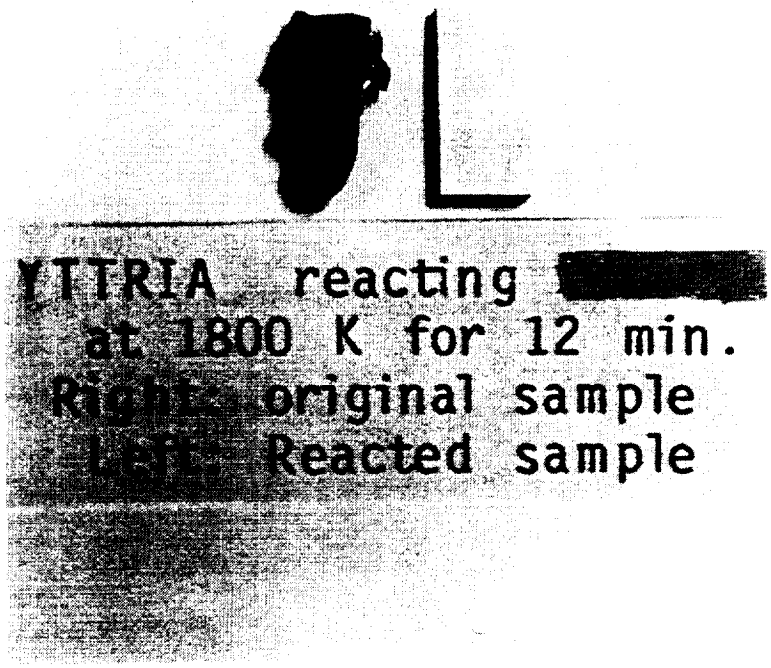

Figure 2.14 Yttria Samples Before and After the Reaction

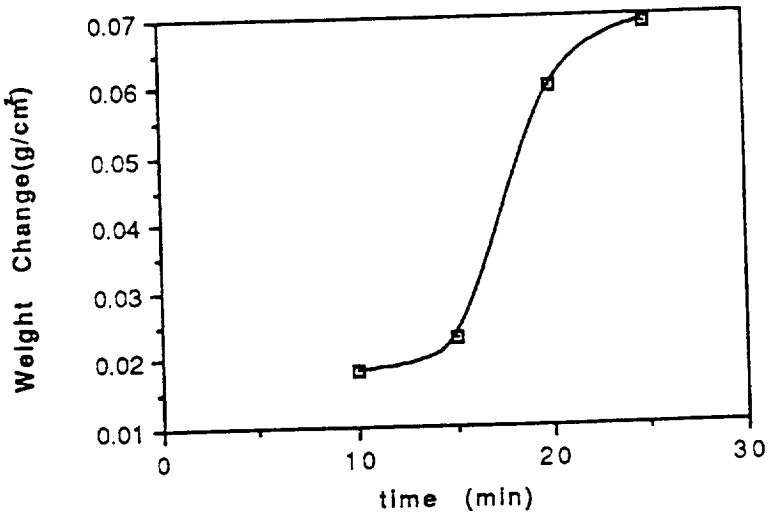

Figure 3.1 Weight Change Analysis of Yttria Samples of 85% Theoretical Density

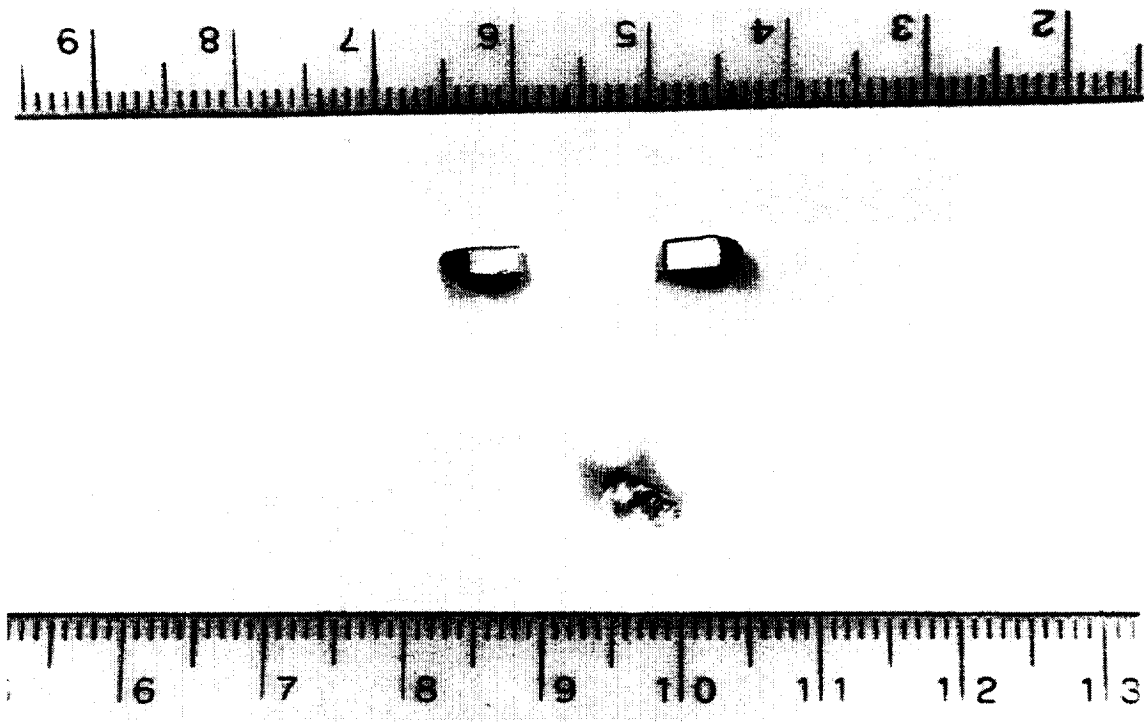

Figure 3.2 Yttria Sample After Being Tested in UF_6 at 1173 K a. 10 min. exposure b. 25 min. exposure [in cm]

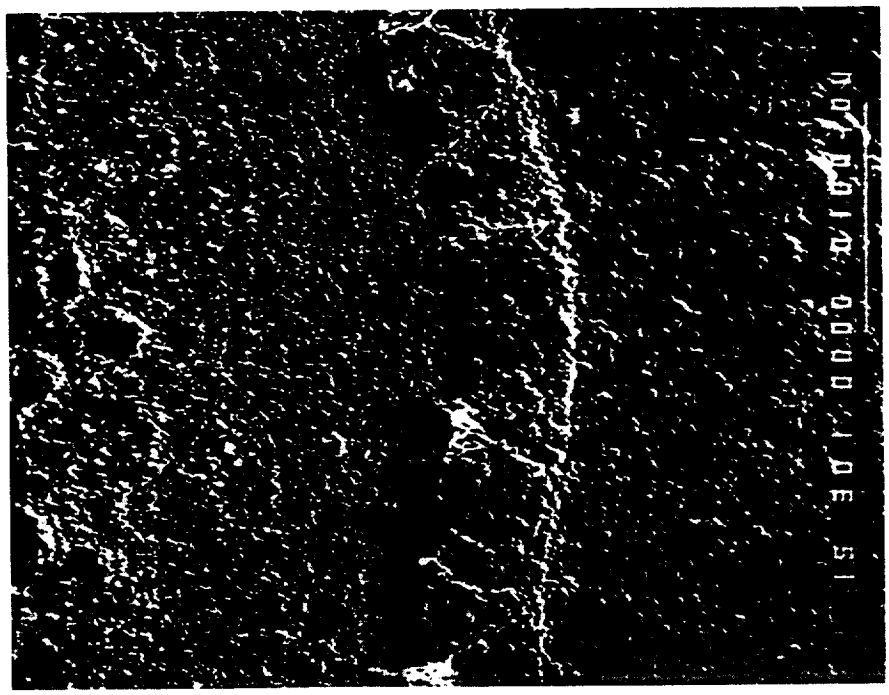

Figure 3.3 SEM Micrograph of Yttria Sample Exposed to UF_6 at 1173 K for 10 min; Outer Layer, Inner Layer, and Yttria Substrate

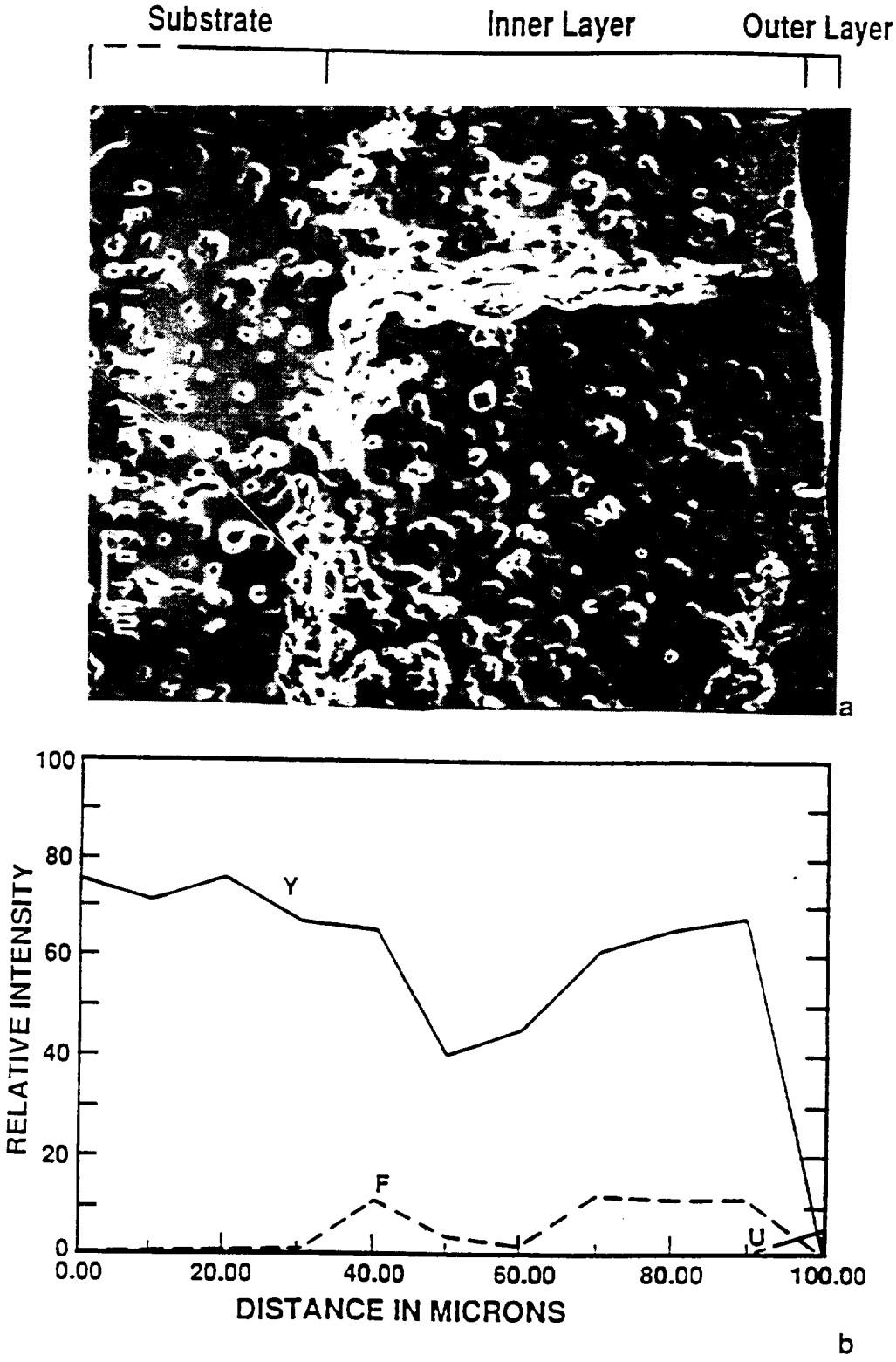

Figure 3.4 EMP Analysis of a Ytt85 Sample Exposed to UF_6
a. Cross Section of the Sample Tested for 5 min at 1173 K
b. Concentration Profiles

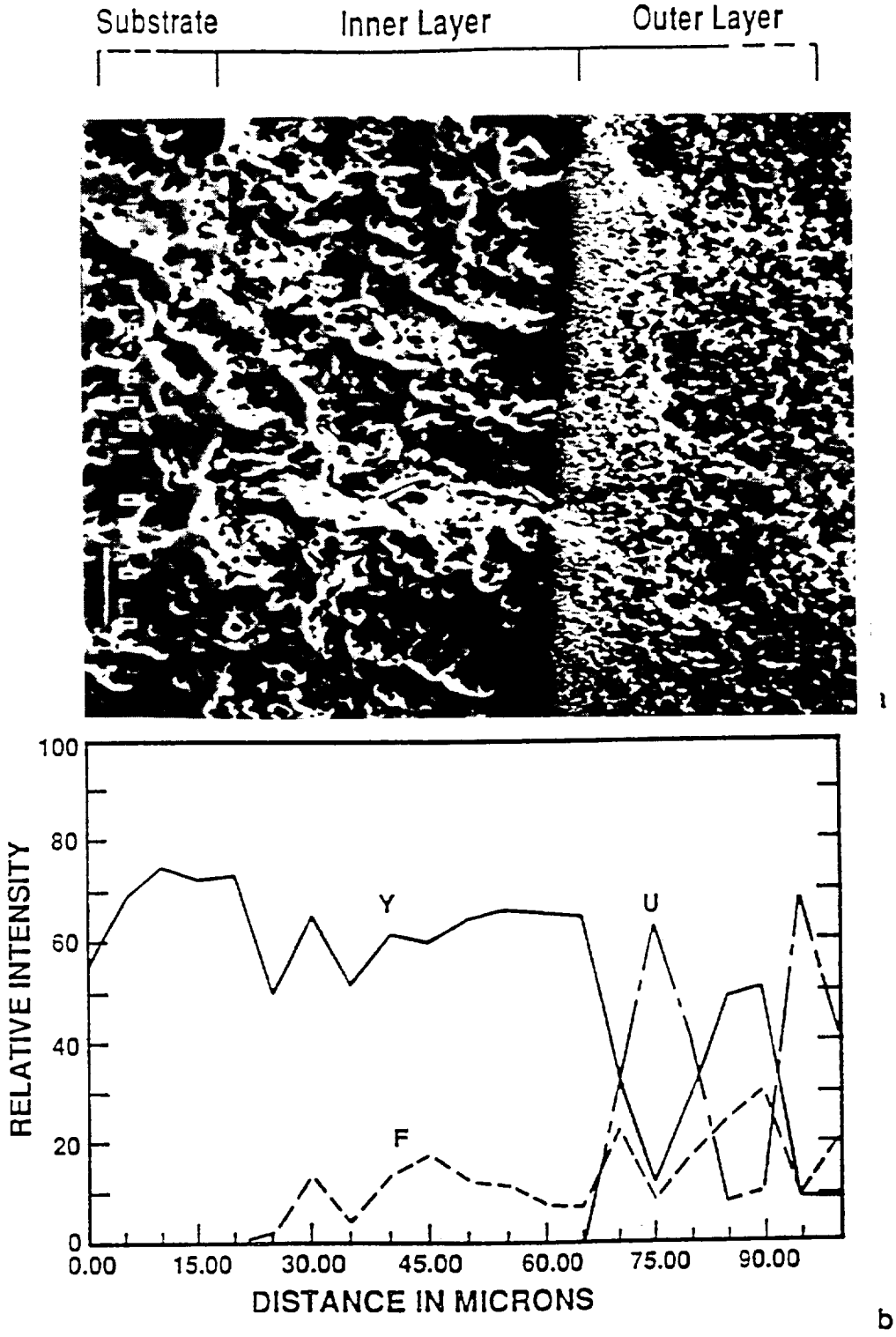

Figure 3.5 EMP Analysis of a Ytt85 Sample Exposed to UF_6
a. Cross Section of the Sample Tested for 10 min at 1173 K
b. Concentration Profiles

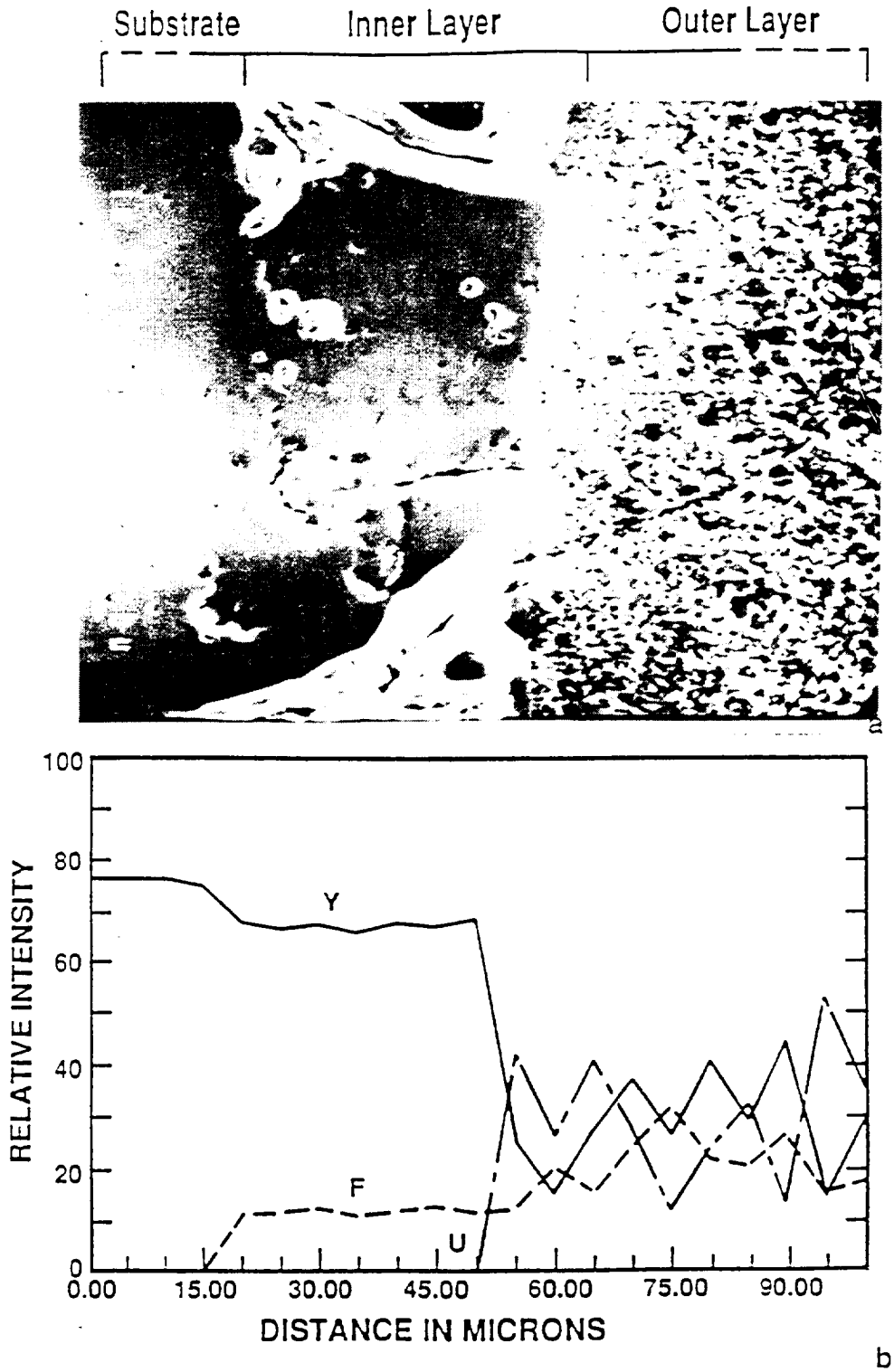

Figure 3.6 EMP Analysis of a Ytt85 Sample Exposed to UF_6
a. Cross Section of the Sample Tested for 20 min at 1173 K
b. Concentration Profiles

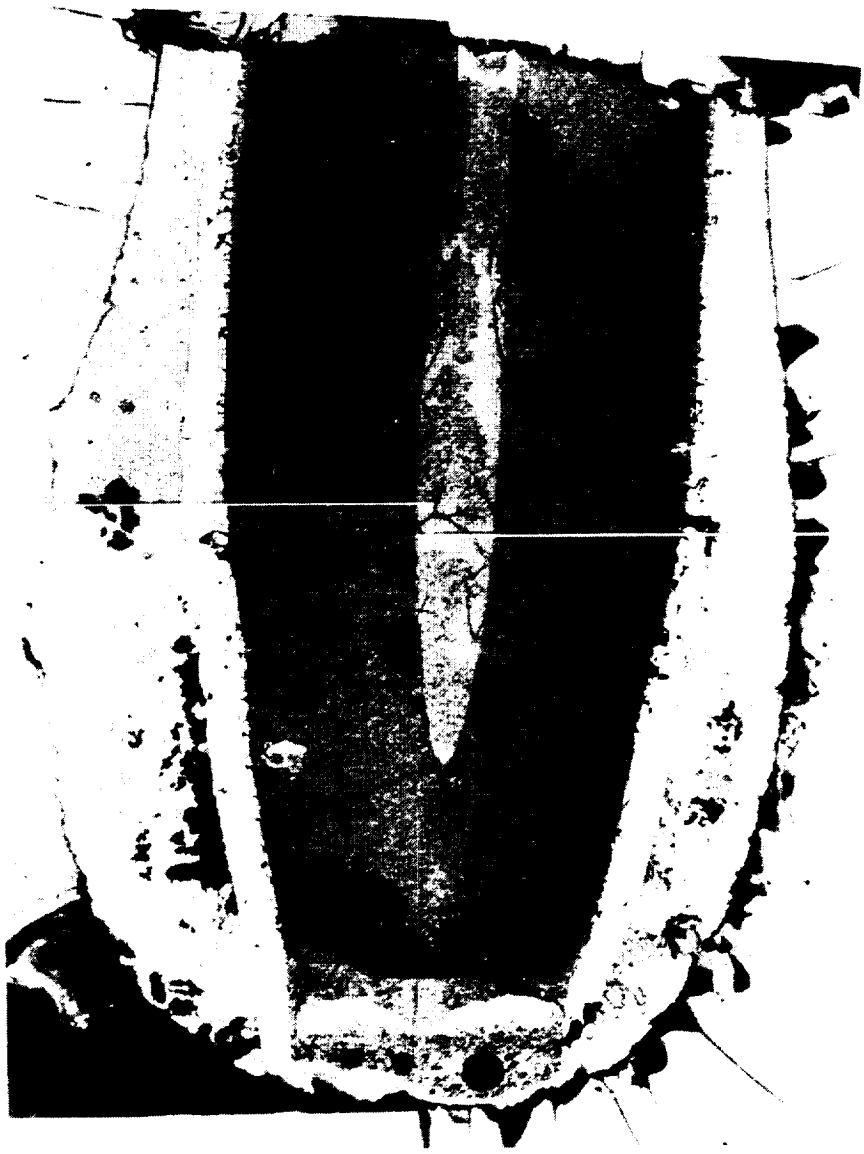

Figure 3.10 Cross Section of the Yttria Sample Tested in UF_4 in Gas Phase at 1740 K for 40 min

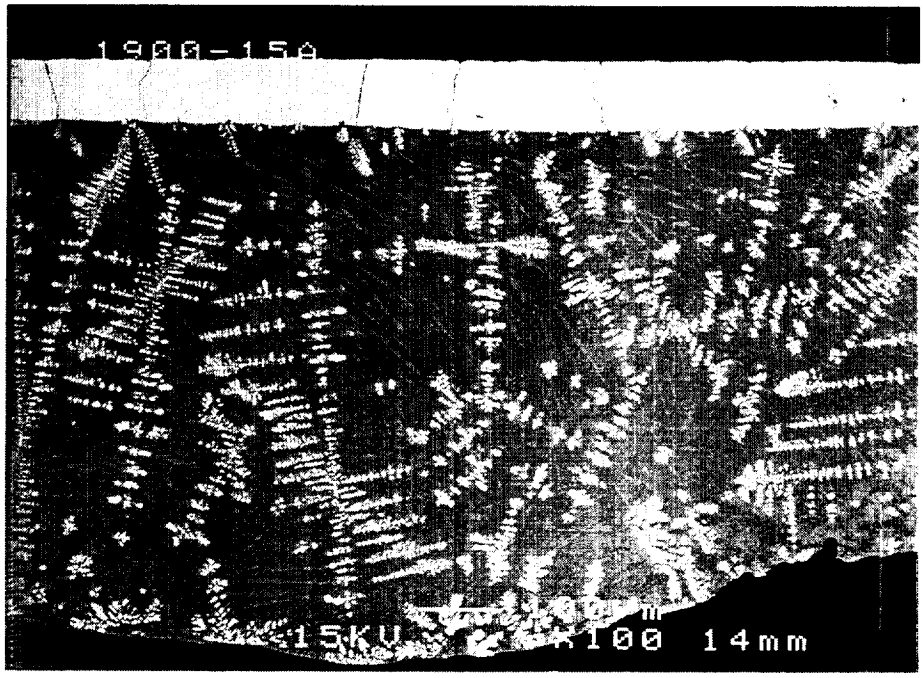

Figure 3.11 SEM Micrographs Taken in Backscattering Mode at 650 mag; Layers with Dendrites and Eutectic.

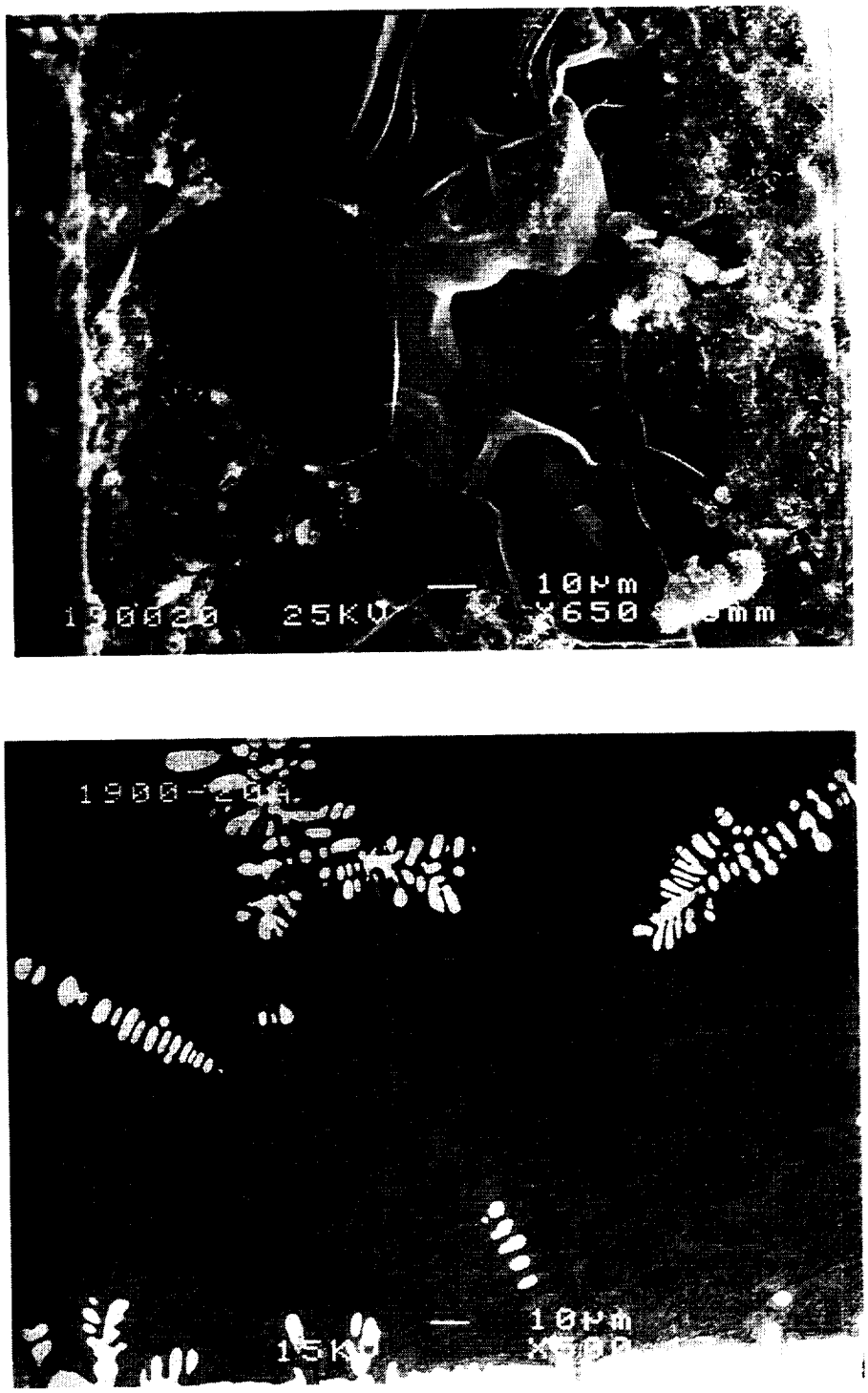

Figure 3.12 SEM Micrographs of a Yttria Sample Tested in UF_4 at 1650 K for 20 min
a. broken cross section of the center layer
b. secondary dentrites, peritectic and eutectic phases in the outer layer

Figure 3.13 Optical Micrographs Taken at 50 mag of the Yttria Samples Exposed to UF_4

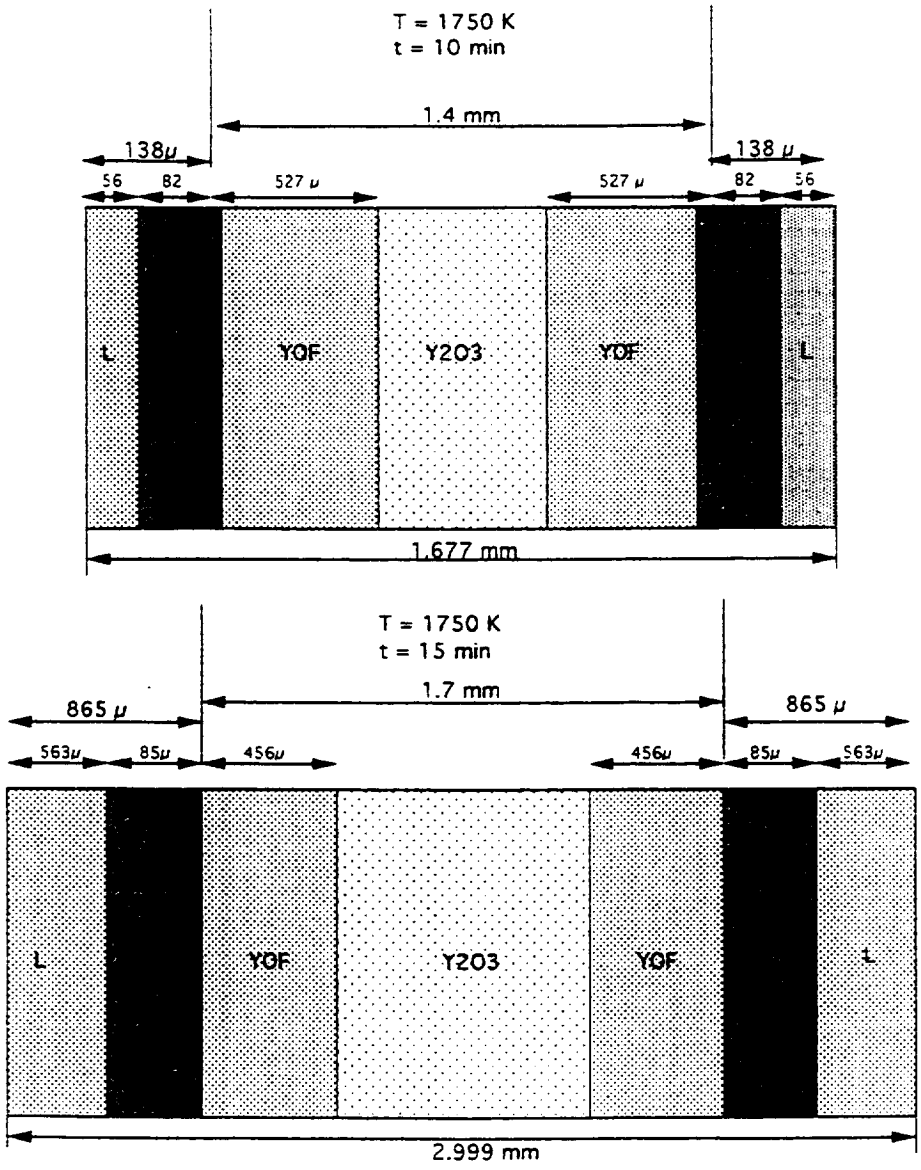

Figure 3.14 Reaction Layers and Original Sample Dimensions for 10 and 15 min Tests at 1750 K in UF_4

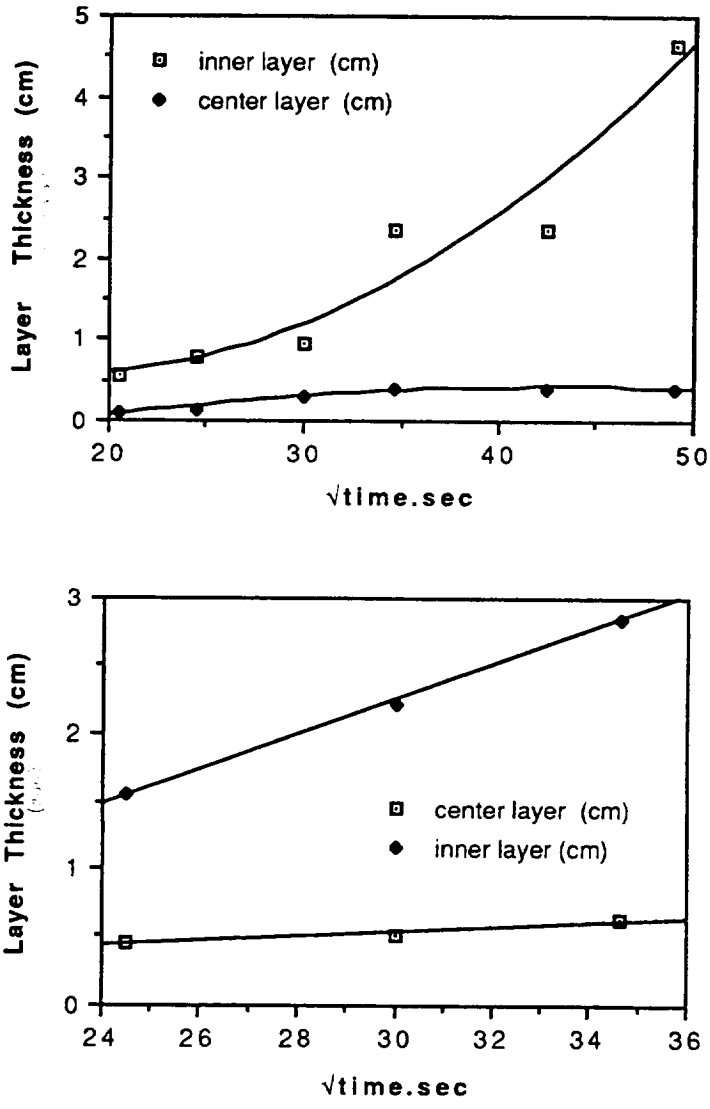

Figure 3.15 Growth Rate of the Layers at 1650 K and 1740 K
a. At 1650 K b. At 1740 K

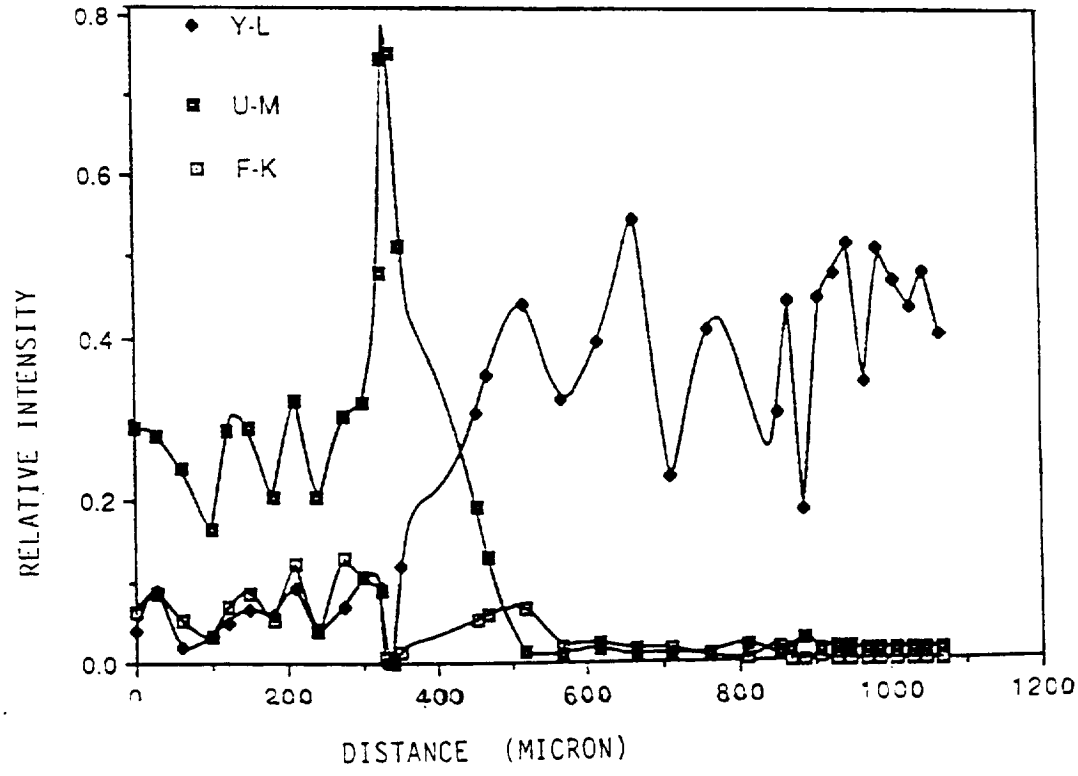

Figure 3.16 EMP Result of a Yttria Sample Tested in UF_4 at 1740 K for 20 min

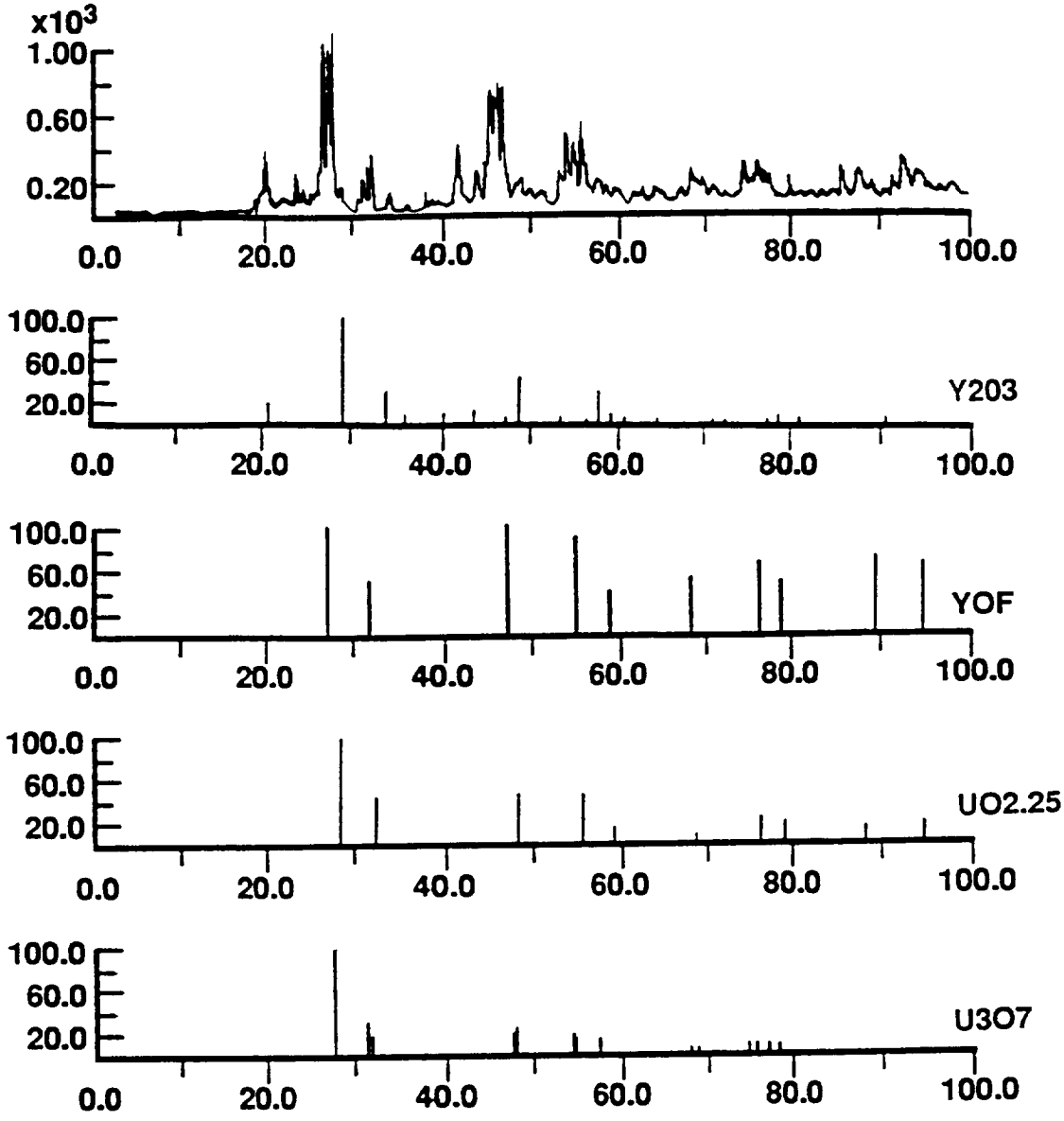

Figure 3.17 XRD Patterns of a Yttria Sample Exposed to UF_4

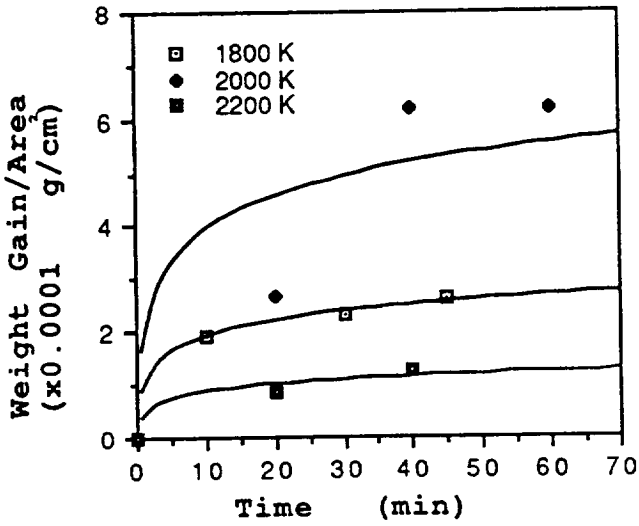

Figure 3.18 Weight Change of Mo Tested at 1800, 2000, 2200 K

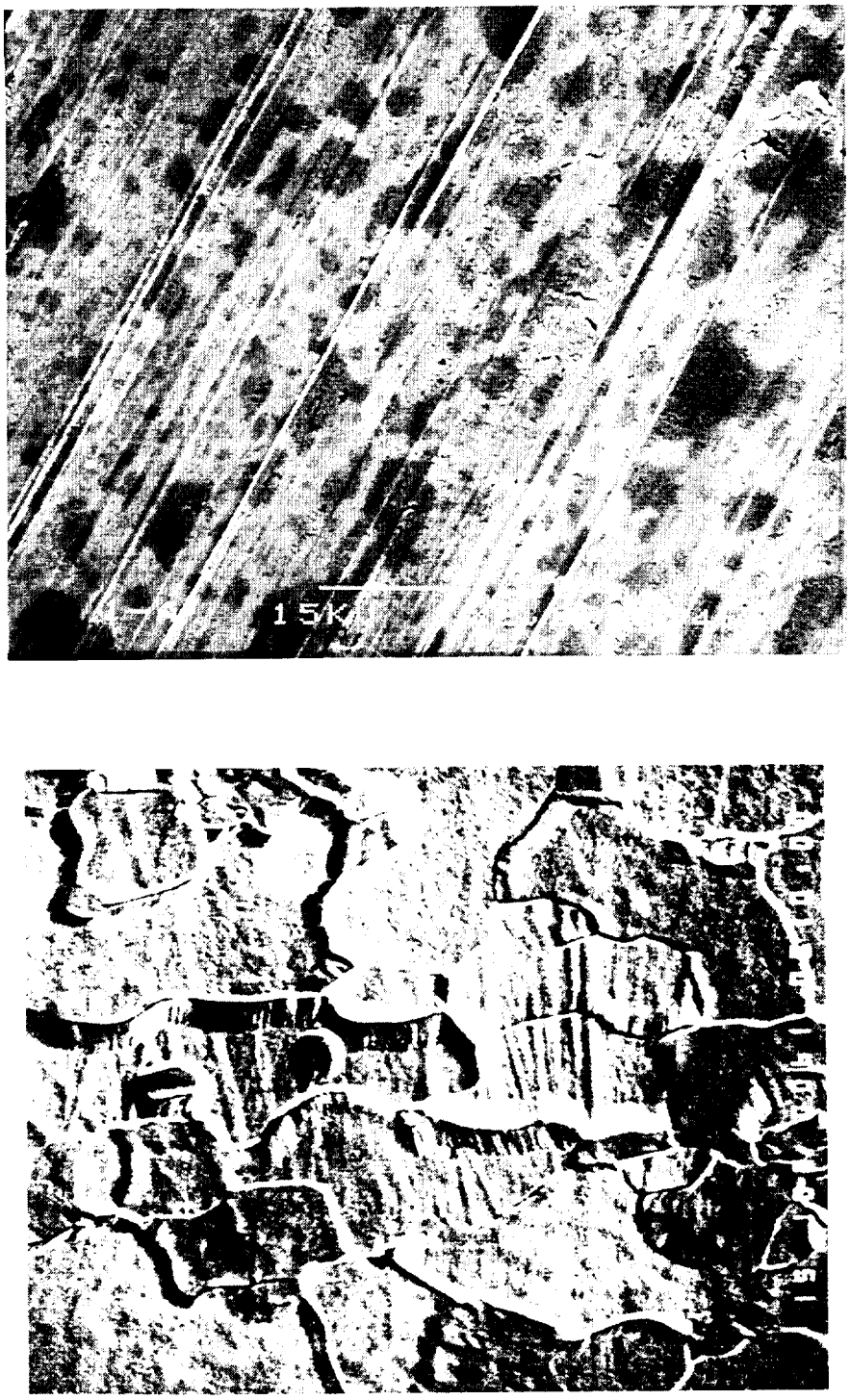

Figure 3.19 Micrographs of a Mo Sample Before and After UF_4 Test

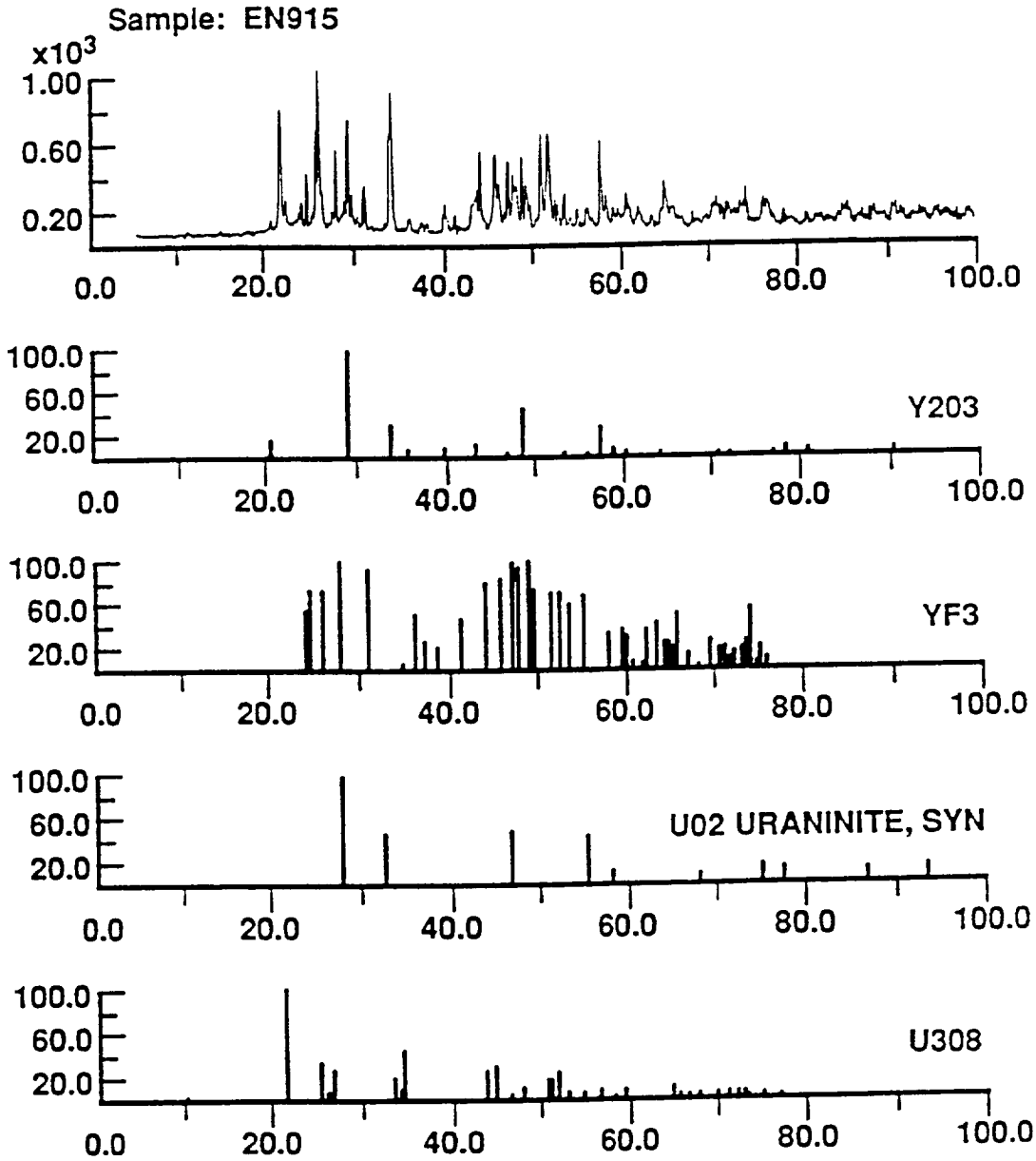

Figure 3.7 XRD Patterns of ytt85 Exposed to UF_6 at 1173 K for 15 min

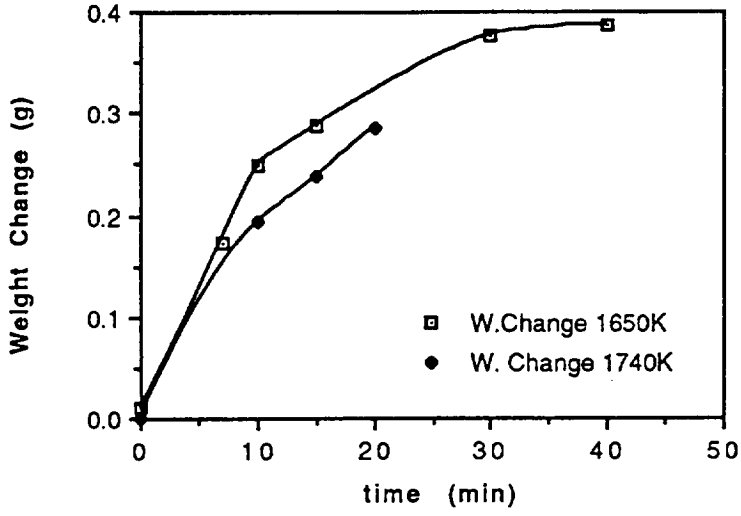

Figure 3.8 Weight Change of Yttria Exposed to UF_4

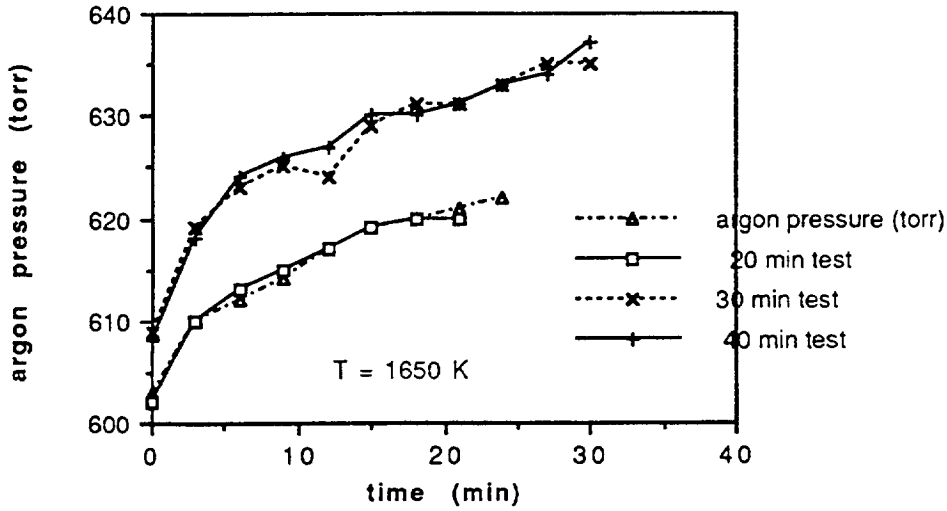

Figure 3.9 Pressure Change During the Test of Yttria in UF_4

†† JSM-6400 Scanning Microscope, Tracor Northern Comp. Sys.

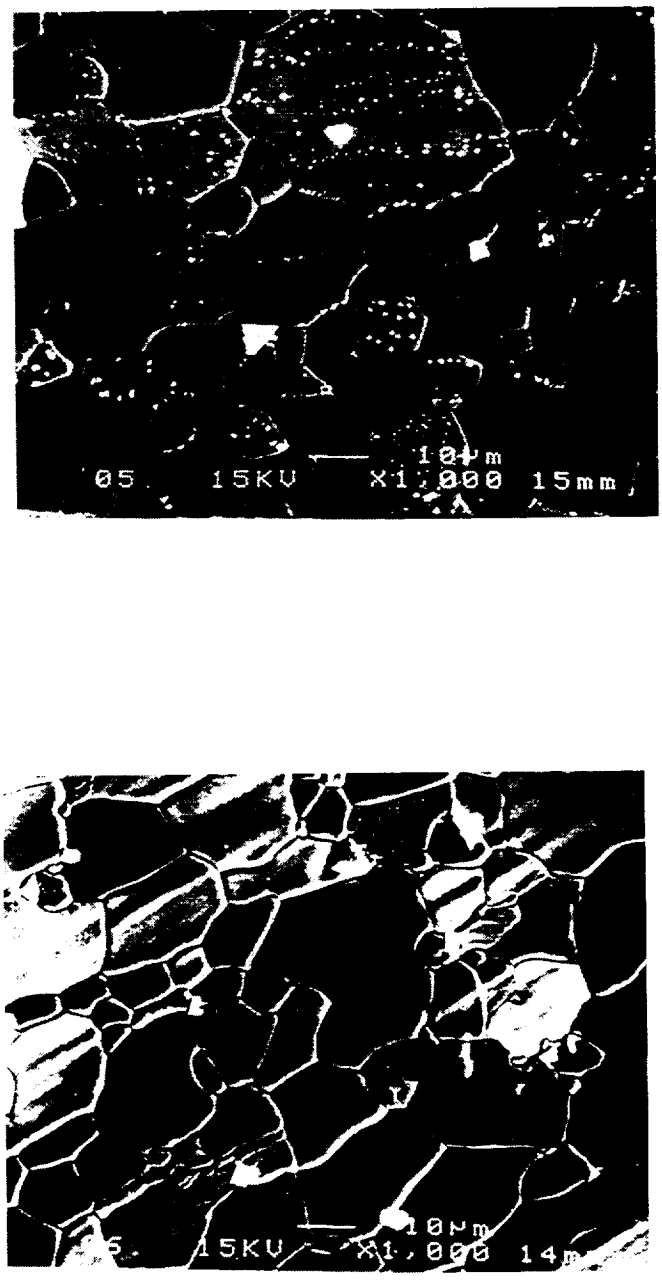

Figure 3.20 SEM Results of Mo Exposed to UF_4 at 2000 K and 2200 K

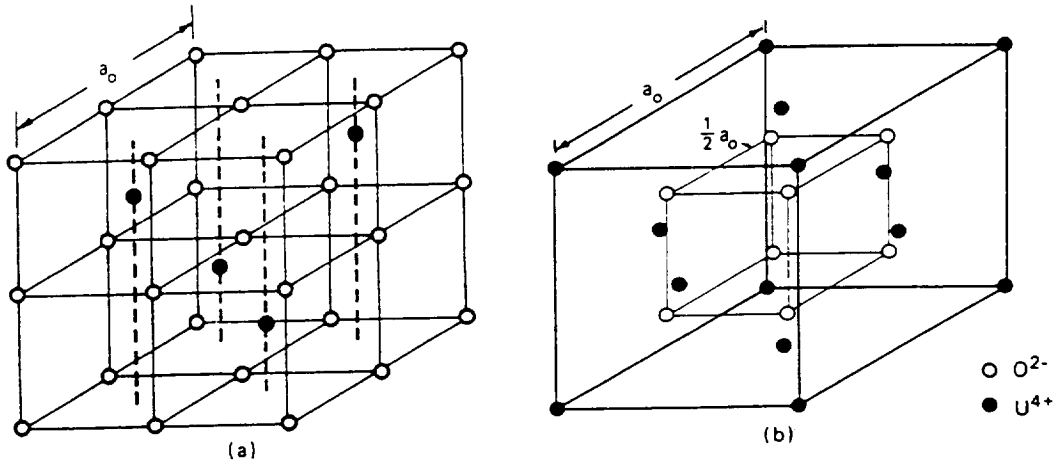

Figure 4.1 The Fluorite Structure of UO_2
a. The sc structure of the anion sublattice
b. The fcc structure of the cation sublattice
From Olander D.R., Fundamental Aspects of the Nuclear Reactor Fuel Elements

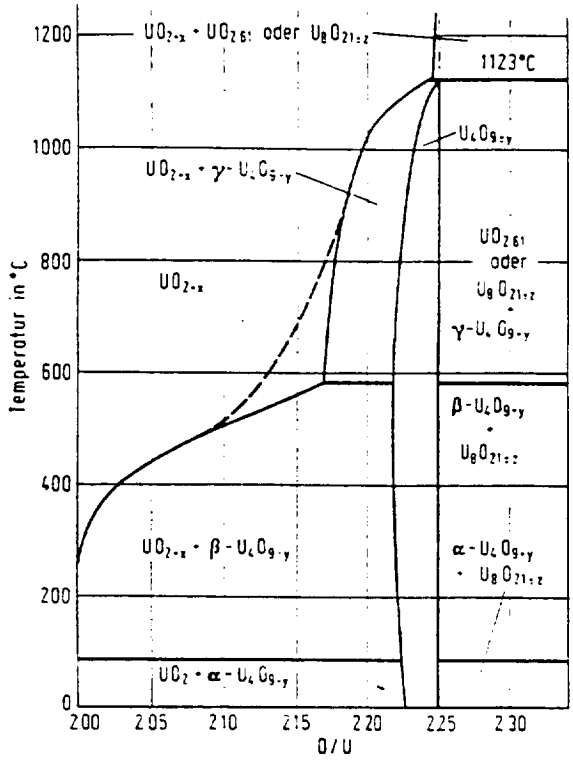

Figure 4.2 Oxygen-Uranium Phase Equilibrium System
From: Gmelin, Handbuch der Anorganishen Chemie, U Uran

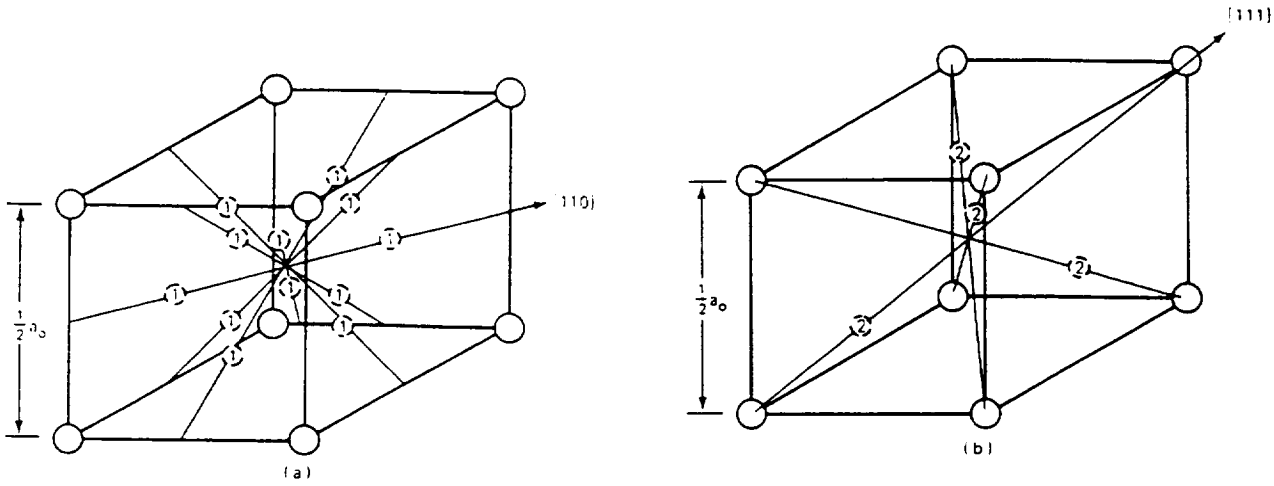

Figure 4.3 Sites for Interstitial Oxygen in UO_2
○, Normal oxygen ions ①, type 1 interstitial sites ②, type 2 interstitial sites

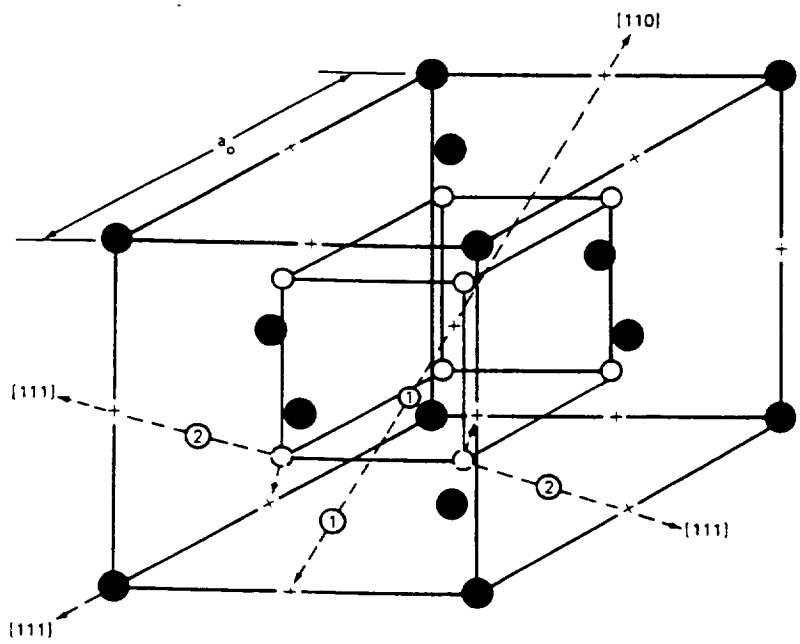

Figure 4.4 Defect complex in UO_2
From: Olander D.R., Fundamental Aspects of the Nuclear Reactor Fuel Elements.

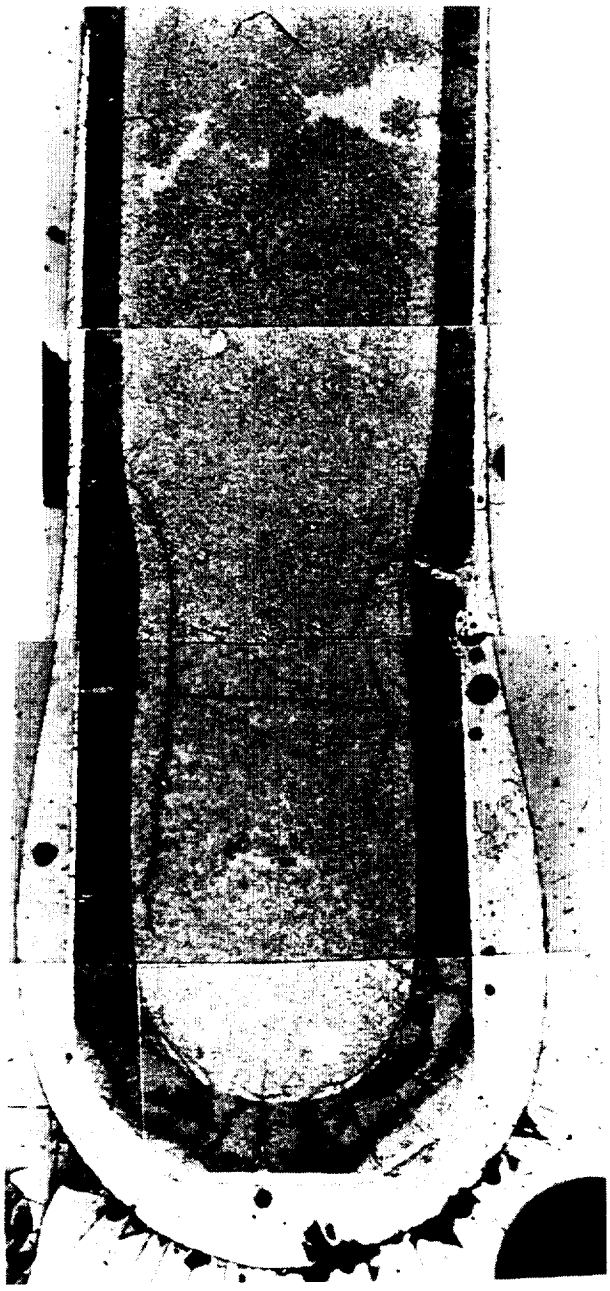

Figure 4.5 Cross Section of a Yttria Sample Exposed to UF_4 at 1650 K for 15 min

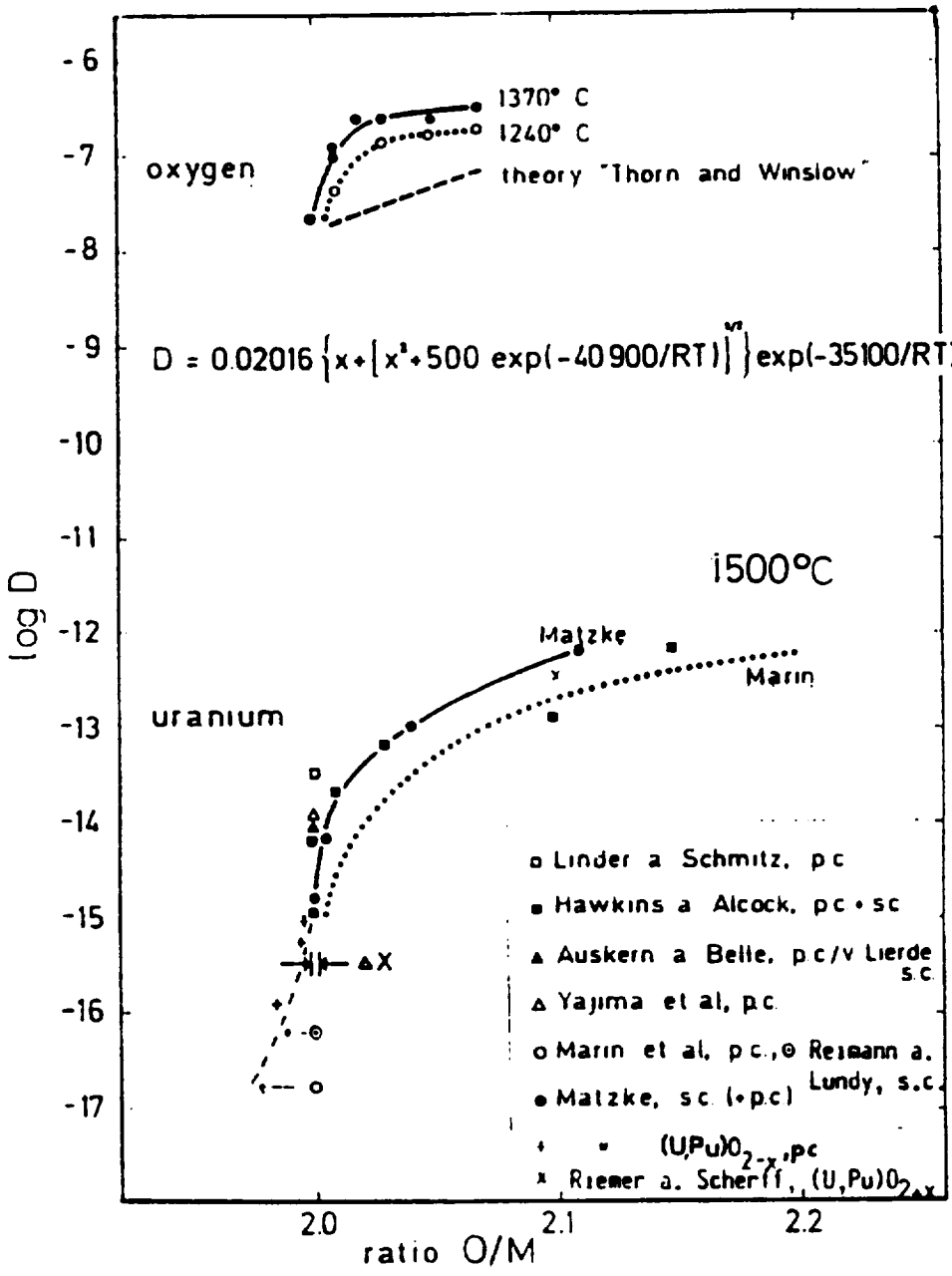

Figure 4.6 Diffusion Coefficient of Uranium with Respect to O/M Ratio
From Matzke, H.J., On Uranium Self-Diffusion in UO_2 and UO_2^+

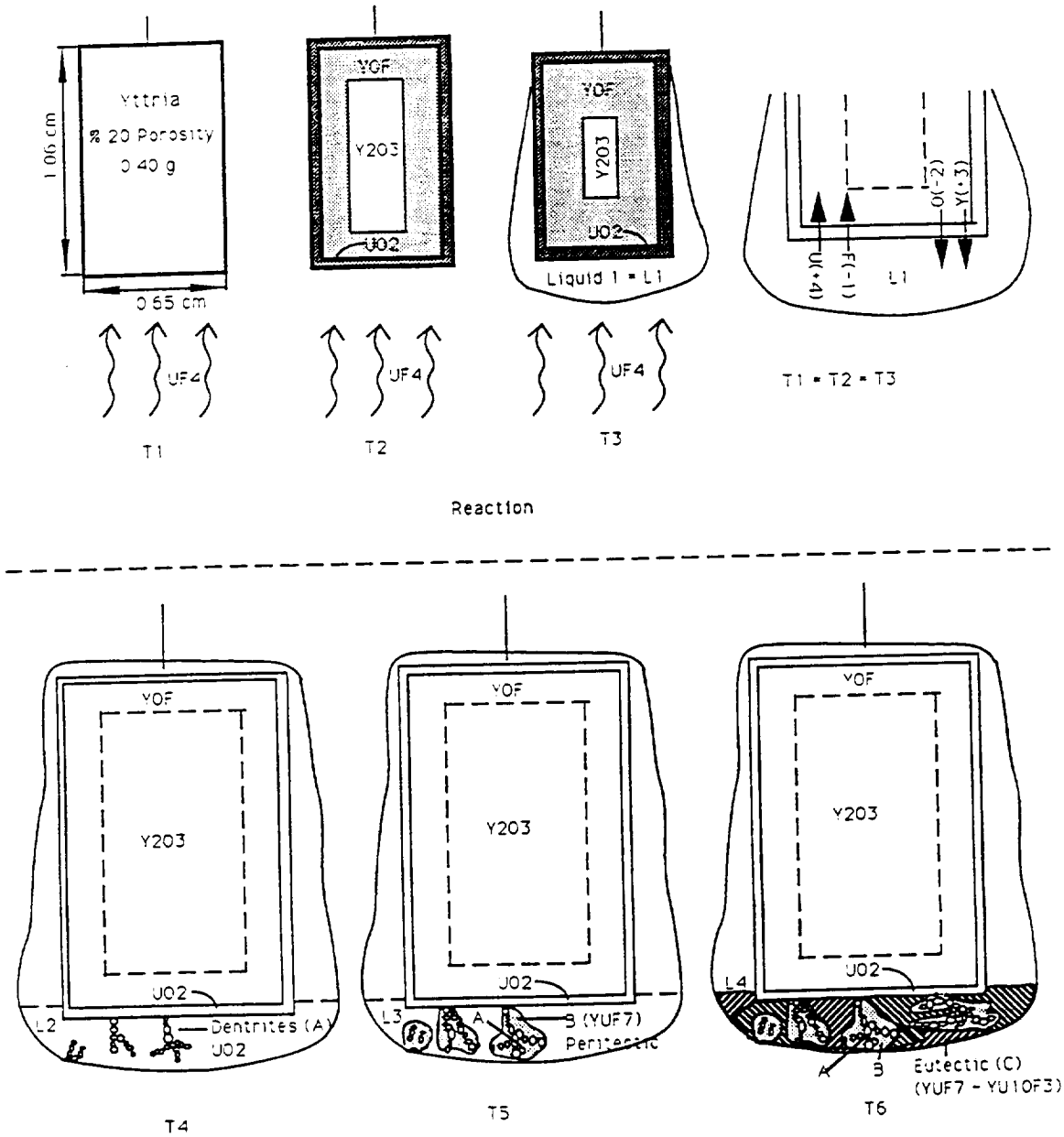

Figure 4.7 Reaction and Solidification Scheme

REPORT DOCUMENTATION PAGE

Form Approved
OMB No. 0704-0188

1. AGENCY USE ONLY (*Leave blank*)	2. REPORT DATE	3. REPORT TYPE AND DATES COVERED
	April 1996	Final Contractor Report

4. TITLE AND SUBTITLE

Materials Compatibility With Uranium Fluorides at High Temperatures

5. FUNDING NUMBERS

WU–233–01–0N
C–NAS3–26314

6. AUTHOR(S)

S. Anghaie, R.J. Hanrahan, Jr., and Z.E. Erkmen

7. PERFORMING ORGANIZATION NAME(S) AND ADDRESS(ES)

University of Florida
Ultrahigh High Temperature Reactor and Energy Conversion Program
Innovative Nuclear Space Power and Propulsion Institute
Gainesville, Florida 32611

8. PERFORMING ORGANIZATION REPORT NUMBER

E–9883

9. SPONSORING/MONITORING AGENCY NAME(S) AND ADDRESS(ES)

National Aeronautics and Space Administration
Lewis Research Center
Cleveland, Ohio 44135–3191

10. SPONSORING/MONITORING AGENCY REPORT NUMBER

NASA CR–198390

11. SUPPLEMENTARY NOTES

Project Manager, Harvey S. Bloomfield, Power Technology Division, NASA Lewis Research Center, organization code 5440, (216) 433–6131.

12a. DISTRIBUTION/AVAILABILITY STATEMENT

Unclassified - Unlimited
Subject Categories 20 and 27

This publication is available from the NASA Center for Aerospace Information, (301) 621–0390.

12b. DISTRIBUTION CODE

13. ABSTRACT (*Maximum 200 words*)

The objective of an ongoing study being conducted by the Innovative Nuclear Space Power and Propulsion Institute (INSPI) at the University of Florida, is to find suitable materials for use in contact with uranium tetrafluoride from approximately 1200 to 3000 C. This temperature range encompasses both the liquid and gas phase of UF_4. In this project ceramic materials were investigated which have been used in the fuel of nuclear reactors. These materials, if compatible with UF_4, would be extremely valuable due to their very high melting temperatures, familiar chemistry, and well characterized nuclear properties. Experiments were conducted on thorium dioxide (ThO_2) and uranium dioxide (UO_2). Samples were exposed to liquid UF_4 at 1100 C and to UF_4 vaporized at above 1450 C. Exposures took place in a graphite crucible inside an evacuated quartz tube. An inductive heating system was used to heat the crucible and thereby the UF_4. Use of the quartz tube allowed direct observation of the ongoing reactions. At the conclusion of each exposure samples of residual gases diluted with nitrogen were run through a gas chromatograph (GC) to determine which gases were released as corrosion products. Subsequent to each experiment remaining samples were weighed then photographed at 2.5x magnification. Power samples of the surface scales and the bulk samples were then prepared for x-ray diffraction analysis (XRD) to determine composition. Data from the GC and XRD were then correlated with equilibrium reaction product data obtained from F*A*C*T to determine the reactions present. Surface analysis of the samples was conducted using Scanning Electron Microscopy (SEM) to examine the scales formed at high magnification, and Energy Dispersive X-Ray Spectroscopy (EDS), to qualitatively determine the elements present in various parts of the scales. Experiments with uranium dioxide showed that although UO_2 does not react significantly with UF_4, it does dissolve in liquid UF_4 and apparently suffers from ablation when exposed to UF_4 vapor. Thoria did react with UF_4 in both the liquid and gas phase exposures, forming a mixture of uranium dioxide and uranium-thorium oxyfluorides.

14. SUBJECT TERMS

Uranium fluoride; Compatibility; High temperature

15. NUMBER OF PAGES

159

16. PRICE CODE

A08

17. SECURITY CLASSIFICATION OF REPORT	18. SECURITY CLASSIFICATION OF THIS PAGE	19. SECURITY CLASSIFICATION OF ABSTRACT	20. LIMITATION OF ABSTRACT
Unclassified	Unclassified	Unclassified	

National Aeronautics and
Space Administration

Lewis Research Center
21000 Brookpark Rd.
Cleveland, OH 44135-3191